Geosci. Model Dev. Discuss., https://doi.org/10.5194/gmd-2018-316
Manuscript under review for journal Geosci. Model Dev.
Discussion started: 19 December 2018

Geoscientific Model Development Discussions

Chemistry and deposition in the Model of Atmospheric composition at Global and Regional scales using Inversion Techniques for Trace gas Emissions (MAGRITTEv1.0). Part A. Chemical mechanism

Jean-François Müller[1], Trissevgeni Stavrakou[1], and Jozef Peeters[2]

[1]Royal Belgian Institute for Space Aeronomy, Avenue Circulaire 3, 1180, Brussels, Belgium
[2]Department of Chemistry, University of Leuven, Celestijnenlaan 200F, B-3001 Leuven, Belgium

Correspondence: Jean-François Müller (Jean-Francois.Muller@aeronomie.be)

Abstract. A new chemical mechanism for the oxidation of biogenic volatile organic compounds (BVOCs) is presented and implemented in the Model of Atmospheric composition at Global and Regional scales using Inversion Techniques for Trace gas Emissions (MAGRITTE). With a total of 99 organic species and over 240 gas-phase reactions, 67 photodissociations and 7 heterogeneous reactions, the mechanism treats the chemical degradation of isoprene – its main focus – as well as acetaldehyde, acetone, methylbutenol and the family of monoterpenes. Regarding isoprene, the mechanism incorporates a state-of-the-art representation of its oxidation scheme accounting for all major advances put forward in recent theoretical and laboratory studies. The model and its chemical mechanism are evaluated against the suite of chemical measurements from the SEAC^{4}RS (Studies of Emissions and Atmospheric Composition, Clouds and Climate Coupling by Regional Surveys) airborne campaign, demonstrating a good overall agreement for major isoprene oxidation products, although the aerosol hydrolysis of tertiary and non-tertiary nitrates remain poorly constrained. The comparisons for methylnitrate indicate a very low nitrate yield ($< 3 \cdot 10^{-4}$) in the CH_3O_2+NO reaction. The oxidation of isoprene, acetone and acetaldehyde by OH is shown to be a substantial source of enols and keto-enols, primarily through the photolysis of multifunctional carbonyls generated in their oxidation schemes. Oxidation of those enols by OH radicals constitutes a sizable source of carboxylic acids estimated at 8 Tg (HCOOH) yr^{-1} and 17 Tg(CH_3COOH) yr^{-1}, or $\sim$25% of their global identified source. The ozonolysis of alkenes is found to be a smaller source of HCOOH (6 Tg HCOOH yr^{-1}) than previously estimated, due to several factors including the strong deposition sink of hydroxymethylhydroperoxide (HMHP).

1 Introduction

The terrestrial biosphere is, by far, the largest source of non-methane volatile organic compounds (NMVOCs) to the global atmosphere (Guenther et al., 2012). Because those biogenic VOCs (BVOCs) are generally very reactive, their chemical degradation takes mostly place in the boundary layer, in the vicinity of the emission regions, where they have a strong impact on the budget of oxidants and the formation and growth of secondary organic aerosol (SOA), a major component of fine particulate matter (Seinfeld and Pandis, 2006; Hallquist et al., 2009). Even far away from those regions, longer-lived intermediates

Geosci. Model Dev. Discuss., https://doi.org/10.5194/gmd-2018-316
Manuscript under review for journal Geosci. Model Dev.
Discussion started: 19 December 2018

Geoscientific Model Development Discussions
Open Access
EGU

generated in their oxidation (e.g. organic nitrates and peroxynitrates) have a large impact on nitrogen oxides (NOx), hydroxyl radical (OH) and ozone levels (Paulot et al., 2012).

Among the BVOCs, isoprene has by far the largest global emissions, of the order of 500 Tg yr^{-1}, representing about 50% of all BVOCs; other major biogenic compounds in terms of emissions include the monoterpenes, methanol, acetone, acetaldehyde, and ethanol (Guenther et al., 2012). The complex chemical degradation mechanism and the profound impact of isoprene on air quality and the climate has been the topic of numerous field (Trainer et al., 1987; Claeys et al., 2004; Lelieveld et al., 2008; Hofzumahaus et al., 2009; Toon et al., 2016), laboratory (Tuazon and Atkinson, 1989; Paulot et al., 2009a, b; Crounse et al., 2011; Wolfe et al., 2012; Kwan et al., 2012; Lin et al., 2013; Fuchs et al., 2013; Bates et al., 2014, 2016; Nguyen et al., 2015a, 2016; Schwantes et al., 2015; Teng et al., 2017), theoretical (Peeters et al., 2009; Kjaergaard et al., 2012; Crounse et al., 2013; Peeters et al., 2014; Peeters and Nguyen, 2012; Liu et al., 2017; Praske et al., 2018) and modelling studies (Stavrakou et al., 2010; Paulot et al., 2012; Taraborrelli et al., 2012; Jenkin et al., 2015; Squire et al., 2015; Travis et al., 2016; Lelieveld et al., 2016; Silva et al., 2018; Stadtler et al., 2018).

Our understanding of isoprene oxidation has expanded considerably in the last decade. Most importantly perhaps, the traditional views regarding the fate of large, multifunctional peroxy radicals formed in the oxidation of isoprene and other NMVOCs has been radically altered by the realization that H-shift reactions in such radicals can sometimes be fast enough to compete with, or even outrun, their reactions with nitric oxide and peroxy radicals (Peeters et al., 2009; Crounse et al., 2011; Teng et al., 2017). The impact of the 1,6 H-shifts in allylic peroxy radicals formed in the oxidation of isoprene by OH is enhanced by their thermal instability allowing fast interconversion of the different peroxy isomers/conformers (Peeters et al., 2009), such that the 1,6 H-shifts can compete with the conventional bimolecular reactions for the entire pool of initial peroxys, which greatly affects the product yields (Peeters and Müller, 2010; Peeters et al., 2014; Teng et al., 2017). Other examples of peroxy isomerization reactions shown to be of importance include 1,4 aldehyde H-shifts (Asatryan et al., 2010; Crounse et al., 2012) and the very fast enolic H-shifts (Peeters and Nguyen, 2012) as well as hydroperoxide H-shifts (Jorgensen et al., 2016). The resulting autoxidation reactions generate multifunctional hydroperoxides shown in some cases (in monoterpene oxidation) to be of such extremely low volatility as to play a crucial role in SOA and cloud condensation nuclei (CCN) formation (Crounse et al., 2013; Jokinen et al., 2014, 2015), while in other cases, they are believed to be an important source of HOx radicals through photodissociation (Peeters and Müller, 2010; Wolfe et al., 2012; Liu et al., 2017, 2018). The recycling of OH radicals associated with peroxy H-shifts and their subsequent reactions, as well as with other previously unsuspected reactions such as epoxide formation from activated hydroxy hydroperoxy radicals (Paulot et al., 2009a) has led to a reassessment of the overall impact of isoprene (and other BVOCs) on OH and HO_2 levels, now found to be fairly consistent with HOx measurements in isoprene photooxidation experiments (Fuchs et al., 2013; Novelli et al., 2018b) as well as in field experiments in isoprene-rich, low-NOx environments (Bottorff et al., 2018). The importance of isoprene-derived epoxides stems from their major role as precursors of SOA demonstrated by laboratory and field measurements (Paulot et al., 2009a; Surratt et al., 2010; Lin et al., 2012, 2013). Finally, the impact of isoprene on NOx levels has been also reevaluated due to a better assessment of organic nitrate formation in isoprene oxidation by OH (Paulot et al., 2009b; Lee et al., 2014; Teng et al., 2017; Wennberg et al., 2018) and NO_3 (Kwan et al., 2012; Schwantes et al., 2015; Wennberg et al., 2018) as well as of the balance between NOx-recycling path-

Geosci. Model Dev. Discuss., https://doi.org/10.5194/gmd-2018-316
Manuscript under review for journal Geosci. Model Dev.
Discussion started: 19 December 2018

ways such as photolysis (Müller et al., 2014) and NOx terminal losses through heterogeneous hydrolysis in aqueous aerosols (Romer et al., 2016) and dry deposition (Nguyen et al., 2015b).

A proper model assessment of the role of BVOCs in the global troposphere and in issues such as air quality and the interaction between the biosphere, the atmosphere and the climate requires the implementation of up-to-date, state-of-the-art chemical mechanisms in large-scale (global or regional) models. Whereas completely explicit mechanisms are not advisable due to computational cost concerns, oversimplified mechanisms are clearly not appropriate as tools to explore the impact of mechanistic changes, especially in the context of the rapid evolution of our understanding of the mechanisms. We present here a semi-explicit mechanism of intermediate complexity incorporating the major advances reported above. It covers the oxidation of isoprene, monoterpenes, methanol, acetone, acetaldehyde, ethanol and 2-methyl-3-butene-2-ol (short-handed as methyl-butenol or MBO). This mechanism is implemented in the Model of Atmospheric composition at Global and Regional scales using Inversion Techniques for Trace gas Emissions (MAGRITTE) which is based on the previous global model IMAGES (Muller and Brasseur, 1995; Stavrakou et al., 2009a, b, 2015; Bauwens et al., 2016).

Given the very large uncertainties in monoterpene oxidation, their treatment is still very crude in the mechanism, the focus being put on the formation yield of important products. Regarding isoprene, the mechanism relies on the Leuven Isoprene Mechanism (Peeters et al., 2009, 2014) and on the extensive, explicit Caltech oxidation mechanism (ca. 900 reactions and 400 species) recently presented by Wennberg et al. (2018), based on a critical appraisal of the relevant theoretical and laboratory studies. For other reactions not addressed in those studies, it also relies on the Master Chemical Mechanism (MCM) (Saunders et al., 2003; Jenkin et al., 2015) and on our own evaluation. The mechanism also incorporates important new mechanistic developments related to e.g. the revisited role of hydroperoxycarbonyl photolysis (Liu et al., 2017, 2018) and the fate of enols and keto-enols produced from such processes. Due to these developments, the oxidation of isoprene as well as of other compounds (e.g. acetone and acetaldehyde) by OH entails a previously unsuspected source of formic and acetic acid, for which atmospheric observations suggest the existence of large missing sources (Paulot et al., 2011; Stavrakou et al., 2012; Millet et al., 2015) especially since the HCOOH source due to alkene ozonolysis through the Criegee Intermediate CH_2OO recently turned out smaller than previously thought (Sheps et al., 2017; Allen et al., 2018).

The complete chemical mechanism of BVOC oxidation is presented in Sect. 2. The parameterization of Henry's law constants and dry deposition velocities is presented and evaluated in a companion paper (Müller et al., 2018). Simulations with the MAGRITTE model and the updated chemical mechanism are presented in Sect. 3, including an evaluation against airborne measurements over the Eastern United States (Sect. 3.3) and a presentation of the global sources of carboxylic acids (Sect. 3.4) and glyoxal(Sect. 3.5) resulting from the implementation of the chemical mechanism.

2 The chemical mechanism of BVOC oxidation in MAGRITTE

The list of chemical species and the complete gas-phase BVOC oxidation mechanism are given in Tables 1–3.

Geosci. Model Dev. Discuss., https://doi.org/10.5194/gmd-2018-316
Manuscript under review for journal Geosci. Model Dev.
Discussion started: 19 December 2018

Geoscientific Model Development Discussions

2.1 Isoprene + OH

2.1.1 Initial steps of mechanism

To limit the number of species and reactions, the OH-adducts formed from the reaction of isoprene with OH are not explicitly represented, and the isoprene peroxys are lumped into three compounds: ISOPBO2 and ISODO2 resulting from addition of OH to carbons 1 and 4, respectively, and ISOPEO2 resulting from OH addition to the central carbons (see Peeters et al. (2014) regarding carbon numbering). For example, ISOPBO2 includes the 1,2-OH-peroxy as well as the 1,4-OH-peroxy which can undergo a 1,6-H shift leading to a $\delta-$hydroperoxy aldehyde (HPALD1) and other products. The ratio of OH addition to C_4 to addition to C_1 is 37:63 (Wennberg et al., 2018). Accounting for the fast interconversion of β- and δ-OH-peroxys, the bulk isomerisation rate of ISOPBO2 and ISOPDO2 was shown to increase linearly with the sink rate (k_p) of the traditional peroxy reaction (Peeters et al., 2014). The following expressions of the bulk 1,6 isomerisation rates are obtained by linear regression of the bulk rates between 285 and 305 K, based on the experimental estimates of the peroxy unimolecular reaction rates (Wennberg et al., 2018):

$$k_{\mathrm{ISOPBO2}} = 3.409 \cdot 10^{12} \cdot \exp\left(-10698/T\right) + k_p \cdot 1.07 \cdot 10^{-3} \cdot \exp\left(64/T\right) \quad (1)$$

$$k_{\mathrm{ISOPDO2}} = 4.253 \cdot 10^{8} \cdot \exp\left(-7254/T\right) + k_p \cdot 2.33 \cdot 10^{-7} \cdot \exp\left(3662/T\right) \quad (2)$$

As MAGRITTE is not intended to model local urban conditions with very high NO levels, we omit the products of the bimolecular reactions of the δ-hydroxyperoxy radicals, which at NO levels below 1 ppbv carry less than 5% of the reactive flux. The $\delta-$HPALD yield in the 1,6 H-shift is taken equal to 25% (Teng et al., 2017), and dihydroperoxy carbonyl peroxy radicals (DIHPCARP1,$CH_3C(OO)(CHO)CH(OOH)CH_2OOH$ and its isomer DIHPCARP2) are assumed to make up the rest (Peeters et al., 2014). Unidentified species isobaric with the $\delta-$HPALDs were also measured by Teng et al. (2017) at a 15% yield, and assumed by Wennberg et al. (2018) to consist of β-HPALDs (e.g. $O{=}CHC(OOH)(CH_3)CH{=}CH_2$) also formed from the 1,6 H-shift of the δ-OH-peroxys. However, the proposed formation route would require O_2 loss from one of the equilibrated hydroperoxy-peroxy radicals, which is unlikely to be competitive with the HO_2 expulsion from the initial hydroperoxy-peroxy radical to form δ-HPALDs (Peeters et al., 2014). Those pathways are not included here, such that our DIHPCARP yield (75%) could be somewhat overestimated.

Besides bimolecular reactions with NO and HO_2, the DIHPCARPs were proposed to undergo aldehyde H-shifts to trihydroperoxy acyl radicals which can eliminate CO and OH and form dihydroperoxycarbonyls (DIHPMEK or DIHPCHO, see Table 1) (Peeters et al., 2014; Wennberg et al., 2018). Direct experimental evidence is still lacking for these reactions. They are assumed to be very fast and therefore largely dominant in atmospheric conditions by Wennberg et al. (2018), although the DIHPCARPs were bypassed in their reduced mechanism and replaced by simpler (C_1-C_3) compounds, including hydroperoxyacetaldehyde (HPAC) and hydroperoxyacetone (HPACET), which were observed in the laboratory and quantified relative to the sum of HPALDs by Teng et al. (2017). The bimolecular reactions of the DIHPCARPs are believed to form HPAC and

Geosci. Model Dev. Discuss., https://doi.org/10.5194/gmd-2018-316
Manuscript under review for journal Geosci. Model Dev.
Discussion started: 19 December 2018

HPACET, along with other compounds inlcuding glyoxal and methylglyoxal (Peeters et al., 2014; Wennberg et al., 2018). The ratio of HPAC and HPACET to the sum of HPALDs was found by Teng et al. (2017) to show very little dependence on NO levels, which is difficult to rationalize if those compounds are formed by DIHPCARP bimolecular reactions in competition with H-shifts. On the other hand, such competition was strongly suggested by the finding (Crounse et al. (2011), amendment published in 2012) that the HPAC and HPACET relative yields were larger (comparable to that of HPALD) in the deuterated isoprene system, since D-shifts are known to be much slower than H-shifts. Nevertheless, HPAC and HPACET formation from the bimolecular DIHPCARP reactions would require very slow H-shifts, which is very unlikely. Very fast H-shift is therefore assumed here, supported by recent theoretical calculations (Novelli et al., 2018b). Note that besides CO elimination, the tri-hydroperoxy acyl radicals might also add O_2 (Novelli et al., 2018b); the resulting acylperoxy could undergo an H-shift to form a dihydroperoxy peracid of which the subsequent fate requires further investigation. Although CO elimination could be dominant in the case of DIHPCARP1, O_2 addition could be the major fate of the tri-hydroperoxy acyl radical resulting from the H-shift in DIHPCARP2.

2.1.2 Hydroperoxycarbonyl photolysis

The isoprene oxidation mechanism (in particular the DIHPCARP pathways) generates several hydroperoxycarbonyls. Photolysis is expected to dominate the loss of all α-hydroperoxy aldehydes (e.g. HPAC, $O{=}CHCH_2OOH$) and of several hydroperoxyketones (among which HPACET, $CH_3C(O)CH_2OOH$) due to estimated near-unit quantum yields and to the strong enhancement of the absorption cross sections caused by the interaction between the hydroperoxy and carbonyl chromophores (Jorand et al., 2000; Liu et al., 2018). The expected likely major pathway in the photolysis of 2-hydroperoxy propanal was theoretically determined to be a 1,5 H-shift in the S1 state leading to enol formation (along with triplet O_2), at an estimated yield of 84%, whereas intersystem crossing (ISC) resulting in C–C scission (i.e. formyl elimination) and OH expulsion, makes up the rest (Liu et al., 2018). Similar yields are expected (and adopted here) for e.g. HPAC and HPACET. However, the enol yield should be lower for heavier compounds due to expected faster ISC rates. It is taken to be 50% for e.g. $CH_3C(O)CH(OOH)CH{=}O$ (HPKETAL) and $O{=}CHC(OOH)(CH_3)CH{=}O$ (HPDIAL). Furthermore, when H-bonding between the carbonyl-O and the hydroperoxide-H supposed to undergo the H-shift leading to enol formation is not favoured, e.g. because of possible H-bonds of this hydrogen with another oxygen in the molecule, enol formation is disadvantaged and therefore neglected here for simplicity. This situation applies in particular to the dihydroperoxycarbonyls produced in the reactions of the DIHPCARPs. For these compounds, formyl or acetyl elimination, followed by OH expulsion, is taken to be the only photolysis channel. Note that, to limit the number of compounds and reactions in the mechanism, several hydroperoxycarbonyls are not considered explicitly, and are replaced by their estimated photolysis products.

The theoretical investigation of the reaction of OH with vinyl alcohol (VA) (So et al., 2014) and with propenols (Lei et al., 2018) is the basis for our evaluation of OH-reactions with enols. OH-addition generally follows e.g.

Geosci. Model Dev. Discuss., https://doi.org/10.5194/gmd-2018-316
Manuscript under review for journal Geosci. Model Dev.
Discussion started: 19 December 2018

Geoscientific Model Development Discussions

$$\mathrm{RCH{=}CHOH + OH(+O_2) \rightarrow RCH(O_2)CH(OH)_2 \xrightarrow{\text{1,5 H-shift}} HC(O)OH + OH + RCHO}$$
$$\mathrm{\rightarrow RCH(OH)CH(OH)O_2 \rightarrow HO_2 + RCH(OH)CHO}$$

In the case of vinyl alcohol (generated in HPAC photolysis), the formic acid yield is ca. 60% according to So et al. (2014). Acetic acid is similarly formed from the OH-reaction of 2-propenol generated in the photolysis of hydroperoxyacetone (Lei et al., 2018). $HCOOH$ should also be formed in the OH-reaction of hydroxyvinylmethylketone (HMVK, $HOCH{=}CHC(O)CH_3$) and hydroxymethacrolein (HMAC, $O{=}CHC(CH_3){=}CHOH$), although at a lower yield due to the competition with other possible reactions. Note that the acid-catalyzed tautomerization of enols is neglected, based on the theoretical study of the case of vinyl alcohol (Peeters et al., 2015).

2.1.3 HPALD photolysis

The HPALD photolysis quantum yield is taken equal to 0.8, a compromise between the experimental value of $1{\pm}0.4$ for a C_6 HPALD proxy (Wolfe et al., 2012) and the theoretical value (actually a lower limit) of 0.55 by Liu et al. (2017). The mechanism following HPALD photolysis is based on the theoretical study of Liu et al. (2017):

$$\begin{aligned}\mathrm{HPALD1 + h\nu \rightarrow\ } & \mathrm{OH + 0.11\,(HO_2 + O{=}CHCH{=}C(CH_3)CH{=}O\ (MBED))}\\ & \mathrm{+0.11\,(CO + OH + O{=}CHCH(OOH)C(O)CH_3\ (HPKETAL))}\\ & \mathrm{+0.56\,(CO + OH + O{=}CHCH{=}C(CH_3)(OH)\ (HMVK))}\\ & \mathrm{+0.22\,(CO + CH_3C(O_2){=}CHCH_2OH^{\dagger}\ (V1O2^{\dagger}))}\end{aligned}$$

$$\begin{aligned}\mathrm{HPALD2 + h\nu \rightarrow\ } & \mathrm{OH + 0.18\,(HO_2 + O{=}CHCH{=}C(CH_3)CH{=}O\ (MBED))}\\ & \mathrm{+0.18\,(CO + OH + O{=}CHCH(OOH)C(O)CH_3\ (HPKETAL))}\\ & \mathrm{+0.46\,(CO + OH + O{=}CHC(CH_3){=}CHOH\ (HMAC))}\\ & \mathrm{+0.18\,(CO + HOCH_2C(CH_3){=}CHO_2{}^{\dagger}\ (V2O2^{\dagger}))}\end{aligned}$$

Note that the formation of $OCHC(CH_3)(OOH)CHO$, considered in Wennberg et al. (2018) besides HPKETAL formation in the second photolysis channel of each HPALD, is neglected here as it was found to be minor (Liu et al., 2017).

Based on a reaction chamber study of butenedial and 4-oxo-2-pentenal photolysis (Thuner et al., 2003), the photolysis of methylbutenedial (MBED) should be very fast (lifetime of minutes) and lead to a furanone-type compound as major product, as well as methylmaleic anhydride (MMAL) and other compounds. Relying on MCM for the further oxidation of the furanone by OH, we replace MBED by its assumed photooxidation products:

$$\begin{aligned}\mathrm{MBED} \xrightarrow{\text{fast}} & \mathrm{0.55\,(-OH + 2CO_2 + HCHO + CH_3CO_3)}\\ & \mathrm{+0.20\,MMAL + 0.15\,(MGLY + CO + HO_2 + CO_2) + 0.10\,(GLY + CH_3CO_3 + CO_2)}\end{aligned}$$

Geosci. Model Dev. Discuss., https://doi.org/10.5194/gmd-2018-316
Manuscript under review for journal Geosci. Model Dev.
Discussion started: 19 December 2018

Geoscientific Model Development Discussions

The major sink of the enols HMAC and HMVK should be their reaction with OH, leading in part to formic acid formation (see Table 2). Based on the experimental study of Yoon et al. (1999), photolysis of the analogous form of acetylacetone ($CH_3C(O)CH{=}C(OH)CH_3$) yields OH and a vinylic co-product radical up to a wavelength of 312 nm, with an OH appearance rate of 10^8 s^{-1} or higher around 300 nm, implying a quantum yield at atmospheric pressure of order 0.1 (instead of a near-unit quantum yield as assumed by Liu et al. (2017)). The absorption cross sections of the enols are obtained from the acetylacetone study of Nakanishi et al. (1977). By analogy with the $CH_2{=}CH^\circ$ + O_2 reaction (Mebel and Kislov, 2005), we assume that the vinylic co-product radicals of HMAC and HMVK photolysis react rapidly with O_2 to give HCO + MGLY and CH_3CO + GLY, respectively.

The activated vinylperoxy radicals $V1O2^\dagger$ and $V2O2^\dagger$ might be stabilized by collisions and undergo reactions with NO, HO_2 and NO_2 (Liu et al., 2017), but a more probable fate is decomposition (Mebel and Kislov, 2005), to CH_3CO + GLYALD in the case of V1O2, and HCO + HYAC, in the case of V2O2.

2.2 Isoprene + O_3

The ozonolysis mechanism follows the experimentally-derived model of Nguyen et al. (2016), except regarding the fate of the Criegee intermediate CH_2OO, formed with a yield of 58% (and assumed to be entirely stabilized). Whereas Nguyen et al. attributed a significant role to the reaction of CH_2OO with the water monomer, motivated by the dependence of the observed yields on relative humidity, the reaction of CH_2OO with the water dimer has been shown by several groups to be largely dominant at all relevant conditions (Berndt et al., 2014; Chao et al., 2015; Smith et al., 2015; Lewis et al., 2015; Sheps et al., 2017) and is therefore the only reaction considered here. More work is needed to elucidate the humidity dependence of the yields. Reaction with the dimer follows the recent study of Sheps et al. (2017):

$$\begin{aligned} CH_2OO + (H_2O)_2 \rightarrow\ & 0.55\,(HOCH_2OOH + H_2O) \\ & + 0.4\,(HCHO + H_2O_2 + H_2O) \\ & + 0.05\,(HCOOH + 2\,H_2O) \end{aligned}$$

2.3 Isoprene + NO_3

The mechanism for NO_3-initiated oxidation follows largely the laboratory study of Schwantes et al. (2015). Several minor pathways are neglected, however, as the further degradation mechanism of several products remain unclear. The title reaction, followed by O_2–addition, forms several peroxy radical isomers lumped into one compound (NISOPO2). Generalizing the mechanism proposed by Schwantes et al., the reaction of NISOPO2 with non-tertiary peroxy radicals proceeds following

$$\begin{aligned} NISOPO2 + RO_2 \rightarrow\ & 0.2\,(NISOPO + RO + O_2) \\ & + 0.4\,(0.88\,NC4CHO + 0.12\,MACR + 0.12\,HCHO + 0.12\,NO_2 + ROH) \\ & + 0.4\,(0.88\,ISOPCNO3 + 0.12\,ISOPDNO3 + R'CHO) \end{aligned}$$

whereas for tertiary peroxy radicals the reaction reads

Geosci. Model Dev. Discuss., https://doi.org/10.5194/gmd-2018-316
Manuscript under review for journal Geosci. Model Dev.
Discussion started: 19 December 2018

Geoscientific Model Development Discussions

$$\mathrm{NISOPO2 + RO2 \rightarrow 0.5\,(NISOPO + RO + O_2)}$$
$$\mathrm{+0.5\,(0.88\,NC4CHO + 0.12\,MACR + 0.12\,HCHO + 0.12\,NO_2 + ROH)}$$

The proposed 1,6 H-shift of the trans-[1,4] isomer of NISOPO2 radicals (Schwantes et al., 2015) is neglected, as it is slow ($4{\cdot}10^{-4}$ s^{-1}) compared to the other reactions. The different isomers of the oxy radical NISOPO have different fates: decomposition to MVK or MACR (for the β-nitroxy oxys), reaction with O_2 (for the δ's), and a fast 1,5 H-shift (Kwan et al., 2012) (ca. $2{\cdot}10^5$ s^{-1}) for the δ-(1-ONO_2,4-O) radical, outrunning the O_2-reaction by a factor of about 4. The isomerisation leads, after O_2-addition, to a peroxy of which the reaction with NO or NO_3 forms an enal nitrate, $O_2NOCH_2C(=CH_2)CH{=}O$, along with HCHO and HO_2 (Wennberg et al., 2018). The main expected fate of this enal nitrate is photolysis, to NO_2 + HCHO + $O{=}CH{-}C(=CH_2)O_2$. The latter radical can undergo a fast 1,4 H-shift to give CO + OH + $H_2C{=}C{=}O$ (ketene). Ketene can react with OH, at a rate of ca. $1.7{\cdot}10^{-11}$ molec^{-1} cm^3 s^{-1}, producing CO + $^\circ CH_2OH$ (Calvert et al., 2011); it also photolyzes to $^1CH_2$ (or $^3CH_2$) + CO. The fate of methylene is mainly oxidation to CO or CO_2 (Baulch et al., 2005). Based on photolysis parameter data provided by Calvert et al. (2011), photolysis is estimated to be slightly less important than the OH-reaction, and is therefore neglected here for simplicity.

Based on the above, the lumped oxy radical undergoes the condensed fast reaction

$$\mathrm{NISOPO \rightarrow 0.42\,MVK + 0.04\,MACR + 1.54\,HCHO + 0.82\,NO_2 + 0.18\,NC4CHO + 0.9\,HO_2 + 0.72\,CO}$$

The β- and δ-nitroxy hydroperoxides formed in the $\mathrm{NISOPO2 + HO_2}$ reaction are explicitly considered. Their reactions with OH forms nitroxy hydroxy epoxides (IHNE) as well as hydroperoxy and nitroxy carbonyls, also explicitly considered in the mechanism. A major product of the NISOPO2 reaction with NO or RO_2 is the enal nitrate NC4CHO. Laboratory work on an analogous compound (Xiong et al., 2016) has shown that photolysis is by far its dominant sink, owing to high quantum yields and to enhanced absorption cross sections attributed to the interaction of the nitrate and carbonyl chromophore. The NC4CHO photolysis cross sections and quantum yield recommendation follow Xiong et al. (2016). The reaction produces the same oxy radicals as in HPALD photolysis (see above, Sect. 2.1.

2.4 Cross-reactions of peroxy radicals

The channel ratios and rates of the cross reactions of peroxy radicals generally follow Capouet et al. (2004), except when more recent recommendations exist (e.g. Schwantes et al. (2015) for peroxys resulting from NO_3 addition to isoprene). The cross reaction rates are calculated as twice the geometric mean of the self-reaction rates, except for acylperoxy radicals for which the rate and channel data reported for CH_3CO_3 are used (Atkinson et al., 2006). The self-reaction rates are obtained from compiled data for similar compounds (Capouet et al., 2004; Peeters and Müller, 2010; Atkinson et al., 2006).

Geosci. Model Dev. Discuss., https://doi.org/10.5194/gmd-2018-316
Manuscript under review for journal Geosci. Model Dev.
Discussion started: 19 December 2018

Geoscientific Model Development Discussions

2.5 Peroxy radical reactions with NO and HO_2

We adopt the recommendations of Wennberg et al. (2018) for the rates of non-acyl peroxy radical reactions with NO ($2.7 \cdot 10^{-12} \exp(350/T)$ cm^3 molec^{-1} s^{-1}) as well as with HO_2 ($2.82 \cdot 10^{-13} \exp(1300/T) \cdot [1 - \exp(-0.231\, n)]$ cm^3 molec^{-1} s^{-1}, with n the number of heavy atoms in the radical, excluding the peroxy moiety).

The organic nitrate yield in the reactions of organic peroxys with NO is calculated according to the temperature and pressure-dependent expression of Arey et al. (2001), scaled in order to match experimental values at chamber conditions, when available. The ratio of the nitrate formation pathway to the oxy radical forming pathway is given (Arey et al., 2001) by

$$R_{\text{nit}} = \frac{k_0[M]}{1 + k_0[M]/k_\infty} F^{\{1+[\log_{10}(k_0[M]/k_\infty)]^2\}^{-1}} \quad (3)$$

$$k_0 = \alpha \exp(\beta \cdot n_{\text{C}})\, (T/298)^{-m_0} \quad (4)$$

$$k_\infty = Y_\infty^{298}\, (T/298)^{-m_\infty} \quad (5)$$

with α = 2·10^{-22} cm^3 molec^{-1}, β = 1.0, Y_∞^{298} = 0.3, F = 0.1, m_0 = 0, m_∞ = 8, and n_{C} is the number of carbon atoms in the peroxy radical. Although this expression was derived for secondary alkyl nitrates, we apply it to compute all nitrate yields, given the scarcity of data for tertiary and primary nitrates (Carter and Atkinson, 1989). The altitude and latitude dependence of the yields is shown in Fig. 1 for several values of n_{C}. It has been proposed that the nitrate yield should increase with the number of heavy atoms, instead of with the number of carbons, implying higher yields for highly functionalized compounds (Matsunaga and Ziemann, 2010; Lee et al., 2014; Wennberg et al., 2018), because more heavy atoms increase the lifetime of the ROONO* adduct. However, such procedure often overestimates the measured nitrate yield (Wennberg et al., 2018).

2.6 $CH_3O_2 + OH$

Methylperoxy radical (CH_3O_2) was shown to react rapidly with OH (Bossolasco et al., 2014) although two more recent experimental studies inferred a lower rate constant (Yan et al., 2016; Assaf et al., 2016). The possible pathways include

$$\begin{aligned} CH_3O_2 + OH &\xrightarrow{a} CH_3O + HO_2 \\ &\xrightarrow{b} CH_3OH + O_2 \\ &\xrightarrow{c} CH_2O_2 + H_2O \\ &\xrightarrow{d} CH_3OOOH \end{aligned}$$

The stabilized trioxide (CH_3OOOH) formed in channel d has several possible fates, among which reaction with OH and uptake by aqueous aerosols followed by decomposition into $CH_3OH + O_2$ are expected to be the most important (Müller et al., 2016). An upper limit of 5% for the yield of Criegee radicals was also determined by Assaf et al. (2017), in agreement with the theoretical expectation that it should be negligible (Müller et al., 2016). A yield of 0.9±0.1 for the methoxy + HO_2 channel was determined experimentally at low pressure (50 Torr) (Assaf et al., 2018), in good agreement with the best theoretical

Geosci. Model Dev. Discuss., https://doi.org/10.5194/gmd-2018-316
Manuscript under review for journal Geosci. Model Dev.
Discussion started: 19 December 2018

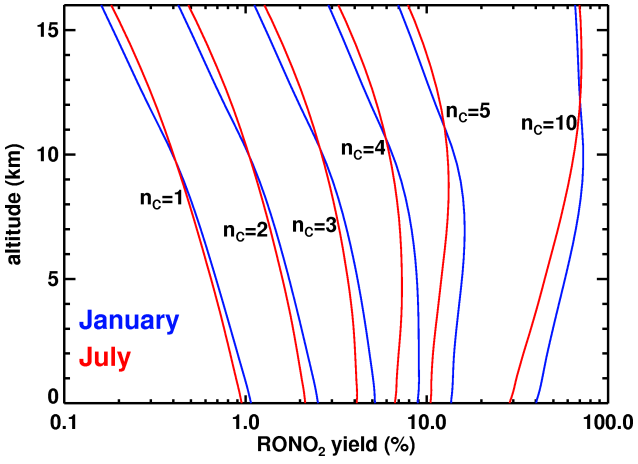

Figure 1. Organic nitrate yield in the reaction of secondary peroxy radicals with NO (Arey et al., 2001), calculated as functions of altitude using temperature and pressure profiles typical of January (in blue) and July (in red) at 40° N (zonal average of ECMWF analyses). n_C is the number of carbons.

estimate (0.92, range 0.77–0.97) determined in Müller et al. (2016) and used in our mechanism. It is also consistent with the methanol yield measurements reported recently by Caravan et al. (2018) at both low and high pressure (0.06±0.02 at 740 Torr). Those results imply however a methanol yield much lower than the value (0.23) used in our global model to reconcile its predictions with atmospheric methanol observations at remote locations (Müller et al., 2016). Note that at low pressure (as used in the experiments by Assaf et al. (2017) and Assaf et al. (2018)), stabilisation of the trioxide is negligible, given the quadratic dependence of the stabilisation fraction (f_{stab}) on atmospheric pressure (Müller et al., 2016),

$$f_{\text{stab}} = f_0 \cdot p^2 \cdot (T/298)^{-5}, \quad (6)$$

where p is atmospheric pressure (atm) and T is temperature (K). In the lower troposphere, however, stabilisation is significant, with a best theoretical estimate of f_0 =0.107. Significant experimental evidence for this partial stabilisation was found by Caravan et al. (2018) at 740 Torr (but not at low pressure).

The mechanism does not account for the possible reaction of OH with other peroxy radicals. As noted by Müller et al. (2016), its relevance for larger peroxys (such as those formed in the oxidation of biogenic VOCs) is expected to be lower than in the case of CH_3O_2. Furthermore, the fate of the stabilised trioxide formed at high yield (Müller et al., 2016; Assaf et al., 2018) in the reaction of large RO_2 radicals with OH is so far unexplored.

2.7 Model species and chemical mechanism

Geosci. Model Dev. Discuss., https://doi.org/10.5194/gmd-2018-316
Manuscript under review for journal Geosci. Model Dev.
Discussion started: 19 December 2018

Geoscientific Model Development Discussions
Open Access
EGU

Table 1. Chemical species of the oxidation mechanism of isoprene, monoterpenes and methylbutenol (MBO).

Notation	*Chemical formula*
	C_1 compounds
HCHO	HCHO
CO	CO
CH_3OH	CH_3OH
HCOOH	HCOOH
CH_3OOH	CH_3OOH
CH_3OOOH	CH_3OOOH
CH_3ONO_2	CH_3ONO_2
PAN	$CH_3CO_3NO_2$
HMHP	$HOCH_2OOH$
	C_2 compounds
CH_3CHO	CH_3CHO
GLYALD	CH_2OHCHO
GLY	CHOCHO
C_2H_5OH	C_2H_5OH
CH_3COOH	CH_3COOH
PAA	CH_3COOOH
ETHLN	$OCHCH_2ONO_2$
HPAC	$OCHCH_2OOH$
GCO3H	$HOCH_2CO(OOH)$
GCOOH	$HOCH_2COOH$
GPAN	$HOCH_2CO_3NO_2$
VA	$CH_2{=}CHOH$
	C_3 compounds
CH_3COCH_3	CH_3COCH_3
HYAC	$CH_2OHCOCH_3$
MGLY	CH_3COCHO
PYRA	$CH_3COCOOH$
C_2H_5COOH	CH_3CH_2COOH

Geosci. Model Dev. Discuss., https://doi.org/10.5194/gmd-2018-316
Manuscript under review for journal Geosci. Model Dev.
Discussion started: 19 December 2018

Geoscientific Model Development Discussions
Open Access
EGU

Notation	*Chemical formula*
NOA	$CH_3C(O)CH_2ONO_2$
HPACET	CH_3COCH_2OOH
MVA	$CH_2{=}C(CH_3)OH$
DHA	$CH_3C(O)CH(OH)_2$
	C_4 compounds
MACR	$CH_2{=}CCH_3CHO$
MVK	$CH_2{=}CHCOCH_3$
MPAN	$CH_2{=}CCH_3CO_3NO_2$
MCO3H	$CH_2{=}CH(CH_3)CO(OOH)$
MCOOH	$CH_2{=}CH(CH_3)COOH$
MVKOOH	$0.55\,CH_3C(O)CH(OOH)CH_2OH + 0.45\,CH_3C(O)CH(OH)CH_2OOH$
MACRNO3	$OCHC(CH_3)(ONO_2)CH_2OH$
MVKNO3	$0.2\,CH_3COCH(OH)CH_2ONO_2 + 0.8\,CH_3COCH(ONO_2)CH_2OH$
MACROH	$HOCH_2C(CH_3)(OH)CHO$
BIACETOH	$CH_3COCOCH_2OH$
DHBO	$CH_3C(O)CH(OH)CH_2OH$
HOBA	$CH_3C(O)CH(OH)CHO$
DIHPMEK	$CH_3C(O)CH(OOH)CH_2OOH$
HPKETAL	$CH_3C(O)CH(OOH)CHO$
HPDIAL	$OCHC(CH_3)(OOH)CHO$
DIHPCHO	$CH_3C(OOH)(CHO)CH_2OOH$
HMVK	$CH_3C(O)CH{=}CHOH$
HMAC	$OCHC(CH_3){=}CHOH$
HMML	$HOCH_2\overline{C(CH_3)OC}{=}O$
	C_5 compounds
ISOP	$CH_2{=}C(CH_3)CH{=}CH_2$
MBO	$CH_3C(OH)(CH_3)CH{=}CH_2$
HCOC5	$CH_2{=}C(CH_3)C(O)CH_2OH$
ISOPBOOH	$CH_2{=}CHC(CH_3)(OOH)CH_2OH$
ISOPDOOH	$CH_2{=}C(CH_3)CH(OOH)CH_2OH$
ISOPEOOH	$CH_2{=}C(CH_3)CH(OH)CH_2OOH$

Geosci. Model Dev. Discuss., https://doi.org/10.5194/gmd-2018-316
Manuscript under review for journal Geosci. Model Dev.
Discussion started: 19 December 2018

Geoscientific Model Development Discussions

Notation	*Chemical formula*
INDOOH	$HOCH_2CH(ONO_2)C(CH_3)(OOH)CH_2OH$
ISOPBNO3	$CH_2{=}CHC(CH_3)(ONO_2)CH_2OH$
ISOPCNO3	$0.86\,HOCH_2CH{=}C(CH_3)CH_2ONO_2 + 0.16\,HOCH_2C(CH_3){=}CHCH_2ONO$
ISOPDNO3	$CH_2{=}C(CH_3)CH(ONO_2)CH_2OH$
ISOPENO3	$CH_3C(=CH_2)CH(OH)CH_2ONO_2$
MBONO3	$0.67\,CH_3C(OH)(CH_3)CH(ONO_2)CH_2OH + 0.33\,CH_3C(OH)(CH_3)CH(OH)CH_2ONO_2$
INCCO	$HOCH_2C(O)C(CH_3)(OH)CH_2ONO_2$
INCNO3	$HOCH_2CH(ONO_2)C(CH_3)(OH)CH_2ONO_2$
NISOPOOHB	$0.9\,CH_2{=}CHC(CH_3)(OOH)CH_2ONO_2 + 0.1\,CH_2{=}C(CH_3)CH(OOH)CH_2ONO_2$
NISOPOOHD	$0.84\,HOOCH_2CH{=}C(CH_3)CH_2ONO_2 + 0.26\,O_2NOCH_2CH{=}C(CH_3)CH_2OOH$
IEPOX	$HOCH_2\overline{CHOC}(CH_3)CH_2OH$
ICHE	$HOCH_2\overline{CHOC}(CH_3)CHO$ and 3 isomers
DHHEPOX	$HOCH_2C(CH_3)(OOH)\overline{CHOCH}(OH)$
NC4CHO	$0.75\,OCHCH{=}C(CH_3)CH_2ONO_2 + 0.25\,OCHC(CH_3){=}CHCH_2ONO_2$
ISOPBOH	$CH_2{=}CHC(CH_3)(OH)CH_2OH$
ISOPDOH	$CH_2{=}C(CH_3)CH(OH)CH_2OH$
HPALD1	$OCHC(CH_3){=}CHCH_2(OOH)$
HPALD2	$OCHCH{=}C(CH_3)CH_2(OOH)$
MMAL	$O{=}\overline{CCH{=}C(CH_3)C(=O)O}$
IHNE	$0.57\,O_2NOCH_2\overline{C(CH_3)OCHCH_2OH}$ + $0.25\,O_2NOCH_2C(CH_3)(OH)\overline{CHOCH_2}$ and isomers
	C_{10} compounds
APIN	$C_{10}H_{16}$ (sum of monoterpenes)
APINONO2	$C_{10}H_{16}(OH)(ONO_2)$
	Peroxy radicals
CH_3O_2	CH_3O_2
CH_3CO_3	CH_3CO_3
$OCHCH_2O_2$	$OCHCH_2O_2$
$HOCH_2CH_2O_2$	$HOCH_2CH_2O_2$
GCO3	$HOCH_2CO_3$
QO2	$HOCH_2CH_2O_2$
ACETO2	$CH_3COCH_2O_2$

Geosci. Model Dev. Discuss., https://doi.org/10.5194/gmd-2018-316
Manuscript under review for journal Geosci. Model Dev.
Discussion started: 19 December 2018

Geoscientific Model Development Discussions
Open Access
EGU

Notation	*Chemical formula*
MVKO2	$0.75\,CH_3COCH(O_2)CH_2OH + 0.25\,CH_3COCH(OH)CH_2O_2$
MCO3	$CH_2{=}C(CH_3)CO_3$
ISOPBO2	$HOCH_2C(CH_3)(O_2)CH{=}CH_2$
ISOPDO2	$CH_2{=}C(CH_3)CH(O_2)CH_2OH$
ISOPEO2	$CH_3C(=CH_2)CH(OH)CH_2O_2$
DIHPCARP1	$CH_3C(OO)(CHO)CH(OOH)CH_2OOH$
DIHPCARP2	$OCHCH(OO)C(CH_3)(OOH)CH_2OOH$
IEPOXAO2	$HOCH_2C(OH)(CH_3)CH(O2)CHO$
IEPOXBO2	$HOCH_2CH(OH)C(CH_3)(O2)CHO$
C59O2	$HOCH_2C(CH_3)(O_2)C(O)CH_2OH$
INBO2	$0.85\,HOCH_2CH(O_2)C(CH_3)(ONO_2)CH_2OH + 0.15\,O_2CH_2CH(OH)C(CH_3)(ONO_2)CH_2OH$
INDO2	$HOCH_2CH(ONO_2)C(CH_3)(O_2)CH_2OH$
INCO2	$HOCH_2CH(O_2)C(OH)(CH_3)CH_2ONO_2$ and isomers
NISOPO2	$0.45\,O_2CH_2CH{=}C(CH_3)CH_2ONO_2 + 0.45\,CH_2{=}CHC(CH_3)(O_2)CH_2ONO_2 +$
	$0.085\,O_2NOCH_2CH{=}C(CH_3)CH_2O_2 + 0.045\,CH_2{=}C(CH_3)CH(O_2)CH_2ONO_2$
MBOO2	$0.67\,CH_3C(OH)(CH_3)CH(O_2)CH_2OH + 0.33\,CH_3C(OH)(CH_3)CH(OH)CH_2O_2$
APINOHO2	peroxy radical from APIN + OH
APINO3O2	peroxy radical from APIN + O_3

Geosci. Model Dev. Discuss., https://doi.org/10.5194/gmd-2018-316
Manuscript under review for journal Geosci. Model Dev.
Discussion started: 19 December 2018

Geoscientific Model Development Discussions

Table 2. Chemical reaction mechanism and kinetic rates. Read $2.14(-11)$ as $2.14{\cdot}10^{-11}$; KRO2NO=$2.7(-12)\exp(350/T)$; T=temperature (K); $[M]$ is air density (molec.cm^{-3}); Y_n^{Arey} is the pressure- and temperature- dependent nitrate yield from Arey et al. (2001), where n is carbon number; units for 1^{st}-, 2^{nd}-, and 3^{d}-order reactions are s^{-1}, cm^{3}molec.$^{-1}$s^{-1} and cm^{6}molec.$^{-2}$s^{-1} respectively. Three-body reaction rates are calculated with $k = \frac{k_0[M]}{1+k_0[M]/k_\infty} F_c^{\{1+[\log_{10}(k_0[M]/k_\infty)]^2\}^{-1}}$. Rates for equilibrium reactions calculated as $k = k_f/K_{eq}$, with k_f the forward reaction rate and K_{eq} the equilibrium constant. **References:** 1, MCM (Saunders et al., 2003; Jenkin et al., 2015); 2, Nguyen et al. (2016); 3, Wennberg et al. (2018); 4, Liu et al. (2013); 5, Peeters and Müller (2010); 6, Capouet et al. (2004); 7, Atkinson et al. (2006); 8, Peeters et al. (2014); 9, St. Clair et al. (2016); 10, D'Ambro et al. (2017); 11, Lee et al. (2014); 12, Jacobs et al. (2014); 13, Paulot et al. (2009b); 14, Bates et al. (2016); 15, Schwantes et al. (2015); 16, Xiong et al. (2016); 17, Crounse et al. (2012); 18, Gross et al. (2014); 19, Burkholder et al. (2015); 20, Nguyen et al. (2015a); 21, Galloway et al. (2011); 22, Praske et al. (2015); 23, Vu et al. (2013); 24, Baeza-Romero et al. (2007); 25, Magneron et al. (2005); 26, Taraborrelli et al. (2012); 27, So et al. (2014); 28, Assaf et al. (2016); 29, Assaf et al. (2018); 30, Müller et al. (2016); 31, Allen et al. (2018); 32, Chan et al. (2009).

Reaction	*Rate*	*Ref.*	*Note*
	C_5 compounds		
$\text{ISOP} + \text{OH} \rightarrow 0.586\,\text{ISOPBO2} + 0.344\,\text{ISOPDO2} + 0.02\,\text{ISOPEO2}$ $+0.10\,\text{HO}_2 + 0.05\,\text{ACETO2} + 0.05\,\text{HCHO} + 0.05\,\text{CO}_2$	$2.7(-11)\exp(360/T)$		N1
$\text{ISOP} + \text{NO}_3 \rightarrow \text{NISOPO2}$	$3.15(-12)\exp(-450/T)$	1	
$\text{ISOP} + \text{O}_3 \rightarrow 0.41\,\text{MACR} + 0.17\,\text{MVK} + 0.86\,\text{HCHO} + 0.03\,\text{MCOOH}$ $+0.3\,\text{CO}_2 + 0.3\,\text{HO}_2 + 0.1\,\text{CH}_3\text{O}_2 + 0.24\,\text{CO} + 0.05\,\text{CH}_3\text{CO}_3$ $+0.14\,\text{OH} + 0.58\,(0.55\,\text{HMHP} + 0.4\,\text{HCHO} + 0.4\,\text{H}_2\text{O}_2$ $+0.05\,\text{HCOOH})$	$1.03(-14)\exp(-1995/T)$	2	N2
$\text{ISOPBO2} + \text{NO} \rightarrow \text{MVK} + \text{HCHO} + \text{HO}_2 + \text{NO}_2$	$\text{KRO2NO} \cdot (1 - Y_5^{\text{Arey}} \cdot 1.35)$	1,3	N3
$\text{ISOPBO2} + \text{NO} \rightarrow \text{ISOPBNO3}$	$\text{KRO2NO} \cdot Y_5^{\text{Arey}} \cdot 1.35$	1,3	N3
$\text{ISOPBO2} + \text{NO}_3 \rightarrow \text{MVK} + \text{HCHO} + \text{HO}_2 + \text{NO}_2$	$2.3(-12)$	1	
$\text{ISOPBO2} + \text{HO}_2 \rightarrow 0.937\,\text{ISOPBOOH} + 0.063\,\text{OH}$ $+0.063\,\text{MVK} + 0.063\,\text{HCHO} + 0.063\,\text{HO}_2$	$2.1(-13)\exp(1300/T)$	1,3,4	
$\text{ISOPBO2} + \text{ISOPBO2} \rightarrow 2\,\text{MVK} + 2\,\text{HCHO} + 2\,\text{HO}_2$	$7.0(-14)$	5	
$\text{ISOPBO2} + \text{ISOPDO2} \rightarrow 0.7\,\text{MVK} + 1.4\,\text{HCHO} + 1.4\,\text{HO}_2$ $+0.3\,\text{ISOPBOH} + 0.7\,\text{MACR} + 0.3\,\text{HCOC5}$	$1.3(-12)$	5	
$\text{ISOPBO2} + \text{CH}_3\text{O}_2 \rightarrow 0.7\,\text{MVK} + 1.7\,\text{HCHO} + 0.7\,\text{HO}_2$ $+0.3\,\text{ISOPBOH}$	$8.0(-13)$	5	
$\text{ISOPBO2} + \text{CH}_3\text{CO}_3 \rightarrow \text{MVK} + \text{HCHO} + \text{HO}_2 + \text{CH}_3\text{O}_2 + \text{CO}_2$	$1.8(-12)\exp(500/T)$	6,7	
$\text{ISOPBO2} \rightarrow 0.25\,\text{HPALD1} + 0.25\,\text{HO}_2 + 0.75\,\text{DIHPMEK}$ $+0.75\,\text{OH} + 0.75\,\text{CO}$	$3.409(+12)\exp(-10698/T)$ $+ 2.89(-15)\exp(414/T) \cdot [\text{NO}]$ $+ 2.26(-16)\exp(1364/T) \cdot [\text{HO}_2]$	8,3	N4

Geosci. Model Dev. Discuss., https://doi.org/10.5194/gmd-2018-316
Manuscript under review for journal Geosci. Model Dev.
Discussion started: 19 December 2018

Geoscientific Model Development Discussions
Open Access
EGU

Reaction	*Rate*	*Ref.*	*Note*
$ISOPBO2 \rightarrow MVK + HCHO + OH$	$1.04(+11)\exp(-9746/T)$	8	
$ISOPBOOH + OH \rightarrow 0.855\,IEPOX + 0.145\,DHHEPOX + OH$	$1.7(-11)\exp(390/T)$	9,3,10	N5
$ISOPBOOH + OH \rightarrow 0.75\,ISOPBO2 + 0.2\,HCOOH + 0.3\,HO_2$ $+0.05\,HCHO + 0.05\,OH + 0.25\,MVK$	$4.6(-12)\exp(200/T)$	9,3	N6
$ISOPDO2 + NO \rightarrow MACR + HCHO + HO_2 + NO_2$	$KRO2NO \cdot (1 - Y_5^{Arey} \cdot 1.23)$	1,3	N3
$ISOPDO2 + NO \rightarrow ISOPDNO3$	$KRO2NO \cdot Y_5^{Arey} \cdot 1.23$	1,3	N3
$ISOPDO2 + NO_3 \rightarrow MACR + HCHO + HO_2 + NO_2$	$2.3(-12)$	1	
$ISOPDO2 + HO_2 \rightarrow 0.937\,ISOPDOOH + 0.063\,OH$ $+0.063\,MACR + 0.063\,HCHO + 0.063\,HO_2$	$2.1(-13)\exp(1300/T)$	1,3	
$ISOPDO2 + ISOPDO2 \rightarrow MACR + HCHO + HO_2$ $+0.5\,HCOC5 + 0.5\,ISOPDOH$	$6.0(-12)$	5	
$ISOPDO2 + CH_3O \rightarrow 0.5\,MACR + 1.25\,HCHO + HO_2$ $+0.25\,ISOPDOH + 0.25\,HCOC5 + 0.25\,CH_3OH$	$2.9(-12)$	5	
$ISOPDO2 + CH_3CO_3 \rightarrow 0.9\,MACR + 0.9\,HCHO + 0.9\,HO_2$ $+0.9\,CH_3O_2 + 0.9\,CO_2 + 0.1\,CH_3COOH + 0.1\,HCOC5$	$2.0(-12)\exp(500/T)$	6,7	
$ISOPDO2 \rightarrow 0.25\,HPALD2 + 0.25\,HO_2 + 0.75\,DIHPCHO$ $+0.75\,OH + 0.75\,CO$	$4.253(+8)\exp(-7254/T)$ $+ 6.29(-19)\exp(4012/T) \cdot [NO]$ $+ 4.90(-20)\exp(4012/T) \cdot [HO_2]$	8,3	N4
$ISOPDO2 \rightarrow MACR + HCHO + OH$	$1.88(+11)\exp(-9752/T)$	8	
$ISOPDOOH + OH \rightarrow 0.855\,IEPOX + 0.145\,DHHEPOX + OH$	$3.0(-11)\exp(390/T)$	9,3,10	N5
$ISOPDOOH + OH \rightarrow 0.6\,ISOPDO2 + 0.32\,HCOOH + 0.48\,HO_2$ $+0.08\,HCHO + 0.08\,OH + 0.4\,MACR$	$4.1(-12)\exp(200/T)$	9,3	N7
$ISOPEO2 + NO \rightarrow MACR + HO_2 + HCHO + NO_2$	$KRO2NO \cdot (1 - Y_5^{Arey} \cdot 1.23)$	1,3	N3
$ISOPEO2 + NO \rightarrow ISOPENO3$	$KRO2NO \cdot Y_5^{Arey} \cdot 1.23$	1,3	N3
$ISOPEO2 + HO_2 \rightarrow ISOPEOOH$	$2.1(-13)\exp(1300/T)$	1,3	
$ISOPEO2 + ISOPBO2 \rightarrow 0.7\,MVK + 1.4\,HCHO + 1.4\,HO_2$ $+0.3\,ISOPBOH + 0.7\,MACR + 0.3\,HCOC5$	$1.2(-12)$	5	
$ISOPEO2 + ISOPDO2 \rightarrow MACR + HCHO + HO_2 + 0.5\,HCOC5$ $+0.5\,ISOPDOH$	$1.1(-11)$	5	
$ISOPEO2 + ISOPEO2 \rightarrow MACR + HCHO + HO_2$ $+0.5\,HCOC5 + 0.5\,ISOPDOH$	$5.0(-12)$	5	
$ISOPEOOH + OH \rightarrow 0.83\,HYAC + 0.83\,GLY + 0.17\,MACR + HO_2$	$1.0(-10)$	1	N8
$ISOPENO3 + OH \rightarrow HYAC + ETHLN + HO_2$	$6.0(-11)$	1,11	N8
$ISOPBNO3 + OH \rightarrow 0.85\,INBO2 + 0.15\,IEPOX + 0.15\,NO_2$	$8.4(-12)\exp(390/T)$	1,3	

Geosci. Model Dev. Discuss., https://doi.org/10.5194/gmd-2018-316
Manuscript under review for journal Geosci. Model Dev.
Discussion started: 19 December 2018

Geoscientific Model Development Discussions
Open Access
EGU

Reaction	*Rate*	*Ref.*	*Note*
$INBO2 + NO \rightarrow HNO_3$	$KRO2NO \cdot Y_5^{Arey} \cdot 1.73$	1	N9
$INBO2 + NO \rightarrow 1.85\,NO_2 + 0.85\,GLYALD + 0.85\,HYAC + 0.15\,MACRNO3 + 0.15\,HO_2 + 0.15\,HCHO$	$KRO2NO \cdot (1 - Y_5^{Arey}) \cdot 1.73$	1,13,3	N10
$INBO2 + NO_3 \rightarrow 1.85\,NO_2 + 0.85\,GLYALD + 0.85\,HYAC + 0.15\,MACRNO3 + 0.85\,HO_2 + 0.15\,HCHO$	$2.3(-12)$	1	N10
$INBO2 + HO_2 \rightarrow HNO_3$	$2.5(-13)\exp(1300/T)$	1,3	N11
$ISOPDNO3 + OH \rightarrow 0.85\,INDO2 + 0.15\,IEPOX + 0.15\,NO_2$	$3.9(-11)$	1,3	
$INDO2 + NO \rightarrow HNO_3$	$KRO2NO \cdot Y_5^{Arey} \cdot 1.73$	1,3	N12
$INDO2 + NO \rightarrow HCHO + HO_2 + MVKNO3 + NO_2$	$KRO2NO \cdot (1 - Y_5^{Arey} \cdot 1.73)$	1,3,11,12	N12
$INDO2 + NO3 \rightarrow HCHO + HO_2 + MVKNO3 + NO_2$	$2.3(-12)$	1	
$INDO2 + HO_2 \rightarrow 0.39\,INDOOH + 0.65\,HCHO + 0.65\,HO_2 + 0.65\,MVKNO3$	$2.5(-13)\exp(1300/T)$	1,3	
$INDOOH + OH \rightarrow 0.39\,INDO2 + 1.22\,HO_2 + 0.61\,CO + 0.61\,MVKNO3 + 0.61\,OH$	$9.2(-12)$	1	N13
$IEPOX + OH \rightarrow 0.19\,ICHE + 0.58\,IEPOXAO2 + 0.23\,IEPOXBO2$	$4.4(-11)\exp(-400/T)$	3	N14
$ICHE + OH \rightarrow 0.28\,OH + 1.28\,CO + 0.28\,HYAC + 0.72\,MVKOOH$	$1.5(-11)$		N15
$ICHE + OH \rightarrow CO + HO_2 + 0.28\,HPDIAL + 0.72\,HPKETAL$	$2.0(-11)$		N16
$IEPOXAO2 \rightarrow DHBO + OH + CO$	$1.0(7)\exp(-5000/T)$	3	N17
$IEPOXAO2 \rightarrow CO + 2.5\,HO_2 + 1.5\,OH + 0.5\,HOBA + 0.5\,HPDIAL$	$1.875(13)\exp(-10000/T)$	3	N18
$IEPOXAO2 + NO \rightarrow NO_2 + HO_2 + 0.8\,MGLY + 0.8\,GLYALD + 0.2\,DHBO + 0.2\,CO$	$KRO2NO$	1,3	
$IEPOXAO2 + HO_2 \rightarrow OH + HO_2 + 0.8\,MGLY + 0.8\,GLYALD + 0.2\,DHBO + 0.2\,CO$	$1.6(-13)\exp(1300/T)$	3	N19
$IEPOXAO2 + HO_2 \rightarrow CO + HO_2 + OH + DHBO$	$0.8(-13)\exp(1300/T)$	3	N20
$IEPOXBO2 \rightarrow MACROH + OH + CO$	$1.0(7)\exp(-5000/T)$	3	N17
$IEPOXBO2 \rightarrow 1.5\,CO + 3\,HO_2 + 0.5\,MGLY + 0.5\,HPKETAL$	$1.875(13)\exp(-10000/T)$	3	N21
$IEPOXBO2 + NO \rightarrow NO_2 + HO_2 + 0.8\,GLY + 0.8\,HYAC + 0.2\,MACROH + 0.2\,CO$	$KRO2NO$	1,3	
$IEPOXBO2 + HO_2\ rightarrow OH + HO_2 + 0.8\,GLY + 0.8\,HYAC + 0.2\,MACROH + 0.2\,CO$	$1.6(-13)\exp(1300/T)$	3	N19
$IEPOXBO2 + HO_2 \rightarrow CO + HO_2 + OH + MACROH$	$0.8(-13)\exp(1300/T)$	3	N22
$HCOC5 + OH \rightarrow C59O2$	$3.81(-11)$	1	
$C59O2 + NO \rightarrow HYAC + GCO3 + NO_2$	$KRO2NO$	1	

Geosci. Model Dev. Discuss., https://doi.org/10.5194/gmd-2018-316
Manuscript under review for journal Geosci. Model Dev.
Discussion started: 19 December 2018

Geoscientific Model Development Discussions
Open Access
EGU

Reaction	*Rate*	*Ref.*	*Note*
$C59O2 + NO_3 \rightarrow HYAC + GCO3 + NO_2$	$2.3(-12)$	1	
$C59O2 + HO_2 \rightarrow HYAC + GCO3 + OH$	$2.4(-13)\exp(1300/T)$	1,3	N23
$C59O2 + CH_3O_2 \rightarrow HYAC + GCO3 + HCHO + HO_2$	$9.2(-14)$	1	
$C59O2 + CH_3CO_3 \rightarrow HYAC + GCO3 + CO_2 + CH_3O_2$	$1.8(-12)\exp(500/T)$	6,7	
$ISOPBOH + OH \rightarrow DHBO + CO$	$3.85(-11)$	10	N24
$ISOPDOH + OH \rightarrow 0.9\,DHBO + 0.9\,CO + 0.1\,HCOC5 + 0.1\,HO_2$	$7.38(-11)$	10	N24
$HPALD1 + OH \rightarrow 0.45\,OH + 1.35\,CO_2 + 0.55\,HCHO + 0.65\,CH_3CO_3$ $+0.2\,MMAL + 0.15\,MGLY + 0.15\,CO + 0.1\,GLY$	$1.0(-11)$	5,3	N25
$HPALD1 + OH \rightarrow MVK + OH + 0.5\,CO + 0.5\,CO_2$	$0.5(-11)$	5,3	N25
$HPALD1 + OH \rightarrow MVK + OH + CO_2$	$1.5(-11)$	5,3	N25
$HPALD1 + OH \rightarrow MVKOOH + OH + CO$	$1.4(-11)$	5,3	N25
$HPALD1 + OH \rightarrow ICHE$	$0.8(-11)$	5,3	N25
$HPALD1 + O_3 \rightarrow 0.35\,MGLY + 0.27\,GLY + 1.19\,OH + 0.65\,CO$ $+0.65\,CH_3CO_3 + 0.08\,H_2O_2 + 0.73\,HPAC$	$2.4(-17)$	1	
$HPALD2 + OH \rightarrow 0.45\,OH + 1.35\,CO_2 + 0.55\,HCHO + 0.65\,CH_3CO_3$ $+0.2\,MMAL + 0.15\,MGLY + 0.15\,CO + 0.1\,GLY$	$1.0(-11)$	5,3	N26
$HPALD2 + OH \rightarrow MACR + OH + 0.5\,CO + 0.5\,CO_2$	$0.5(-11)$	5,3	N25
$HPALD2 + OH \rightarrow MACR + OH + CO_2$	$1.5(-11)$	5,3	N25
$HPALD2 + OH \rightarrow OH + 2\,CO + 2\,HO_2 + HPACET$	$0.8(-11)$	5,3	N26
$HPALD2 + OH \rightarrow ICHE$	$1.4(-11)$	5,3	N26
$HPALD2 + O_3 \rightarrow 0.27\,HPACET + 1.7\,OH + 0.24\,HO_2$ $+0.48\,CO + 0.73\,MGLY + 0.74\,GLY + 0.02\,OCHCOOH$	$2.4(-17)$	1	
$MMAL + OH \rightarrow MGLY + HO_2 + 2\,CO_2$	$1.5(-12)$	1	N27
$DIHPMEK + OH \rightarrow 2\,OH + CH_3CO_3 + CO + HCHO$	$1.63(-11)$	1	N28
$DIHPMEK + OH \rightarrow OH + HPKETAL$	$1.28(-11)$	1	
$HPKETAL + OH \rightarrow 0.6\,OH + CO + 0.6\,MGLY$ $+0.4\,CH_3CO_3 + 0.4\,HO_2$	$3.0(-11)$		N29
$DIHPCHO + OH \rightarrow OH + CO + HPACET$	$2.6(-11)$	1	
$DIHPCHO + OH \rightarrow OH + HPDIAL$	$1.2(-11)$	1	
$HPDIAL + OH \rightarrow OH + CO + MGLY$	$3.0(-11)$		N30
$NISOPO2 + NO \rightarrow 1.82\,NO_2 + 0.42\,MVK + 0.04\,MACR$ $+1.54\,HCHO + 0.18\,NC4CHO + 0.9\,HO_2 + 0.72\,CO$	KRO2NO	1,15,3	N31
$NISOPO2 + NO_3 \rightarrow 1.82\,NO_2 + 0.42\,MVK + 0.04\,MACR$ $+1.54\,HCHO + 0.18\,NC4CHO + 0.9\,HO_2 + 0.72\,CO$	$2.3(-12)$	1,15,3	

Geosci. Model Dev. Discuss., https://doi.org/10.5194/gmd-2018-316
Manuscript under review for journal Geosci. Model Dev.
Discussion started: 19 December 2018

Geoscientific Model Development Discussions
Open Access
EGU

Reaction	*Rate*	*Ref.*	*Note*
NISOPO2 + HO_2 → 0.535 NISOPOOHD + 0.22 NISOPOOHB + 0.245 OH + 0.245 NO_2 + 0.225 MVK + 0.02 MACR + 0.245 HCHO	$2.5(-13)\exp(1300/T)$	1,15,3	
NISOPO2 + NISOPO2 → 0.17 MVK + 0.11 MACR + 0.7 HCHO + 0.42 NO_2 + 0.78 NC4CHO + 0.36 HO_2 + 0.28 CO + 0.7 ISOPCNO3 + 0.1 ISOPDNO3	$3.5(-12)$	15,3	N32
NISOPO2 + CH_3O_2 → 0.08 MVK + 0.06 MACR + 0.95 HCHO + 0.21 NO_2 + 0.39 NC4CHO + 0.38 HO_2 + 0.14 CO + 0.4 CH_3OH + 0.35 ISOPCNO3 + 0.05 ISOPDNO3	$2.2(-12)$	15,3	N32
NISOPO2 + CH_3CO_3 → 0.38 MVK + 0.05 MACR + 1.39 HCHO + 0.75 NO_2 + 0.25 NC4CHO + 0.81 HO_2 + 0.64 CO + 0.9 CH_3O_2 + 0.9 CO_2 + 0.1 CH_3COOH	$2.0(-12)\exp(500/T)$	15,3	N32
NISOPO2 + ISOPBO2 → 0.71 MVK + 0.08 MACR + 1.33 HCHO + 0.47 NO_2 + 0.53 NC4CHO + 0.95 HO_2 + 0.36 CO + 0.5 ISOPBOH	$1.0(-12)$	15,3	N32
NISOPO2 + ISOPDO2 → 0.08 MVK + 0.26 MACR + 0.55 HCHO + 0.21 NO_2 + 0.39 NC4CHO + 0.38 HO_2 + 0.14 CO + 0.4 ISOPDOH + 0.35 ISOPCNO3 + 0.05 ISOPDNO3 + 0.4 HCOC5	$9.2(-12)$	15,3	N32
NISOPOOHD + OH → NISOPO2	$3.4(-12)\exp(200/T)$	3	N33
NISOPOOHD + OH → OH + NC4CHO	$7.5(-12)\exp(20/T)$	3	N33
NISOPOOHD + OH → 0.19 CO + 0.95 HO_2 + 0.43 OH + 0.69 NOA + 0.19 HCHO + 0.5 HPAC + 0.07 HPACET + 0.07 ETHLN + 0.24 IHNE	$2.37(-11)\exp(390/T)$	3	N34
NISOPOOHD + O_3 → 0.2 OH + 0.87 NOA + 0.13 HPACET + 0.84 HPAC + 0.16 ETHLN	$1.3(-17)$	15	N35
NISOPOOHB + OH → NISOPO2	$3.4(-12)\exp(200/T)$	3	N36
NISOPOOHB + OH → 0.23 GLYALD + 0.47 NOA + 0.76 OH + 0.09 CO + 0.33 HO_2 + 0.09 HCHO + 0.15 HPAC + 0.04 HYAC + 0.04 ETHLN + 0.51 IHNE	$8.72(-12)\exp(390/T)$	3	N37
IHNE + OH → 0.23 HMVK + 0.03 HMAC + 0.82 HCHO + 0.8 NO_2 + 0.8 CO + 0.17 NOA + 0.45 MGLY + 0.72 HO_2 + 0.38 OH + 0.03 MVKNO3 + 0.09 HYAC + 0.09 CO_2	$3.22(-11)\exp(-400/T)$	3	N38
NC4CHO + OH → 0.45 CO_2 + 1.08 CO + 0.85 HO_2 + 0.58 NOA + 0.5 OH + 0.12 HCHO + 0.12 MGLY + 0.17 NO_2 + 0.11 MVKNO3 + 0.05 ICHE + 0.14 CH_3CO_3 + 0.14 ETHLN	$4.1(-11)$	15,3	N39
NC4CHO + NO_3 → HNO_3 + CO_2 + 0.75 NOA + 0.75 CO + 0.75 HO_2	$6.0(-12)\exp(-1860/T)$	1,3	N39

Geosci. Model Dev. Discuss., https://doi.org/10.5194/gmd-2018-316
Manuscript under review for journal Geosci. Model Dev.
Discussion started: 19 December 2018

Geoscientific Model Development Discussions
Open Access
EGU

Reaction	*Rate*	*Ref.*	*Note*
$+0.25\,CH_3CO_3 + 0.25\,ETHLN$			
$NC4CHO + O_3 \rightarrow 0.555\,NOA + 0.89\,CO + 0.89\,OH + 0.445\,MGLY$ $+0.445\,HO_2 + 0.075\,H_2O_2 + 0.445\,NO_2 + 0.52\,GLY$ $+0.035\,OCHCOOH$	$4.4(-18)$	1	
$ISOPCNO3 + O_3 \rightarrow 0.555\,NOA + 0.52\,GLYALD + 0.07\,C_2H_5COOH$ $+0.075\,H_2O_2 + 0.89\,OH + 0.445\,NO_2 + 0.445\,MGLY$ $+0.445\,HO_2 + 0.445\,CO + 0.445\,HCHO$	$2.8(-17)$	1,11	
$ISOPCNO3 + OH \rightarrow 1.2\,OH + 1.1\,CO + 0.9\,HO_2 + 0.5\,NOA$ $+0.1\,CH_3CO_3 + 0.1\,ETHLN + 0.4\,NC4CHO$	$7.5(-12)\exp(20/T)$	3	N40
$ISOPCNO3 + OH \rightarrow INCO2$	$2.2(-11)\exp(390/T)$	3	N41
$INCO2 \rightarrow HO_2 + 2\,CO + 3\,HO2 + OH + NOA$	$1.14(13)\exp(-10000/T)$	3	N42
$INCO2 + NO \rightarrow INCNO3$	$KRO2NO \cdot Y_5^{Arey} \cdot 1.4$	1	
$INCO2 + NO \rightarrow NO_2 + HO_2 + 0.79\,NOA + 0.79\,GLYALD + 0.07\,HCHO$ $+0.05\,MACRNO3 + 0.14\,HYAC + 0.14\,ETHLN + 0.02\,MVKNO3$	$KRO2NO \cdot (1 - Y_5^{Arey} \cdot 1.4)$	3	N41
$INCO2 + NO_3 \rightarrow NO_2 + HO_2 + 0.79\,NOA + 0.79\,GLYALD + 0.07\,HCHO$ $+0.05\,MACRNO3 + 0.14\,HYAC + 0.14\,ETHLN + 0.02\,MVKNO3$	$2.3(-12)$	1	N41
$INCO2 + HO_2 \rightarrow 0.32\,INCCO + 0.11\,INCO2 + 0.46\,NOA + 0.46\,GLYALD$ $+0.03MACRNO3 + 0.04\,HCHO + 0.57\,HO_2 + 0.46\,OH + 0.07\,HYAC$ $+0.07\,ETHLN + 0.01\,MVKNO3$	$2.5(-13)\exp(1300/T)$	3	N43
$INCCO + OH \rightarrow HCHO + 3\,HO_2 + CH_3CO_3 + 2\,CO + NO_2$	$3.3(-12)$	1	N44
$INCNO3 + OH \rightarrow 0.445\,INCCO + 0.414\,GLY + 0.414\,HO_2$ $+0.555\,NOA + 0.141\,GLYALD + NO_2$	$1.98(-12)$	1	N45
C_4 compounds			
$MACR + OH \rightarrow CO + 0.036\,HPACET + 0.036\,HO_2 + 0.964\,HYAC$ $+0.964\,OH$	$4.4(-12)\exp(380/T)$	3	N46
$MACR + OH \rightarrow MCO3$	$2.7(-12)\exp(470/T)$	3	
$MACR + O_3 \rightarrow 0.9\,MGLY + 0.12\,HCHO + 0.1\,CO + 0.1\,OH$ $+0.1\,CH_3CO_3 + 0.88\,(0.55\,HMHP + 0.4\,HCHO + 0.4\,H_2O_2$ $+0.05\,HCOOH)$	$1.4(-15)\exp(-2100/T)$	1	N2
$MACR + NO_3 \rightarrow MCO3 + HNO_3$	$3.4(-15)$	1	
$MCO3 + NO \rightarrow CO_2 + 0.65\,CH_3O_2 + 0.65\,CO + 0.35\,CH_3CO_3$ $+HCHO + NO_2$	$8.70(-12)\exp(290/T)$	1	
$MCO3 + NO_3 \rightarrow CO_2 + 0.65\,CH_3O_2 + 0.65\,CO + 0.35\,CH_3CO_3$ $+HCHO + NO_2$	$4.0(-12)$	1	

Geosci. Model Dev. Discuss., https://doi.org/10.5194/gmd-2018-316
Manuscript under review for journal Geosci. Model Dev.
Discussion started: 19 December 2018

Reaction	*Rate*	*Ref.*	*Note*
$MCO3 + HO_2 \rightarrow MCO3H$	$2.43(-13)\exp(980/T)$	1,18	
$MCO3 + HO_2 \rightarrow MCOOH + O_3$	$1.25(-13)\exp(980/T)$	1,18	
$MCO3 + HO_2 \rightarrow CO_2 + 0.65\,CH_3O_2 + 0.65\,CO + 0.35\,CH_3CO_3$ $+HCHO + OH$	$4.15(-13)\exp(980/T)$	1,18	
$MCO3 + CH_3O_2 \rightarrow 0.585\,CH_3O_2 + 0.585\,CO + 0.315\,CH_3CO_3$ $+1.9\,HCHO + 0.9\,HO_2 + 0.9\,CO_2 + 0.1\,MCOOH$	$2.0(-12)\exp(500/T)$	1,6,7	
$MCO3 + CH_3CO_3 \rightarrow 1.65\,CH_3O_2 + 0.65\,CO + 0.35\,CH_3CO_3$ $+HCHO + 2\,CO_2$	$5.4(-12)\exp(500/T)$	1,6,7	
$MCO3 + ISOPBO2 \rightarrow 0.65\,CH_3O_2 + 0.65\,CO + 0.35\,CH_3CO_3$ $+2\,HCHO + MVK + HO_2 + CO_2$	$1.8(-12)\exp(500/T)$	1,6,7	
$MCO3 + ISOPDO2 \rightarrow 0.585\,CH_3O_2 + 0.585\,CO + 0.315\,CH_3CO_3$ $+1.8\,HCHO + 0.9\,MACR + 0.9\,HO_2 + 0.9\,CO_2$ $+0.1\,MCOOH + 0.1\,HCOC5$	$2.0(-12)\exp(500/T)$	1,6,7	
$MCO3 + NO_2 \rightarrow MPAN$	$k_0 = 9.7(-29)(300/T)^{5.6}$ $k_\infty = 9.3(-12)(300/T)^{1.5}$ $F_c = 0.6$	19	
$MPAN \rightarrow MCO3 + NO_2$	$K_{eq} = 9.0(-29)\exp(14000/T)$	19	
$MPAN + OH \rightarrow HYAC + CO + NO_3$	$7.5(-12)$	20	
$MPAN + OH \rightarrow HMML + NO_3$	$2.25(-11)$	20	
$MPAN + O_3 \rightarrow HCHO + CH_3CO_3 + NO_3 + CO_2$	$8.2(-18)$	1	
$MCO3H + OH \rightarrow MCO3$	$3.6(-12)$	1	
$MCO3H + OH \rightarrow 0.83\,HYAC + 0.83\,CO + 0.17\,HMML + OH$	$1.3(-11)$	1	
$MCOOH + OH \rightarrow CO_2 + 0.65\,CH_3O_2 + 0.65\,CO$ $+0.35\,CH_3CO_3 + HCHO$	$1.51(-11)$	1	
$HMML + OH \rightarrow CO_2 + 0.7\,MGLY + 0.7\,OH$ $+0.3\,CH_3CO_3 + 0.3\,HCOOH$	$4.33(-12)$	1	
$MVK + OH \rightarrow MVKO2$	$2.6(-12)\exp(610/T)$	1	
$MVK + O_3 \rightarrow 0.28\,CH_3CO_3 + 0.545\,MGLY + 0.1\,HO_2$ $+0.18\,CO + 0.18\,OH + 0.6\,HCHO + 0.1\,CH_3CHO + 0.1\,CO_2$ $+0.045\,H_2O_2 + 0.075\,PYRA$ $+0.5\,(0.55\,HMHP + 0.4\,HCHO + 0.4\,H_2O_2 + 0.05\,HCOOH)$	$8.5(-16)\exp(-1520/T)$	1	N2
$MVKO2 + N \rightarrow 0.28\,MGLY + 0.28\,HCHO + 0.28\,HO_2$ $+0.72\,GLYALD + 0.72\,CH_3CO_3 + NO_2$	$KRO2NO \cdot (1 - Y_4^{Arey} \cdot 0.61)$	1,21,22	N47
$MVKO2 + NO \rightarrow MVKNO3$	$KRO2NO \cdot Y_4^{Arey} \cdot 0.61$	22	

Geosci. Model Dev. Discuss., https://doi.org/10.5194/gmd-2018-316
Manuscript under review for journal Geosci. Model Dev.
Discussion started: 19 December 2018

Geoscientific Model Development Discussions
Open Access
EGU

Reaction	*Rate*	*Ref.*	*Note*
$MVKO2 + NO_3 \rightarrow 0.28\,MGLY + 0.28\,HCHO + 0.28\,HO_2$ $+0.72\,GLYALD + 0.72\,CH_3CO_3 + NO_2$	$2.3(-12)$	1	N47
$MVKO2 + HO_2 \rightarrow 0.35\,GLYALD + 0.35\,CH_3CO_3 + 0.52\,OH$ $+0.174\,HO_2 + 0.48\,MVKOOH + 0.13\,BIACETOH$ $+0.04\,MGLY + 0.04\,HCHO$	$2.1(-13)\exp(1300/T)$	22,3	N47
$MVKO2 + CH_3O_2 \rightarrow 0.14\,MGLY + 0.36\,GLYALD$ $+0.36\,CH_3CO_3 + 0.89\,HCHO + 0.64\,HO_2 + 0.25\,DHBO$ $+0.18\,BIACETOH + 0.07\,HOBA + 0.25\,CH_3OH$	$1.16(-12)$	1	N47
$MVKO2 + CH_3CO_3 \rightarrow 0.25\,MGLY + 0.65\,GLYALD$ $+0.65\,CH_3CO_3 + 0.25\,HCHO + 0.25\,HO_2 + 0.9\,CH_3O_2$ $+0.9\,CO_2 + 0.1\,CH_3COOH + 0.1\,DHBO$	$2.0(-12)\exp(500/T)$	1,6,7	
$MVKOOH + OH \rightarrow 0.55\,BIACETOH + 0.55\,OH + 0.45\,HOBA$	$4.5(-11)$	1	N48
$MACRNO3 + OH \rightarrow 0.5\,HYAC + 0.5\,MGLY + 0.5\,HO_2 + 0.5\,CO$ $+0.5\,CO_2 + NO_2$	$3.0(-12)$	1	N49
$MVKNO3 + OH \rightarrow 0.5\,BIACETOH + 0.4\,GLY + 0.4\,CH_3CO_3$ $+0.1\,MGLY + 0.1\,CO_2 + 0.5\,HO_2 + NO_2$	$1.76(-12)$	1	N50
$MVKNO3 + OH \rightarrow HOBA + NO_2$	$0.44(-12)$	1	N50
$HOBA + OH \rightarrow 0.84\,MGLY + HO_2 + 0.16\,CH_3CO_3 + 0.32\,CO$	$2.45(-11)$	1,14	N51
$HOBA + NO_3 \rightarrow HNO_3 + MGLY + HO_2$	$5.6(-12)\exp(-1860/T)$	1	
$DHBO + OH \rightarrow 0.61\,BIACETOH + 0.39\,HOBA$	$8.7(-12)\exp(70/T)$	14	
$MACROH + OH \rightarrow HO_2 + 0.84\,HYAC + 0.84\,OH + 0.84\,CO$ $-0.16\,OH + 0.16\,MGLY + 0.16\,HO_2 + 0.16\,CO_2$	$2.4(-11)\exp(70/T)$	3	N52
$BIACETOH + OH \rightarrow CH_3CO_3 + 2\,CO + HO_2$	$2.69(-12)$	14	
$HMVK + OH \rightarrow HCOOH + OH + MGLY$	$6.0(-11)$		N53
$HMVK + OH \rightarrow HO2 + HOBA$	$2.4(-11)$		N53
$HMAC + OH \rightarrow 0.5\,HCOOH + 0.5\,OH + 0.5\,MGLY$ $+0.5\,CO + 0.5\,OH + 0.5\,DHA$	$3.0(-11)$		N54
$HMAC + OH \rightarrow 0.89\,CO + 1.34\,OH + 0.78\,CH_3CO_3$ $+0.89\,CO_2 + 0.44\,HO_2 + 0.22\,MGLY$	$2.7(-11)$		N55
C_3 compounds			
$CH_3COCH_3 + OH \rightarrow ACETO2$	$1.33(-13) + 3.82(-11)\exp(-2000/T)$	1	
$HPACET + OH \rightarrow MGLY + OH$	$8.39(-12)$	1	
$HPACET + OH \rightarrow ACETO2$	$1.9(-12)\exp(190/T)$	1	
$ACETO2 + NO \rightarrow NO_2 + HCHO + CH_3CO_3$	$KRO2NO \cdot (1 - Y_3^{Arey} \cdot 0.4)$	1	

Geosci. Model Dev. Discuss., https://doi.org/10.5194/gmd-2018-316
Manuscript under review for journal Geosci. Model Dev.
Discussion started: 19 December 2018

Geoscientific Model Development Discussions
Open Access
EGU

Reaction	*Rate*	*Ref.*	*Note*
$ACETO2 + NO \rightarrow NOA$	$KRO2NO \cdot Y_3^{Arey} \cdot 0.4$	1	N56
$ACETO2 + NO_3 \rightarrow NO_2 + HCHO + CH_3CO_3$	$2.3(-12)$	1	
$ACETO2 + HO_2 \rightarrow 0.85\,HPACET + 0.15\,HCHO + 0.15\,CH_3CO_3$	$8.6(-13)\exp(700/T)$	1,19	
$ACETO2 + CH_3O_2 \rightarrow 0.3\,CH_3CO_3 + 0.8\,HCHO + 0.3\,HO_2 + 0.2\,HYAC + 0.5\,MGLY + 0.5\,CH_3OH$	$3.8(-12)$	7	
$ACETO2 + CH_3CO_3 \rightarrow CH_3COOH + MGLY$	$2.5(-12)$	7	
$ACETO2 + CH_3CO_3 \rightarrow CH_3O_2 + CO_2 + CH_3CO_3 + HCHO$	$2.5(-12)$	7	
$ACETO2 + ACETO2 \rightarrow HYAC + MGLY$	$3.0(-12)$	7	
$ACETO2 + ACETO2 \rightarrow 2\,CH_3CO_3 + 2\,HCHO$	$5.0(-12)$	7	
$HYAC + OH \rightarrow MGLY + HO_2$	$1.46(-13)\exp(1100/T)\cdot(T/300)^{2.6}$	1,23	
$MGLY + OH \rightarrow 0.6\,CH_3CO_3 + 0.4\,CH_3O_2 + 1.4\,CO + H_2O$	$1.9(-12)\exp(575/T)$	1,24	
$MGLY + NO_3 \rightarrow HNO_3 + CO + CH_3CO_3$	$3.36(-12)\exp(-1860/T)$	1	
$NOA + OH \rightarrow MGLY + NO_2$	$6.7(-13)$	1	
$MVA + OH \rightarrow 0.5\,CH_3COOH + 0.5\,HCHO + 0.5\,OH + 0.5\,HYAC + 0.5\,HO_2$	$9.0(-11)$		N57
$DHA + OH \rightarrow 1.39\,HO_2 + 0.48\,CH3CHO + 0.87\,CO_2 + 0.44\,CH_3CO_3 + 0.08\,CH_3COOH + 0.13\,CO + 0.05\,OH$	$8.0(-12)\exp(70/T)$	3,19	N58
C_2 compounds			
$GLYALD + OH \rightarrow 0.78\,GCO3 + 0.22\,GLY + 0.22\,HO_2$	$1.0(-11)$	1,25	
$GCO3 + NO \rightarrow NO_2 + HO_2 + HCHO + CO_2$	$6.7(-12)\exp(340/T)$	1	
$GCO3 + HO_2 \rightarrow 0.21\,GCO3H + 0.04\,GCOOH + 0.04\,O_3 + 0.75\,HO_2 + 0.75\,HCHO + 0.75\,OH + 0.75\,CO_2$	$7.84(-13)\exp(980/T)$	1,17,26	
$GCO3 + CH_3O_2 \rightarrow 1.9\,HCHO + 1.8\,HO_2 + 0.1\,GCOOH + 0.9\,CO_2$	$1.8(-12)\exp(500/T)$	1,6,7	
$GCO3 + CH_3CO_3 \rightarrow CH_3O_2 + HO_2 + HCHO + 2\,CO_2$	$5.4(-12)\exp(500/T)$	1,6,7	
$GCO3 + NO_2 \rightarrow GPAN$	$k_0 = 9.7(-29)(300/T)^{5.6}$ $k_\infty = 9.3(-12)(300/T)^{1.5}$ $F_c = 0.6$	1,19	
$GPAN \rightarrow GCO3 + NO_2$	$K_{eq} = 9.0(-29)\exp(14000/T)$	1,19	
$GPAN + OH \rightarrow HCHO + CO + NO_2$	$1.12(-12)$	1	
$GCO3H + OH \rightarrow GCO3$	$6.19(-12)$	1	
$GLY + OH \rightarrow 0.72\,HO_2 + 0.28\,OH + 1.55\,CO + 0.45\,CO_2$	$3.1(-12)\exp(340/T)$	1	N59
$GLY + NO_3 \rightarrow HNO_3 + 0.72\,HO_2 + 0.28\,OH + 1.55\,CO + 0.45\,CO_2$	$1.4(-12\exp(-1860/T)$	1	N59
$HPAC + OH \rightarrow GLY + OH$	$1.0(-11)$	1	N60

Geosci. Model Dev. Discuss., https://doi.org/10.5194/gmd-2018-316
Manuscript under review for journal Geosci. Model Dev.
Discussion started: 19 December 2018

Reaction	*Rate*	*Ref.*	*Note*
$HPAC + OH \rightarrow 0.25\,CO + HCHO + OH + 0.75\,CO_2$	$1.8(-11)$	1	N60
$HPAC + OH \rightarrow OCHCH_2O_2$	$1.90(-12)\exp(190/T)$	1	
$C_2H_5OH + OH \rightarrow 0.95\,CH_3CHO + 0.95\,HO_2 + 0.05\,HOCH_2CH_2O_2$	$3.0(-12)\exp(20/T)$	1	
$CH_3CHO + OH \rightarrow 0.95\,CH_3CO_3 + 0.05\,OCHCH_2O_2$	$4.7(-12)\exp(345/T)$	1	
$CH_3CHO + NO_3 \rightarrow CH_3CO_3 + HNO_3$	$1.4(-12)\exp(-1860/T)$	1	
$OCHCH_2O_2 + NO \rightarrow NO_2 + HCHO + CO + HO_2$	KRO2NO	1	
$OCHCH_2O_2 + NO_3 \rightarrow NO_2 + HCHO + CO + HO_2$	$2.3(-12)$	1	
$OCHCH_2O_2 + HO_2 \rightarrow HPAC$	$1.4(-13)\exp(1300/T)$	1,3	
$OCHCH_2O_2 + CH_3O_2 \rightarrow 1.25\,HCHO + 0.5\,CO + HO_2$ $+0.25\,GLY + 0.25\,CH_3OH + 0.25\,GLYALD$	$2.0(-12)$	1,5	
$CH_3CO_3 + NO \rightarrow NO_2 + CH_3O_2 + CO_2$	$7.5(-12)\exp(290/T)$	1	
$CH_3CO_3 + NO_3 \rightarrow NO_2 + CH_3O_2 + CO_2$	$4.0(-12)$	1	
$CH_3CO_3 + HO_2 \rightarrow 0.31\,PAA + 0.16\,CH_3COOH + 0.16\,O_3$ $+0.53\,CH_3O_2 + 0.53\,OH + 0.53\,CO_2$	$7.84(-13)\exp(980/T)$	1,18	
$CH_3CO_3 + CH_3O_2 \rightarrow HCHO + 0.9\,HO_2 + 0.9\,CH_3O_2$ $+0.9\,CO_2 + 0.1\,CH_3COOH$	$2.0(-12)\exp(500/T)$	6,7	
$CH_3CO_3 + CH_3CO_3 \rightarrow 2\,CH_3O_2 + 2\,CO_2$	$2.9(-12)\exp(500/T)$	6,7	
$CH_3CO_3 + NO_2 \rightarrow PAN$	$k_0 = 9.7(-29)(300/T)^{5.6}$ $k_\infty = 9.3(-12)(300/T)^{1.5}$ $F_c = 0.6$	19	
$PAN \rightarrow CH_3CO_3 + NO_2$	$K_{eq} = 9.0(-29)\exp(14000/T)$	19	
$PAA + OH \rightarrow CH_3CO_3$	$3.7(-12)$	1	
$CH_3COOH + OH \rightarrow CH_3O_2 + CO_2$	$3.15(-14)\exp(920/T)$	1,19	
$ETHLN + OH \rightarrow HCHO + NO_2 + CO_2$	$2.0(-12)$	1	N61
$VA + OH \rightarrow 0.64\,HCOOH + 0.64\,HCHO + 0.64\,OH$ $+0.36\,GLYALD + 0.36\,HO_2$	$6.8(-11)$	27	N62
C_1 compounds			
$CH_3O_2 + NO \rightarrow NO_2 + HCHO + HO_2$	$2.8(-12)\exp(300/T)$	19	
$CH_3O_2 + NO \rightarrow CH_3ONO_2$	$2.8(-12)\exp(300/T) \cdot Y_1^{Arey} \cdot 0.018$	19	N63
$CH_3O_2 + NO_3 \rightarrow NO_2 + HCHO + HO_2$	$1.2(-12)$	1	
$CH_3O_2 + HO_2 \rightarrow 0.9\,CH_3OOH + 0.1\,HCHO$	$4.1(-13)\exp(750/T)$	19	
$CH_3O_2 + CH_3O_2 \rightarrow 2\,HCHO + 2\,HO_2$	$9.5(-14)\exp(390/T)$ $/(1 + 0.04\exp(1130/T))$	19	
$CH_3O_2 + CH_3O_2 \rightarrow HCHO + CH_3OH$	$9.5(-14)\exp(390/T)$	19	

Geosci. Model Dev. Discuss., https://doi.org/10.5194/gmd-2018-316
Manuscript under review for journal Geosci. Model Dev.
Discussion started: 19 December 2018

Geoscientific Model Development Discussions

Reaction	*Rate*	*Ref.*	*Note*
	$/(1+26.2\exp(-1130/T))$		
$CH_3O_2 + O_3 \rightarrow HCHO + HO_2$	$2.9(-16)\exp(-1000/T)$	19	
$CH_3O_2 + OH \rightarrow 0.92HCHO + 1.84\,HO_2 + 0.08\,CH_3OH$	$1.6(-10)\cdot(1-f_{stab})$	28-30	N64
$CH_3O_2 + OH \rightarrow CH_3OOOH$	$1.6(-10)\cdot f_{stab}$	30	N64
$CH_3OOOH + OH \rightarrow HCHO + HO_2$	$2.2(-11)$	30	
$CH_3OOOH \rightarrow 0.2\,CH_3OH + 0.8\,HCHO + 1.6\,HO_2$	$1.1(14)(T/300)^{3.5}\exp(-12130/T)$	30	
$CH_3OOOH + (H_2O)_2 \rightarrow CH_3OH$	$3.0(-15)\exp(-2500/T)$	30	N65
$CH_3OOH + OH \rightarrow 0.3\,HCHO + 0.3\,OH + 0.7\,CH_3O_2$	$3.8(-12)\exp(200/T)$	19	
$CH_3ONO_2 + OH \rightarrow HCHO + NO_2$	$8.0(-13)\exp(-1000/T)$	19	
$HMHP + OH \rightarrow 0.45\,HCOOH + 0.45\,OH$ $+0.55\,HCHO + 0.55\,HO_2$	$1.3(-12)\exp(500/T)$	3,31	N66
$CH_3OH + OH \rightarrow HCHO + HO_2$	$2.9(-12)\exp(-345/T)$	19	N67
$HCHO + OH \rightarrow CO + HO_2$	$55(-12)\exp(125/T)$	19	
$HCHO + NO_3 \rightarrow CO + HO_2 + HNO_3$	$5.8(-16)$	19	
$HCOOH + OH \rightarrow CO_2 + HO_2$	$4.5(-13)$	1	
oxidation of monoterpenes			
$APIN + OH \rightarrow APINOHO2 + 0.1\,HCOOH + 1.3\,HCHO$ $+CH_3COCH_3 + 0.2\,GLY + 0.05\,MGLY$	$1.2(-11)\exp(440/T)$	1	N68
$APIN + O_3 \rightarrow APINO3O2 + 0.15\,OH + 0.1\,HCOOH$ $+1.3\,HCHO + 0.06\,HMHP + CH_3COCH_3$ $+0.2\,GLY + 0.05\,MGLY$	$8.05(-16)\exp(-640/T)$	1	N68
$APIN + NO_3 \rightarrow 0.74\,NO_2 + 0.26\,APINONO2$ $+1.3\,HCHO + CH_3COCH_3 + 0.2\,GLY + 0.05\,MGLY$	$1.2(-12)\exp(490/T)$	1	N68
$APINOHO2 + NO \rightarrow 0.74\,NO_2 + 0.26\,APINONO2$	KRO2NO	1	N69
$APINOHO2 + NO_3 \rightarrow NO_2$	$2.3(-12)$	1	
$APINOHO2 + HO_2 \rightarrow$ products	$2.6(-13)\exp(1300/T)$	1	
$APINO3O2 + NO \rightarrow 0.74\,NO_2 + 0.26\,APINONO2$	KRO2NO	1	N69
$APINO3O2 + NO_3 \rightarrow NO_2$	$2.3(-12)$	1	
$APINO3O2 + HO_2 \rightarrow$ products	$2.6(-13)\exp(1300/T)$	1	
$APINONO2 + OH \rightarrow NO_2$	$4.5(-12)$	1	
MBO oxidation			
$MBO + OH \rightarrow MBOO2$	$8.1(-12)\exp(610/T)$	1	
$MBO + O_3 \rightarrow 0.308\,HCHO + 0.992\,CH_3COCH_3 + 1.31\,HO_2$ $+0.01\,CH_3CHO + 0.89\,CO_2 + 0.168\,HMHP + 0.64\,CO$	$1.0(-17)$	1	N70

Geosci. Model Dev. Discuss., https://doi.org/10.5194/gmd-2018-316
Manuscript under review for journal Geosci. Model Dev.
Discussion started: 19 December 2018

Geoscientific Model Development Discussions

Reaction	*Rate*	*Ref.*	*Note*
$\mathrm{MBOO2 + NO \rightarrow MBONO3}$	$\mathrm{KRO2NO} \cdot Y_5^{\mathrm{Arey}} \cdot 0.96$	1,32	N71
$\mathrm{MBOO2 + NO \rightarrow 0.67\,GLYALD + CH_3COCH_3 + HO_2}$ $\mathrm{+0.33\,HCHO + 0.33\,CO_2 + NO_2}$	$\mathrm{KRO2NO} \cdot (1 - Y_5^{\mathrm{Arey}} \cdot 0.96)$	1	N71
$\mathrm{MBOO2 + NO_3 \rightarrow 0.67\,GLYALD + CH_3COCH_3 + HO_2}$ $\mathrm{+0.33\,HCHO + 0.33\,CO_2 + NO_2}$	$2.3(-12)$	1	N71
$\mathrm{MBOO2 + HO_2 \rightarrow 0.67\,CO + CH_3COCH_3 + 2\,HO_2 + 1.33\,CO_2}$	$2.3(-13)\exp(1300/T)$	1,3	N72
$\mathrm{MBONO3 + OH \rightarrow NO_2 + 0.67\,CO + 0.33\,CO_2}$ $\mathrm{+CH_3COCH_3 + 2\,HO_2}$	$2.0(-12)$	1	N73

2.8 Notes to Table 2

N1. Rate equal to 90% of evaluation (Burkholder et al., 2015) to account for isoprene–OH segregation (Pugh et al., 2011). See text for main products. The minor addition channels (7%) include a hydroxyperoxy radical (ISOPEO2) as well as unsaturated carbonyls along with $\mathrm{HO_2}$. The unsaturated carbonyls are replaced by their major further oxidation products at high NO according to MCM ($\mathrm{ACETO2 + HCHO + HO_2 + CO_2}$).

N2. See text for details. The stabilized Criegee intermediate ($\mathrm{CH_2OO}$) is currently not a model compound; its production is replaced by the products of its main atmospheric sink, the reaction with water dimer, namely $\mathrm{0.55\,HMHP + 0.4\,HCHO + 0.4\,H_2O_2 + 0.05\,HCOOH}$ (Sheps et al., 2017).

N3. Y_n^{Arey} denotes the pressure- and temperature- dependent nitrate yield from Arey et al. (2001), where n is carbon number. The scaling factor is adjusted to match laboratory-based estimates at room conditions, which is 14% and 13% for the 1,2- and 4,3-isoprene hydroxynitrate (ISOPBNO3 and ISODNO3), respectively (Wennberg et al., 2018).

N4. Bulk 1,6 isomerisation rate. See text for details.

N5. Addition channels (Wennberg et al., 2018). The non-IEPOX products observed by St. Clair et al. (2016) in presence of NO (HYAC, GLYALD, HPAC, $\mathrm{CH_3CHO}$) as well as the dihydroxy dihydroperoxides ($\mathrm{ISOP(OOH)_2}$) proposed to be a potentially significant component of isoprene SOA in low-NOx conditions (Liu et al., 2016) are assumed to have a negligible yield in most atmospheric conditions due to the proposed isomerisation of the peroxy radical formed in the reaction (D'Ambro et al., 2017). The further chemistry of the dihydroxy hydroperoxy epoxide resulting from this isomerisation, DHHEPOX, is not considered. DHHEPOX is assumed to undergo heterogeneous uptake and acid-catalyzed ring opening leading eventually to SOA formation (D'Ambro et al., 2017).

N6. Abstraction of hydroperoxide-H (75%) and of hydroxy-α-H (25%) (Wennberg et al., 2018). The latter leads to a radical proposed to undergo epoxide formation and OH expulsion (Wennberg et al., 2018), which appears unlikely since the reaction is insufficiently activated because, as is well known, the majority of the exothermicity goes to the newly-formed $\mathrm{H-OH}$ bond. Instead, $\mathrm{O_2}$ addition follows, forming $\mathrm{HO_2 + O{=}CHC(CH_3)(OOH)CH{=}CH_2}$. The main fate of the unsaturated hydroperoxy aldehyde is photolysis to an enol, $\mathrm{HOCH{=}C(CH_3)CH{=}CH_2}$ (80%) or to $\mathrm{HCO + OH + MVK}$ (20%) (see Sect. 2.1.2). The enol reacts primarily by OH addition to the first carbon, followed by a 1,5 H-shift to $\mathrm{OH + HCOOH + MVK}$.

N7. Abstraction of hydroperoxide-H (60%) and of hydroxy-α-H (40%), followed by similar reactions as for ISOPBOOH (see previous note). Hydroperoxy-α-H abstraction is neglected.

N8. Assume fast reaction of MCM product with OH, followed by fast reaction with NO, neglecting side products.

N9. Dinitrate yield of 18% at room conditions, as for INDO2 (see Note N12). Assume fast hydrolysis of the dinitrate in the aqueous aerosol phase, as it bears a tertiary nitrate group. The hydrolysis product (besides HNO_3) is very soluble and can be assumed to remain in the particulate phase.

N10. INBO2 is a mix of two peroxys (see Table 1). Assume 85% external and 15% internal OH-addition to ISOPBNO3. The 1,5 and 1,6 H-shifts in the dihydroxynitroxy peroxy radicals (e.g. $HOCH_2C(CH_3)(ONO_2)CH(OO)CH_2OH$) suggested by Wennberg et al. (2018) are neglected because their rates (equal to 0.05 s^{-1} in Wennberg et al.) should be lowered due to 1) the influence of the nitrate group, and 2) H-bonding between hydroxy-H and peroxy group. However, the rate estimation is very uncertain, and the H-shifts could be significant.

N11. The hydroperoxide bears a tertiary nitrate group and asumed to undergo hydrolysis in the aerosol phase. The hydrolysis product (besides HNO_3) is assumed to remain in the aerosol phase.

N12. Dinitrate yield of 18% at room conditions, consistent with the upper limit (18%) estimated by Lee et al. (2014). As in Note N9, assume fast hydrolysis of dinitrate. As for INBO2 (see above), the H-shifts in the peroxys (e.g. $HOCH_2C(O_2)(CH_3)CH(ONO_2)CH_2OH$) Wennberg et al. (2018) are neglected.

N13. The hydroperoxy aldehyde ($O{=}CHC(CH_3)(OOH)CH(ONO_2)CH_2OH$ or INDHPCHO in MCM) formed in the reaction is assumed to photolyze rapidly to HCO + OH + $CH_3C(O)CH(ONO_2)CH_2OH$.

N14. The $trans$ and cis isomers are lumped, adopting the $trans$:cis ratio of Bates et al. (2016). The epoxide-retaining products are lumped into ICHE.

N15. Formyl-H abstraction from the carbonyl hydroxyepoxides (e.g. $HOCH_2\overline{CHOC}(CH_3)CHO$ and isomers) primarily formed from IEPOX + OH. The isomer distribution follows Wennberg et al. (2018). H-abstraction is followed by concerted CO elimination and ring opening, O_2-addition leading to $CH_3C(O)CH(O_2)CH_2OH$ (for the major isomer) and $OCHC(O_2)(CH_3)CH_2OH$ (minor) which undergoes a 1,4 aldehyde H-shift, to CO + OH + HYAC.

N16. Hydroxyl-α-H abstraction from the carbonyl hydroxyepoxides (see previous note), followed by ring opening to give (for the main isomer) $OCHC(CH_3)(O^\circ)CH{=}CHOH$, followed by 1,5 enolic-H shift and O_2-addition to form $OCHC(CH_3)(OH)CH(O_2)CHO$. This is followed by a fast 1,5 aldehydic-H shift and (for a large part) by CO elimination to give, after O_2-addition, $CH_3C(O)CH(OOH)CHO$ + HO_2.

N17. The 1,4 H-shift in $HOCH_2C(OH)(CH_3)CH(O2)CHO$ and its isomer is taken to be fast (0.5 s^{-1} at 298 K), following Wennberg et al. (2018).

N18. The 1,5 H-shift in $HOCH_2CH(OH)C(CH_3)(O2)CHO$ forms HO_2 + $O{=}CHC(OOH)(CH_3)CH(OH)CHO$ assumed to photolyze rapidly either to CHO + OH + $CH_3C(O)CH(OH)CHO$ (HOBA), or to CHO + HO_2 + $OCHC(OOH)(CH3)CHO$ (HPDIAL).

N19. Oxy radical channel (65%) (Wennberg et al., 2018).

N20. The hydroperoxide channel (35%) forms $O{=}CHC(OOH)(CH_3)CH(OH)CH_2OH$, assumed to photolyze very rapidly to HCO + OH + $CH_3C(O)CH(OH)CH_2OH$.

Geosci. Model Dev. Discuss., https://doi.org/10.5194/gmd-2018-316
Manuscript under review for journal Geosci. Model Dev.
Discussion started: 19 December 2018

Geoscientific Model Development Discussions

N21. The 1,5 H-shift in $HOCH_2C(OH)(CH_3)CH(O2)CHO$ forms HO_2 + $O{=}CHC(OH)(CH_3)CH(OOH)CHO$ assuming to photolyze rapidly either to CHO + OH + $OCHC(CH_3)(OH)CHO$, or to CHO + HO_2 + $CH_3C(O)CH(OOH)CHO$ (HPKETAL). The hydroxy-dialdehyde is assumed to react exclusively with OH, forming CO + MGLY + HO_2.

N22. The hydroperoxide channel (35%) forms $O{=}CHCH(OOH)C(OH)(CH_3)CH_2OH$, assumed to photolyze very rapidly to HCO + OH + $O{=}CHC(OH)(CH_3)CH_2OH$.

N23. Neglect hydroperoxide channel, i.e. assume formation of oxy radical + OH. Note that if the hydroperoxide is formed, it is expected to photolyze rapidly (Liu et al., 2018), for a large part to the same products as the oxy radical pathway.

N24. Based on D'Ambro et al. (2017), the main OH-addition channel forms a hydroxyperoxy of which the main fate in low-NO regions should be reaction with HO_2, followed by reaction of the hydroperoxide with OH, forming $HOCH_2CH(OH)C(CH_3)(OOH)CHO$ as main product (C75OOH in MCM). Note that isomerisation of the hydroperoxy forms also C75OOH (along with HO_2). C57OOH is a α-hydroperoxyaldehyde, assumed to photolyze rapidly (Liu et al., 2018) to HCO+OH+$CH_3C(O)CH(OH)CH_2OH$, therefore regenerating OH and HO_2.

N25. The branching ratios are from Peeters and Müller (2010). The further mechanism mostly follows Wennberg et al. (2018); however, collisional deactivation of the radical ($OCHC(CH_3)C^{\circ}CH_2(OOH)$) formed in the minor OH-addition channel is neglected, since epoxide formation should be largely dominant, as for the radical formed by OH-addition to ISOPOOH, for which epoxide formation constitutes ca. 90% of the sink. The unsaturated dialdehyde $O{=}CHC(CH_3){=}CHCH(O)$ (MBED) undergoes very fast photolysis and is replaced by its oxidation products, as described in Sect. 2.1.3.

N26. Branching ratios from Peeters and Müller (2010), further mechanism from Wennberg et al. (2018), except for the collisional stabilisation of the radical formed in the major addition channel, which is neglected (see previous note). As above, the unsaturated dialdehyde $O{=}CHC(CH_3){=}CHCH(O)$ should photolyze rapidly to compounds replaced by their further reaction products. The hydroxyhydroperoxy aldehyde $HOOCH_2C(CH_3)(OH)CH{=}O$ should photolyze rapidly to (and is therefore replaced by) HCO + HO_2 + $CH_3C(O)CH_2OOH$.

N27. The peroxy radical ($CH_3C(O)CH(OH)C(O)O_2$) formed in the reaction is replaced by its further oxidation products in presence of NO.

N28. H-abstraction from CH group leads to $CH_3C(O)C(O)CH_2OOH$ which can be assumed to photolyze very rapidly to OH + CH_3CO_3 + HCHO + CO. H-abstraction of the CH_2 group yields $CH_3C(O)CH(OOH)CHO$ (HPKETAL).

N29. The acyl radical formed from $CH_3C(O)CH(OOH)CHO$ through aldehydic H-abstraction can add O_2 to form an acylperoxy radical which (upon reaction with NO) leads to CO_2 + OH + MGLY. Note that the acyl radical can also decompose to CO + OH + MGLY. Abstraction of the hydroperoxide H is followed by a 1,4 H-shift of the peroxy radical $CH_3C(O)CH(O_2)CHO$ to the same acyl radical as above. H-abstraction from the carbon bearing the OOH group (40% of reactivity) leads to $CH_3COCOCHO$ assumed to photolyze rapidly to CH_3CO + CO + HCO.

N30. The acyl radical formed from $OCHC(CH_3)(OOH)CHO$ can add O_2 to form an acylperoxy radical which (upon reaction with NO) leads to CO_2 + OH + MGLY. Note that the acyl radical can also decompose to CO + OH + MGLY.

N31. NISOPO2 is a mix of several radicals (Schwantes et al., 2015; Wennberg et al., 2018). The dinitrate formed in the reaction is ignored, as its further chemistry is unclear.

Geosci. Model Dev. Discuss., https://doi.org/10.5194/gmd-2018-316
Manuscript under review for journal Geosci. Model Dev.
Discussion started: 19 December 2018

N32. See text (Sect. 2.3). A higher self-reaction rate was used by Schwantes et al. (2015) in their kinetic modelling, but there is suggestion that it might be overestimated (Schwantes et al., 2015).

N33. H-abstraction from $HOOCH_2CH{=}C(CH_3)CH_2ONO_2$ and isomer.

N34. OH-addition to $HOOCH_2CH{=}C(CH_3)CH_2ONO_2$ (for 84%) and isomer (16%). The mechanism follows Wennberg et al. (2018), except that 1) the 1,5-H shift in the peroxy $O_2NOCH_2C(O_2)(CH_3)CH(OH)CH_2OH$ (and isomer) formed in the reaction is neglected, as it should be slow due to stabilization by H-bonding between the peroxy and hydroxy groups, 2) epoxide formation (ca. 9% yield) is neglected, 3) the minor pathways in the bimolecular reactions of the hydroxyperoxy radicals (e.g. dinitrate formation in RO_2+NO and dihydroperoxide formation in RO_2+HO_2, also the minor oxy decomposition channel proposed by Wennberg et al.) are neglected since their yields are small and uncertain, 4) the peroxys are replaced by the products of their reactions with NO or HO_2, and 5) the nitroxy hydroperoxy aldehyde $OCH{-}C(CH_3)(OOH)CH_2ONO_2$ is assumed to photolyze rapidly (Liu et al., 2018) to CHO + OH + $CH_3C(O)CH_2ONO_2$.

N35. The minor products C3CNO2 and C3CPO2 are replaced by assumed further oxidation product (NOA). The nitrooxy hydroperoxy epoxide (IHPE) formed in the reaction (Schwantes et al., 2015) is neglected and the other yields are increased for carbon balance.

N36. H-abstraction from $CH_2{=}CHC(CH_3)(OOH)CH_2ONO_2$ and isomer.

N37. OH-addition to $CH_2{=}CHC(CH_3)(OOH)CH_2ONO_2$ and isomer. The mechanism follows Wennberg et al. (2018), with simplications similar to the case of the δ-hydroperoxynitrates (see Note N34). The peroxy radical $O_2NOCH_2C(CH_3)(OOH)CH(OH)CH_2O_2$ (INPHO2β in Schwantes et al. (2015)) is assumed to react fast with NO or NO_3, leading to $O_2NOCH_2C(CH_3)(OOH)CHO$ (C4CPNA in Schwantes et al.) assumed to photolyze rapidly (Liu et al., 2018) to CHO + OH + NOA.

N38. IHNE is a mix of two β- and two δ-nitroxy hydroxyepoxides. The mechanism follows Wennberg et al. (2018). The peroxy radicals $O_2NOCH_2C(OH)(CH_3)C(O)CH_2O_2$ and $HOCH_2C(O_2)(CH_3)CH_2ONO_2$ formed from the β-IHNE are replaced by the products of their reaction with NO, neglecting dinitrate formation and minor oxy decomposition products. The radical $O{=}C^{\circ}CH_2ONO_2$ formed in these reactions adds O_2, forming an acylperoxy radical replaced by its further reaction product in presence of NO, i.e. CO_2 + HCHO + NO_2. The peroxy $O_2NOC(OH)(CH_3)CH(O_2)CHO$ undergoes a fast 1,4 H-shift outrunning bimolecular reactions, forming CO + OH + $O_2NOCH_2C(OH)(CH_3)CHO$, which is assumed to photolyze rapidly to NO_2 + HCHO + MGLY + HO_2 (Müller et al., 2014). The carbonyl nitroxyepoxides (ICNE in Wennberg et al.) are assumed to react with OH, following the Caltech reduced mechanism: $\mathrm{ICNE} + \mathrm{OH} \rightarrow 2\,\mathrm{CO} + 0.35\,\mathrm{NOA} + 0.65\,\mathrm{MGLY} + 0.65\,\mathrm{HO_2} + 0.65\,\mathrm{NO_2}$. The peroxys $O_2NOCH_2C(OH)(CH_3)CH(O_2)CHO$ and $OCHC(O_2)(CH_3)CH(OH)CH_2ONO_2$ formed from the δ-IHNE undergo fast H-shift reactions outrunning the bimolecular reactions, forming CO + OH + either $O_2NOC(OH)(CH_3)CH(O_2)CHO$ (in the first case) or $CH_3C(O)CH(OH)CH_2ONO_2$ (second case) (Wennberg et al., 2018).

N39. The OH-reaction rate was measured by Xiong et al. (2016) for $OCHC(CH_3){=}CHCH_2ONO_2$. The yields account for the NC4CHO isomer distribution estimated by Schwantes et al. (2015). The OH-reaction essentially follows Wennberg et al. (2018). Aldehyde H-abstraction from $OCHCH{=}C(CH_3)CH_2ONO_2$ by either OH or NO_3 leads to an acylperoxy radical here replaced by its NO-reaction product according to MCM ($\mathrm{CO_2} + \mathrm{CO} + \mathrm{HO_2} + \mathrm{NOA}$). Note that alternative reaction pathways proposed by Wennberg et al. also lead eventually to $\mathrm{CO} + \mathrm{NOA}$. OH-addition generates peroxy radicals undergoing fast isomerisation (Schwantes et al., 2015) leading to the nitroxy hydroxy aldehyde $O_2NOCH_2C(OH)(CH_3)CHO$ assumed to photolyze rapidly to NO_2 + HCHO + HO_2 + MGLY; the nitrooxy hydroperoxyaldehyde $O_2NOCH_2C(CH_3)(OOH)CHO$ assumed to photolyze rapidly to HCO + OH + NOA; and the nitrooxy hydroperoxyketone $CH_3C(O)CH(OOH)CH_2ONO_2$ assumed to photolyze to CH_3CO + OH + $OCHCH_2ONO_2$ (ETHLN).

Geosci. Model Dev. Discuss., https://doi.org/10.5194/gmd-2018-316
Manuscript under review for journal Geosci. Model Dev.
Discussion started: 19 December 2018

Geoscientific Model Development Discussions
Open Access
EGU

N40. Abstraction of α-hydroxy H in the δ-hydroxynitrates (e.g. $HOCH_2CH{=}C(CH_3)CH_2ONO_2$). The mechanism follows Wennberg et al. (2018), leading in part to photolabile hydroperoxynitroxy carbonyls (e.g. $O_2NOCH_2C(OOH)(CH_3)CHO$) assumed to photolyze rapidly (here to HCO + OH + $CH_3C(O)CH_2ONO_2$ (NOA).

N41. OH-addition to the δ-hydroxynitrates (e.g. $HOCH_2CH{=}C(CH_3)CH_2ONO_2$). The mechanism follows Wennberg et al. (2018), except that all different dihydroxy nitroxyperoxy radicals are lumped into one radical (INCO2), and epoxide formation (ca. 8% yield) is neglected.

N42. The 1,5 H-shift in $O_2NOCH_2C(O_2)(CH_3)CH(OH)CH_2OH$ leading to HO_2 + $O_2NOCH_2C(OOH)(CH_3)CH(OH)CHO$ is assumed to be rapidly followed by fast photolysis to CHO + HO_2 + $O_2NOCH_2C(OOH)(CH_3)CHO$, itself followed by photolysis to CHO + OH + $CH_3C(O)CH_2ONO_2$ (NOA).

N43. Mechanism adapted from Wennberg et al. (2018). The hydroperoxide (e.g. $HOCH_2CH(OOH)C(OH)(CH_3)CH_2ONO_2$) formed with a 43 % yield is assumed to react with OH (ca. $1.5 \cdot 10^{-11}$ molec^{-1} cm^3 s^{-1}), primarily by abstraction of its α-hydroperoxide hydrogen, forming OH + $HOCH_2C(O)C(OH)(CH_3)CH_2ONO_2$ (INCCO), and by abstraction of the terminal hydroperoxide hydrogen to regenerate INCO2.

N44. The dicarbonyl nitrate $O_2NOCH_2C(CH_3)(OH)C(O)CHO$ formed in the reaction is assumed to photolyze rapidly to HCO + $O_2NOCH_2C(CH_3)(OH){-}C^{\circ}{=}O$, which decomposes (for a large part) into CO + HO_2 + $O_2NOCH_2C(O)CH_3$ (NOA).

N45. The mechanism follows the MCM. Among the three considered channels, formation of $O_2NOCH(CHO)C(CH_3)(OH)CH_2ONO_2$ + HO_2 is assumed to be followed by photolysis of the carbonyl dinitrate to NO_2 + GLY + NOA + HO_2 (Müller et al., 2014).

N46. Account for the fast isomerisations of the hydroxyperoxys resulting from OH addition to MACR (Crounse et al., 2012; Wennberg et al., 2018).

N47. MVKO2 is a mix of $CH_3COCH(O_2)CH_2OH$ (72%) and $CH_3COCH(OH)CH_2O_2$ (28%). The ratio is adjusted so that the glycolaldehyde yield in MVKO2 + NO is 69% (Galloway et al., 2011), taking the nitrate yield (4%) (Praske et al., 2015) into account.

N48. MVKOOH is a mix of $CH_3COCH(OOH)CH_2OH$ (55%) and $CH_3COCH(OH)CH_2OOH$ (45%). The fractions account for the different hydroperoxide yields in the reaction of their respective peroxy radical precursors with HO_2.

N49. Reaction rate taken equal to the average of the MCM and the structure activity relationship (SAR) of Neeb (2000). Assume 50% formyl-H absraction and 50% alcoholic-H absraction. The former leads ultimately to hydroxyacetone + NO_2 (in presence of NO). The latter leads to a nitrooxydialdehyde assumed to photolyze immediately into methylglyoxal, NO_2 and HCO.

N50. The reaction MVKNO3 + OH is split into two reactions since MVKNO3 represents two isomers, $CH_3C(O)CH(ONO_2)CH_2OH$ (for 80%) and $CH_3C(O)CH(OH)CH_2(ONO_2)$ (for 20%). For the first, assume 50% alcoholic-H abstraction to $CH_3C(O)CH(ONO_2)CHO$ assumed to photolyze (for ca. 80%) into NO_2 + GLY + CH_3CO, the rest reacting with OH to form eventually MGLY+HO_2+CO_2 (in the presence of NO). For the second compound, ignore alcoholic-H absraction.

N51. Assume fast reaction of the acylperoxy radical (84% of reactive flux) with NO. Assume fast photolysis of $CH_3COCOCHO$ (16% of flux) into CH_3CO + CO + HCO.

N52. Assume immediate reaction of product $OCHC(CH_3)(OH)CHO$ with OH, forming MGLY + HO_2 + CO_2 upon reaction with NO.

Geosci. Model Dev. Discuss., https://doi.org/10.5194/gmd-2018-316
Manuscript under review for journal Geosci. Model Dev.
Discussion started: 19 December 2018

N53. The dominant OH-addition, to $(HO)_2CHCH(O_2)C(O)CH_3$, is followed by a 1,5 H-shift from an alcohol-H to the peroxy group and decomposition (So et al., 2014). The minor addition channel forms $HOC^{\circ}HCH(OH)C(O)CH_3$ which reacts with O_2 to HO_2 + $CH_3C(O)CH(OH)CHO$.

N54. The dominant OH-addition ($3{\cdot}10^{-11}$ molec^{-1} cm^3 s^{-1}), to $O{=}CHC(CH_3)(O_2)CH(OH)_2$, is followed by an H-shift from either an alcohol-H (50%) or from the aldehyde-H (50%) to the peroxy group, leading to either $HCOOH + OH + MGLY$ or CO +OH + $CH_3C(O)CH(OH)_2$ (DHA).

N55. Combines the minor addition channel ($1.2{\cdot}10^{-11}$ molec^{-1} cm^3 s^{-1}) and the aldehyde-H abstraction channel ($1.5{\cdot}10^{-11}$ molec^{-1} cm^3 s^{-1}). The minor addition channel leads to HO_2 + $O{=}CHC(CH_3)(OH)CH{=}O$, which reacts primarily with OH, leading to an acyl radical which can eliminate CO and give MGLY + HO_2 or form an acylperoxy radical which can undergo a shift of the aldehyde-H to the peroxy group. The resulting radical can either lose CO, and upon reaction with O_2, form HO_2 + CO + $CH_3C(O)C(O)OOH$ (PPYR), or react with O_2 and then with NO or HO_2, forming CO_2 + HO_2 + PPYR. The H-abstraction channel leads to an acylperoxy radical, $O{=}C(O_2)C(CH_3){=}CHOH$, which undergoes a enolic 1,6 H-shift followed by O_2-addition, to $O{=}C(OOH)C(O_2)(CH_3)CH{=}O$. The latter radical undergoes a 1,4 H-shift of the aldehyde-H, leading to CO + OH + PPYR. PPYR is assumed to photolyze rapidly to CH_3CO + CO_2 + OH (Saunders et al., 2003).

N56. The nitrate yield is 1.6% at room conditions.

N57. Assume equal rates for the two addition channels. See text (Sect. 2.1.2).

N58. The reaction leads to pyruvic acid (along with HO_2), assumed to photolyze very rapidly according to Burkholder et al. (2015).

N59. Yields calculated at room conditions. The acylperoxy radical resulting from O_2 addition to the HCOCO radical (ca. 17% of the reactive flux) is replaced by the final reaction products in presence of NO and O_2 (i.e. CO + HO_2 + CO_2).

N60. Contrary to MCM, consider aldehyde-H abstraction, leading in part to CO + OH + HCHO (for 25%) and in part to $HOOCH_2CO_3$ (75%) which (upon reaction with NO) leads to CO_2 + OH + HCHO.

N61. Reaction rate taken equal to the average of the MCM and the structure activity relationship (SAR) of Neeb (2000). Products assume fast reaction of peroxy radical with NO.

N62. The minor channel (8%, formation of $CH(OH)_2CH_2O_2$) proposed by So et al. (2014) is neglected.

N63. The methyl nitrate yield adopted here is $2{\cdot}10^{-4}$ at room conditions, or ca. $5{\cdot}10^{-5}$ in the lower stratosphere, at the lower end of the range ($(5\text{-}10){\cdot}10^{-5}$) estimated by Flocke et al. (1998) based on stratospheric CH_3ONO_2 observations.

N64. See text for details.

N65. The water dimer concentration (molec.cm^{-3}) is calculated using

$$[\text{dimer}] = p \cdot K_p \cdot [H_2O]^2/[M] \quad (7)$$

where p is atmospheric pressure (atm), $[H_2O]$ and M are the water vapour and dry air number density (molec.cm^{-3}), and K_p (atm^{-1}) is approximated following Scribano et al. (2006) :

$$K_p = 4.7856 \cdot 10^{-4} \exp(1851.09/T - 5.10485 \cdot 10^{-3} T) \quad (8)$$

N66. Rate reported by Wennberg et al. (2018). H-abstraction from the carbon, followed by OH elimination, is dominant (Allen et al., 2018). H-abstraction from hydroperoxide group is followed by decomposition of the hydroxymethylperoxy radical.

N67. Note that he rate coefficient of the $CH_3OH + OH$ reaction was recently shown to be humidity-dependent (Jara-Toro et al., 2017). Although neglected here, this dependence will be implemented in future versions of the mechanism.

N68. The rate constant is for α-pinene although the compound APIN is a surrogate for all monoterpenes. Due to the complexity and poor understanding of monoterpene oxidation, the product yields reflect mostly secondary formation, as calculated from box model calculations using MCM (60-day simulations at either 1 ppbv or 50 pptv NOx, photolysis rates calculated for clear-sky conditions at 30°N on July 15th). The yield of acetone from both α- and $\beta-$pinene is very close to 100% after several days of reaction, independent of the NOx level. The overall yield of formaldehyde obtained in these simulations is ca. 4.2 HCHO per monoterpene oxidized, which comes down to 2.3 after subtracting the contributions of acetone and methylglyoxal oxidation. This yield is further reduced by 45% to account for wet/dry deposition of intermediates and secondary organic aerosol formation. That fraction is higher, but of the same order, as the estimated overall impact of deposition on the average formaldehyde yield from isoprene oxidation (∼30%), based on global model (MAGRITTE) calculations. The higher fraction is justified by to the larger number of oxidation steps and the generally lower volatility of intermediates involved in formaldehyde formation from monoterpene oxidation. The overall carbon balance of monoterpene oxidation in the mechanism is ∼50% due to the combined effects of deposition, SOA formation and CO and CO_2 formation besides their production through the degradation of the explicit products.

N69. The 26% yield is the assumed overall organic nitrate formation from monoterpenes (Rindelaub et al., 2015).

N70. Several carbonyl intermediates formed in the reaction are assumed to react rapidly with OH. $CH_3C(OH)(CH_3)C(O)O_2$ is assumed to react with NO, forming CO_2 + CH_3COCH_3 + HO_2.

N71. The organic nitrate yield is close to 10% at room conditions (Chan et al., 2009). Whereas the major isomer peroxy radical leads to $CH_3COCH_3 + GLYALD + HO_2$ upon reaction with NO, the other isomer leads to HCHO + HO_2 + $CH_3C(OH)(CH_3)CHO$ which is here replaced by its OH-reaction product in presence of NO, namely CO_2 + CH_3COCH_3 + HO_2. Note that the MCMv3.3.1 mechanism for MBO was recently validated by comparisons with chamber measurements, in particular regarding the production of radicals, acetone and formaldehyde (Novelli et al., 2018a), and that the peroxy radical isomerisation reactions proposed by Knap et al. (2015) can be neglected due to their low rates and resulting impacts.

N72. The hydroperoxides formed in the reaction are replaced by the OH-reaction products in presence of NO.

N73. Average reactivity of the two isomer dihydroxynitrates. The products are replaced by their OH-reaction products in presence of NO.

2.9 Photodissociations

Geosci. Model Dev. Discuss., https://doi.org/10.5194/gmd-2018-316
Manuscript under review for journal Geosci. Model Dev.
Discussion started: 19 December 2018

Geoscientific Model Development Discussions

Table 3. Photodissocation reactions. References: 1, Burkholder et al. (2015); 2, Röth and Ehhalt (2015); 3, Shaw et al. (2018); 4, Salter et al. (2013); 5, Pinho et al. (2005); 6, Jenkin et al. (2015); 7, Atkinson et al. (2006); 8, Liu et al. (2018); 9, Müller et al. (2014); 10, Barnes et al. (1993); 11, Xiong et al. (2016); 12, Liu et al. (2017); 13, Nakanishi et al. (1977).

Reaction	*Cross section*	*Quantum yield*	*Products*
$HCHO \rightarrow CO + 2HO_2$	1	2	
$HCHO \rightarrow H_2 + CO$	1	2	
$CH_3CHO \rightarrow CH_3O_2 + CO + HO_2$	1	1	
$CH_3CHO \rightarrow VA$	1	3	
$GLYALD \xrightarrow{83\%} HCHO + CO + 2HO_2$	1	1	
$\xrightarrow{10\%} CH_3OH + CO$	1	1	
$\xrightarrow{7\%} OH + OCHCH_2O_2$	1	1	
$GLY \rightarrow 2CO + 2HO_2$	1	4	
$GLY \rightarrow 2CO + H_2$	1	4	
$GLY \rightarrow HCHO + CO$	1	4	
$CH_3COCH_3 \rightarrow CH_3CO_3 + CH_3O_2$	1	1	
$MGLY \rightarrow CH_3CO_3 + CO + HO_2$	1	1	
$MACR \xrightarrow{50\%} MCO3 + HO_2$	1	5[a]	6
$\xrightarrow{50\%} 0.35\,CH_3CO_3 + HCHO + 1.65\,CO + 0.65\,CH_3O_2 + HO_2$	1	5[a]	6
$MVK \xrightarrow{50\%} C_3H_6 + CO$	1	1	6
$\xrightarrow{50\%} CH_3CO_3 + HCHO + CO + HO_2$	1	1	6
$CH_3OOH \rightarrow HCHO + HO_2 + OH$	1	1[b]	
$HMHP \rightarrow HCOOH + OH + HO_2$	1	*b*	
$ISOPBOOH \rightarrow MVK + HCHO + HO_2 + OH$	1[c]	*b*	6
$ISOPDOOH \rightarrow MACR + HCHO + HO_2 + OH$	1[c]	*b*	6
$ISOPEOOH \rightarrow MACR + HCHO + HO_2 + OH$	1[c]	*b*	6
$MACROH \rightarrow HYAC + CO + 2HO_2$	7[d]	7[d]	6
$MVKOOH \xrightarrow{45\%} CH_3CO_3 + HO_2 + HPAC$	8	8[e]	6[f]
$\xrightarrow{55\%} CH_3CO_3 + GLYALD + OH$	8	8[e]	6[f]
$CH_3ONO_2 \rightarrow HCHO + HO_2 + NO_2$	1	1[b]	
$PAN \xrightarrow{70\%} CH_3CO_3 + NO_2$	1	1[b]	
$\xrightarrow{30\%} CH_3O_2 + CO_2 + NO_3$	1	1[b]	
$PAA \rightarrow CH_3O_2 + OH + CO_2$	1	*b*	6
$HYAC \xrightarrow{50\%} CH_3CO_3 + HCHO + HO_2$	1	1	1
$\xrightarrow{20\%} GCO3 + CH_3O_2$	1	1	1

Geosci. Model Dev. Discuss., https://doi.org/10.5194/gmd-2018-316
Manuscript under review for journal Geosci. Model Dev.
Discussion started: 19 December 2018

Geoscientific Model Development Discussions
Open Access
EGU

Reaction	*Cross section*	*Quantum yield*	*Products*
$\xrightarrow{15\%} CH_3O_2 + CO + HCHO + HO_2$	1	1	1
$\xrightarrow{15\%} OH + ACETO2$	1	1	1
$INDOOH \rightarrow NO_2 + GLYALD + HYAC + OH$	7[g]	*b*	*h*
$INDOOH \rightarrow OH + 0.15\,(HYAC + GLYALD + NO_2)$ $+0.85\,(HCHO + HO_2 + MVKNO3)$	1[c]	*b*	*i*
$MACRNO3 \rightarrow HYAC + CO + HO_2 + NO_2$	9	9[b]	9
$MVKNO3 \rightarrow 0.8\,(CH_3CO_3 + GLYALD + NO_2)$ $+0.2\,(MGLY + HCHO + NO_2)$	9	9[b]	6
$INCCO \rightarrow NO_2 + HYAC + GCO3$	7[j]	9[b]	6
$INCNO3 \rightarrow NO_2 + HCHO + HO_2 + MVKNO3$	7[k]	*b*	*h*
$INCNO3 \rightarrow NO_2 + GLYALD + NOA + HO_2$	7[g]	*b*	*h*
$NOA \rightarrow CH_3CO_3 + HCHO + NO_2$	10	9	6
$ISOPDNO3 \rightarrow MACR + HCHO + HO_2 + NO_2$	7[l]	*b*	6
$ISOPENO3 \rightarrow MACR + HCHO + HO_2 + NO_2$	7[m]	*b*	6
$ETHLN \rightarrow HCHO + CO + HO_2 + NO_2$	9	9	9
$NC4CHO \xrightarrow{16\%} NO_2 + 1.15\,HO_2 + 1.35\,CO_2 + 0.55\,HCHO + 0.65\,CH_3CO_3$ $+0.2\,MMAL + 0.15\,MGLY + 0.15\,CO + 0.1\,GLY - 0.55\,OH$	11	11[n]	6[o]
$NC4CHO \xrightarrow{16\%} NO_2 + OH + CO + 0.5\,HPKETAL + 0.5\,HPDIAL$			
$NC4CHO \xrightarrow{48\%} NO_2 + CO + OH + 0.3\,HMVK + 0.7\,HMAC$			
$NC4CHO \xrightarrow{20\%} NO_2 + 1.7\,CO + 0.3\,MVKO2 + 0.7\,HYAC$			
$DHBO \rightarrow CH_3CO_3 + GLYALD$	6	6	6
$HOBA \rightarrow MGLY + CO + 2\,HO_2$	6	6	6
$HOBA \rightarrow CH_3CO_3 + GLY + HO_2$	7[p]	7[p]	
$HCOC5 \rightarrow CH_3CO_3 + HCHO + GCO3$	6	6	6
$MCO3H \rightarrow OH + CO_2 + 0.65\,(CH_3O_2 + CO + HCHO)$ $+0.35(CH_3CO_3 + HCHO)$	1[q]	*b*	6
$GCO3H \rightarrow OH + HO_2 + HCHO + CO_2$	1[q]	*b*	6
$HPAC \xrightarrow{84\%} VA$	8	8[e]	8[r]
$\xrightarrow{16\%} HO_2 + CO + HCHO + OH$			
$HPACET \xrightarrow{84\%} MVA$	8	8[e]	8[r]
$\xrightarrow{16\%} CH_3CO_3 + HCHO + OH$			
$HPKETAL \xrightarrow{50\%} HMVK$	8	8[e]	*r*
$\xrightarrow{25\%} CH_3CO_3 + OH + GLY$			
$\xrightarrow{25\%} CO + HO_2 + OH + MGLY$			

Geosci. Model Dev. Discuss., https://doi.org/10.5194/gmd-2018-316
Manuscript under review for journal Geosci. Model Dev.
Discussion started: 19 December 2018

Geoscientific Model Development Discussions
Open Access
EGU

Reaction	*Cross section*	*Quantum yield*	*Products*
$\mathrm{HPDIAL} \xrightarrow{50\%} \mathrm{HMAC}$	8	8^{e}	r
$\xrightarrow{50\%} \mathrm{CO + HO_2 + OH + MGLY}$			
$\mathrm{DIHPCHO} \rightarrow \mathrm{HO_2 + CO + OH + HPACET}$	8	8^{e}	6^{r}
$\mathrm{DIHPMEK} \rightarrow \mathrm{OH + CH_3CO_3 + HPAC}$	8	8^{e}	6^{r}
$\mathrm{BIACETOH} \rightarrow \mathrm{CH_3CO_3 + GCO3}$	7^{t}	7^{s}	6
$\mathrm{HPALD1} \xrightarrow{11\%} \mathrm{0.45\,OH + 1.15\,HO_2 + 1.35\,CO_2 + 0.55\,HCHO + 0.65\,CH_3CO_3}$	1^{t}	t	12^{t}
$\mathrm{+0.2\,MMAL + 0.15\,MGLY + 0.15\,CO + 0.1\,GLY}$			
$\xrightarrow{11\%} \mathrm{2\,OH + CO + HPKETAL}$			
$\xrightarrow{56\%} \mathrm{CO + 2\,OH + HMVK}$			
$\xrightarrow{22\%} \mathrm{CO + CH_3CO_3 + GLYALD}$			
$\mathrm{HPALD2} \xrightarrow{18\%} \mathrm{0.45\,OH + 1.15\,HO_2 + 1.35\,CO_2 + 0.55\,HCHO + 0.65\,CH_3CO_3}$	1^{t}	t	12^{t}
$\mathrm{+0.2\,MMAL + 0.15\,MGLY + 0.15\,CO + 0.1\,GLY}$			
$\xrightarrow{18\%} \mathrm{2\,OH + CO + HPKETAL}$			
$\xrightarrow{46\%} \mathrm{CO + 2\,OH + HMAC}$			
$\xrightarrow{18\%} \mathrm{2\,CO + HO_2 + HYAC}$			
$\mathrm{HMAC} \rightarrow \mathrm{OH + CO + HO_2 + MGLY}$	13	u	v
$\mathrm{HMVK} \rightarrow \mathrm{OH + CH_3CO_3 + GLY}$	13	u	v
$\mathrm{APINONO2} \rightarrow \mathrm{NO_2}$	7^{g}	b	

Notes:

a) Total quantum yield of 0.004.

b) Unit quantum yield.

c) As for $\mathrm{CH_3OOH}$.

d) As for $\mathrm{i-C_3H_7CHO}$.

e) Total quantum yield of 0.8.

f) See text regarding hydroperoxycarbonyl photolysis, and note N48 above.

g) As for $\mathrm{CH_3CH(ONO_2)CH_3}$.

h) Oxy radical decomposition follows Vereecken and Peeters (2009).

i) Oxy decomposition as in $\mathrm{INDO2 + NO}$ (Table 2).

j) Sum of absorption cross sections of $\mathrm{CH_3COC_2H_5}$ and $\mathrm{n-C_4H_9ONO_2}$.

k) As $\mathrm{n-C_4H_9ONO_2}$.

l) Cross sections of $\mathrm{n-C_4H_9ONO_2}$ divided by 3 to account for effect of OH group (Roberts and Fajer, 1989).

m) Cross sections of $\mathrm{n-C_4H_9ONO_2}$ divided by 3 to account for effect of OH group (Roberts and Fajer, 1989).

n) Quantum yield of 1 below 336 nm, zero above.

o) NC4CHO photolysis follows HPALD2 photolysis for 75% and HPALD1 for 25% (isomer distribution of Schwantes et al. (2015)).

p) As for $\mathrm{CH_3COC_2H_5}$.

q) As for $\mathrm{CH_3COOOH}$.

Geosci. Model Dev. Discuss., https://doi.org/10.5194/gmd-2018-316
Manuscript under review for journal Geosci. Model Dev.
Discussion started: 19 December 2018

r) See text regarding hydroperoxycarbonyl photolysis.

s) Photorate taken as 25% of $J(\mathrm{CH_3COCOCH_3})$ (Praske et al., 2015).

t) Absorption cross sections of MACR, quantum yield of 0.8. See text.

u) Quantum yield of 0.1 below the threshold of 312 nm (see text).

v) See text.

2.10 Uptake by aerosols

The heterogeneous reactions on aerosols are listed in Table 2.10 with their associated reactive uptake coefficients. The rate (λ) for the heterogeneous uptake of a chemical compound on aqueous aerosols is calculated using

$$\lambda = \frac{A}{r_n/D_g + 4/(\omega \cdot \gamma)}, \tag{9}$$

where A is the aerosol surface density ($\mathrm{m^2\ m^{-3}}$), r_n is the number mean particle radius (m), D_g is the gas-phase diffusivity parameterized as described in Müller et al. (2008), ω is the mean molecular speed ($\mathrm{m\ s^{-1}}$), and γ the reactive uptake coefficient (Table 2.10). The aerosol surface density is calculated following (Stavrakou et al., 2009b). Aqueous aerosols include inorganic (sulfate/ammonium/nitrate/water) and carbonaceous (OC and BC) calculated by the model as described in Stavrakou et al. (2013) and sea-salt aerosol from the MACC (Monitoring Atmospheric Composition and Climate) Reanalysis (apps.ecmwf.int/datasets/data/macc-reanalysis/levtype=sfc/).

The heterogeneous uptake of alkyl nitrates by aqueous aerosols followed by their hydrolysis has been suggested as a substantial organic nitrate sink and a large source of nitric acid in forested environments (Romer et al., 2016). Since tertiary nitrates were shown in the laboratory to undergo hydrolysis much faster than primary and secondary nitrates, we neglect the hydrolysis of non-tertiary nitrates while assuming fast hydrolysis of tertiary nitrates from isoprene. The reactive uptake coefficient (γ) calculated by Marais et al. (2016) based on measured hydrolysis rates of a primary and a secondary hydroxynitrate from isoprene in neutral solution (Jacobs et al., 2014) is much too low ($1.3{\cdot}10^{-7}$ – $5.2{\cdot}10^{-5}$) to account for the loss observed during the Southern Oxidant and Aerosol Study (SOAS) campaign (Romer et al., 2016), due to the relatively low estimated Henry's law constant of isoprene hydroxynitrates. A much higher γ (0.1) is assumed here for the major (tertiary) 1,2-hydroxynitrate from isoprene (ISOPBNO3), such that heterogeneous loss is its dominant fate in the troposphere, whereas the uptake of non-tertiary isoprene hydroxynitrates is neglected. Although crude, this assumption leads to a good model agreement against aircraft observations of isoprene hydroxynitrates over the Southeastern U.S. (see Sect. 3.2). Furthermore, the calculated average γ for the sum of isoprene hydroxynitrates weighted by their respective abundances is ∼0.02, consistent with the upper limit (0.02) inferred for the isoprene hydroxynitrate family by Wolfe et al. (2015) based on SOAS measurements. An uncertain, but likely significant, fraction of the monoterpene nitrates (represented in the mechanism by a unique lumped compound APINONO2) is assumed to be tertiary and undergoes hydrolysis (Browne et al., 2013, 2014) with γ = 0.01 (Fisher et al., 2016). Other, minor tertiary nitrates generated in the mechanism (INB1CO, INB1OOH, INB2OOH, INB1NO3 in MCM) are also assumed to undergo rapid uptake followed by hydrolysis in the aerosol, generating $\mathrm{HNO_3}$ and a usually very soluble and condensable co-product assumed to remain in the particulate phase. The hydrolysis of non-tertiary nitrates is slow compared to tertiary nitrates, and is therefore neglected here. Gas-aerosol partitioning might occur, leading to possible loss by aerosol dry or wet deposition; this loss could be significant if repartitioning of particulate nitrates to the gas phase would be inhibited (Fisher et al., 2016). These effects are however very uncertain, and are not considered here for simplicity.

Geosci. Model Dev. Discuss., https://doi.org/10.5194/gmd-2018-316
Manuscript under review for journal Geosci. Model Dev.
Discussion started: 19 December 2018

Geoscientific Model Development Discussions

Table 4. Heterogeneous reactions on aqueous aerosols. γ denotes the reactive uptake coefficient. References: 1, Liggio et al. (2005); 2, Marais et al. (2016); 3, Fisher et al. (2016); 4, Müller et al. (2016). Notes:*a*) The dependence on aerosol pH (Marais et al., 2016; Stadtler et al., 2018) is ignored.

Reaction	γ	*Ref.*
$\mathrm{GLY} \rightarrow \mathrm{GLY(aerosol)}$	$2.9(-3)$	1
$\mathrm{IEPOX} \rightarrow \mathrm{IEPOX(aerosol)}$	$4.2(-3)$	2^a
$\mathrm{HMML} \rightarrow \mathrm{HMML(aerosol)}$	$1.3(-4)$	2^a
$\mathrm{ISOPBNO3} \rightarrow \mathrm{ISOPBOH} + \mathrm{HNO_3}$	0.1	*b*
$\mathrm{MACRNO3} \rightarrow \mathrm{MACROH} + \mathrm{HNO_3}$	0.1	*b*
$\mathrm{APINONO2} \rightarrow \mathrm{HNO_3} + \mathrm{product}$	0.01	3
$\mathrm{CH_3OOOH} \rightarrow \mathrm{CH_3OH} + \mathrm{O_2}$	0.1	4

3 Regional and global modelling

3.1 Model description and simulations

The MAGRITTE model calculates the distribution of 175 chemical compounds, among which 136 species undergo transport processes (advection, deep convection and turbulent diffusion) in the model. MAGRITTE can be run either globally at 2° (latitude) $\times$ 2.5° (longitude) resolution, or regionally at $0.5^\circ \times 0.5^\circ$ resolution. The lateral boundary conditions of the regional model are provided by the global model. In the vertical, the model uses a hybrid (σ-pressure) coordinate, with 40 levels between the Earth's surface and the lower stratosphere (44 hPa level). The meteorological fields are provided by ECMWF ERA-Interim analyses (Dee et al., 2011). Most model parameterizations, including the transport scheme, inherit from the IMAGES model (Muller and Brasseur, 1995; Stavrakou et al., 2009a, b, 2015; Bauwens et al., 2016). The deposition scheme is described in a companion paper (Müller et al., 2018).

The model uses anthropogenic emissions of CO, NOx, OC, BC, and SO_2 from the HTAPv2 dataset for year 2010 (Janssens-Maenhout et al., 2015). Following Travis et al. (2016), the anthropogenic NOx emissions over the U.S. are first scaled down to match the U.S. total (3.5 TgN/yr) for the year 2013 reported by the National Emission Inventory (NEI), and the U.S. NOx emissions due to industry and transport are further reduced by 60% to match observed aircraft NO_x concentrations and nitric acid deposition data, consistent with the recommendation of Anderson et al. (2014). Anthropogenic NMVOC emissions are provided by the EDGARv4.3.2 inventory (Huang et al., 2017) for the year 2012. The global annual anthropogenic NMVOC source is 154 TgNMVOC (118 TgC). Biomass burning emissions (78 TgNMVOC or 45 TgC in 2013) are obtained from the Global Fire Emission Database version 4 (GFED4s) (van der Werf et al., 2017) and are vertically distributed according to Sofiev et al. (2013).

Isoprene and monoterpene fluxes (366 and 91.5 TgC, respectively, in 2013) are calculated by the MEGAN-MOHYCAN model (Müller et al., 2008; Guenther et al., 2012; Bauwens et al., 2018) and are available online (http://emissions.aeronomie.be). Biogenic emissions of acetaldehyde and ethanol (amounting to 92 and 88 Tg(C) yr^{-1} globally) are parameterized as in Millet et al. (2010). The methanol biogenic emissions are provided by an inverse modelling study constrained by spaceborne methanol abundances and are estimated at 37.5 Tg(C) yr^{-1} (Stavrakou et al., 2011). Biogenic emissions of C_2H_4 (scaled to a global total of 4 Tg(C) yr^{-1}), CH_2O (1.6 Tg(C) yr^{-1}) and CH_3COCH_3 (18 Tg(C) yr^{-1}) are also provided by MEGAN (Guenther et al., 2012) (available on http://eccad.aeris-data.fr).

Geosci. Model Dev. Discuss., https://doi.org/10.5194/gmd-2018-316
Manuscript under review for journal Geosci. Model Dev.
Discussion started: 19 December 2018

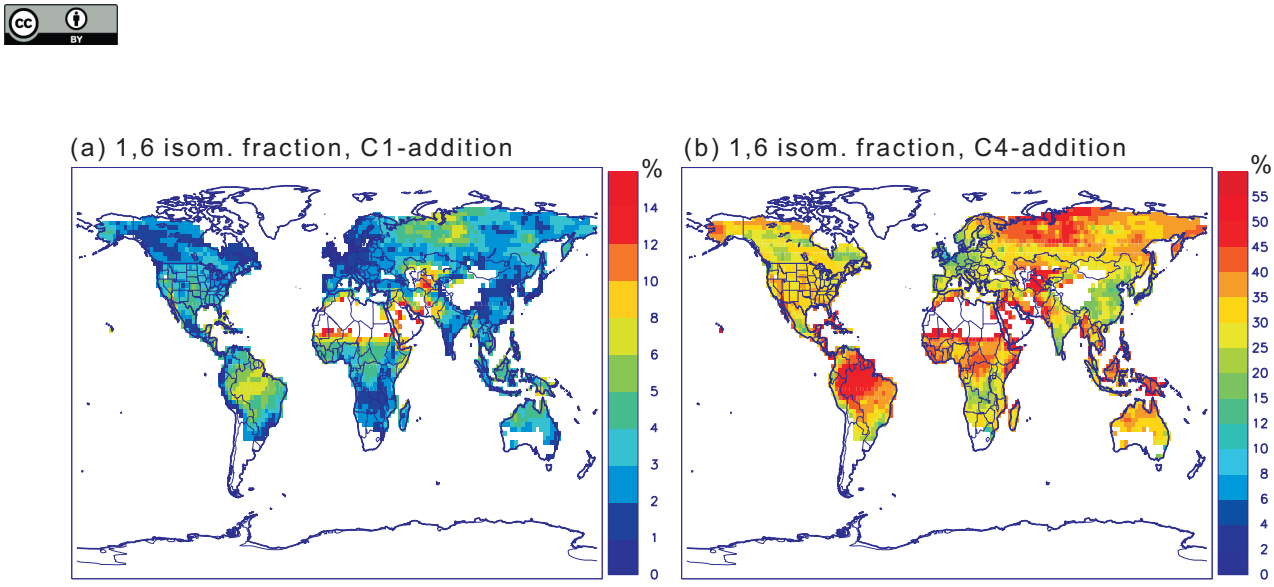

Figure 2. Calculated percentage contribution of Z-δ-hydroxyperoxy 1,6 H-shift to the overall sink of the pool of peroxys resulting from addition of OH (a) to carbon C1, and (b) to carbon C4 of isoprene (column average, July 2013). Note the different color scales in (a) and (b).

The model also includes oceanic emissions of methanol (18.4 Tg(C) yr^{-1}), acetone (39.3 Tg(C) yr^{-1}) and acetaldehyde (30.4 Tg(C) yr^{-1}) (Müller et al., 2018), similar to previous model estimations (Stavrakou et al., 2011; Fischer et al., 2012; Millet et al., 2010). Finally, oceanic emissions of alkyl nitrates are also included, based on comparisons with aircraft campaign measurements as originally proposed by Neu et al. (2008), but taking into account the updated alkylnitrate calibration of the campaign data (Simpson et al., 2011). The adopted rates over Tropical oceans (10°S – 10°N) are $6 \cdot 10^8$, $2.5 \cdot 10^8$, 10^8 and 10^8 molec. cm^{-2} s^{-1} for C_1, C_2, C_3 and $C_{>3}$ alkyl nitrates, respectively; $3 \cdot 10^7$, $3 \cdot 10^7$, $1.5 \cdot 10^7$ and 10^7 molec. cm^{-2} s^{-1} over the Southern Ocean (>10°S); a uniform rate of 10^7 molec. cm^{-2} s^{-1} is adopted elsewhere over ice-free oceans. The calculated global emissions are respectively 0.35, 0.3, 0.2 and 0.25 Tg(C) (or 0.4, 0.18, 0.08, 0.07 Tg(N)) for C_1, C_2, C_3 and higher alkylnitrates.

MAGRITTE is run for a period of 18 months starting on July 1, 2012, both at the global scale (2°×2.5° resolution) and regional scale for the U.S. (0.5°×0.5°, 10-54°N, 65-130°W). Only the results for the year 2013 are discussed hereafter.

3.2 Model general results

Oxidation of isoprene by OH radicals is by far the largest sink of isoprene, representing ∼85% of the global sink according to the model calculations, in agreement with previous model studies (Paulot et al., 2012), whereas ozonolysis and the NO_3-reaction contribute for ∼9% and 5%, respectively. The isomerisation reactions control the fate of about one fifth of the total flux of hydroperoxy radicals formed from the reaction of isoprene with OH (16.5% and 3% for the 1,6 and 1,5 H-shifts, respectively). However, the contribution of 1,6 H-shift is much higher, by about one order of magnitude, for the peroxys resulting from OH-addition to carbon C4 than for those resulting from addition at C1 (Peeters et al., 2014; Wennberg et al., 2018). Furthermore, this contribution is dependent on temperature and on the concentrations of NO and HO_2 radicals, as illustrated on Fig. 2: of the order of 50% over remote forests such as Amazonia, it drops to ∼35% over the Southeastern U.S. and below 20% over cooler, more NOx-polluted areas (for C4-addition).

The isomerisation reactions of isoprene peroxys regenerate HOx ($HO_2 + OH$) radicals, in part directly (as co-products of the HPALDs and of the dihydroperoxycarbonyls formed from the 1,4 H-shift of the DIHPCARPs, see Sect. 2.1.1) and in part from the subsequent reactions of the stable products (Peeters et al., 2014; Wennberg et al., 2018), although our recently proposed enol-forming pathway in the fast photolysis

Geosci. Model Dev. Discuss., https://doi.org/10.5194/gmd-2018-316
Manuscript under review for journal Geosci. Model Dev.
Discussion started: 19 December 2018

Geoscientific Model Development Discussions

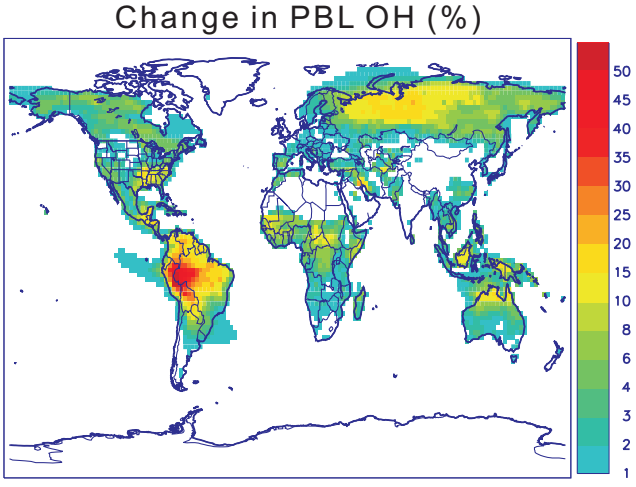

Figure 3. Calculated change (in %) in boundary layer OH concentration upon inclusion of isomerisation reactions of isoprene peroxy radicals (column average, July 2013).

of several key hydroperoxycarbonyls (e.g. HPACET and HPAC) decreases substantially the recycling of OH compared with the previous assumption of O−OH bond scission. The overall impact of isoprene peroxy radical isomerisation reactions on boundary-layer averaged OH concentrations reaches up to about 50% over Western Amazonia and 15% over Southeastern U.S. and Siberia in July (Fig. 3), whereas their impact on HO_2 is comparatively lower, by up to a factor of ∼2 over Amazonia. The isomerisation reactions lead also to reduced isoprene nitrate formation, by up to ∼40% over Amazonia, as the $RO_2 + NO$ reactions compete with unimolecular reactions. The decreased NOx loss through organic nitrate formation and partial removal implies longer NOx effective lifetime and concentrations (by a few % over Amazonia), in spite of the higher OH levels and increased NOx loss through $NO_2 + OH$. These changes lead to slightly enhanced O_3 concentrations over Amazonia (a few percent). The impact on HCHO concentrations and vertically-integrated columns is very small, also of the order of a few percent at most.

The dry or wet deposition of organic (peroxy-)nitrates and the irreversible sink of organic nitrates through hydrolysis or other processes on aerosols are significant net sinks of NOx over vegetated areas (Browne et al., 2014; Romer et al., 2016; Fisher et al., 2016). As shown on Fig. 4, the combined deposition and aerosol sink of organic (peroxy-)nitrates is found to be the dominant sink of NOx over rainforests in South America and Africa, as well as over boreal forests in Siberia and Canada during the summer. This fraction even exceeds 70% over the most remote areas (e.g. Western Amazonia) where high isoprene and low NOx levels both contribute to low OH concentrations (of the order of 10^6 molec. cm^{-3} during daytime in the boundary layer). These estimates should be considered with caution given the large uncertainties in the assumed aerosol uptake coefficient and poor understanding of aerosol chemical processes. Over the Southeastern U.S. (80-94.5°W, 29.5-40°N) during August-September 2013, the MAGRITTE model calculations (regional version over the U.S., 0.5° resolution) suggest that the NOx sink through aerosol hydrolysis amounts to 14.5% of NOx emissions in the region, whereas the deposition of organic nitrates and peroxynitrates account for additional 7 and 5% of NOx emissions. The estimated total net loss of NOx through $RONO_2$ formation amounts therefore to 21.5% of NOx emissions, in good agreement with previous calculations using the GEOS-Chem model (Fisher et al., 2016) (21%). This agreement might be partly fortuitous, given the important differences in the treatment of $RONO_2$ aerosol sink: a unique uptake coefficient (0.005) was used by Fisher et al. (2016) for all isoprene nitrates except nitroxyacetone and ethanal nitrate, whereas only

Geosci. Model Dev. Discuss., https://doi.org/10.5194/gmd-2018-316
Manuscript under review for journal Geosci. Model Dev.
Discussion started: 19 December 2018

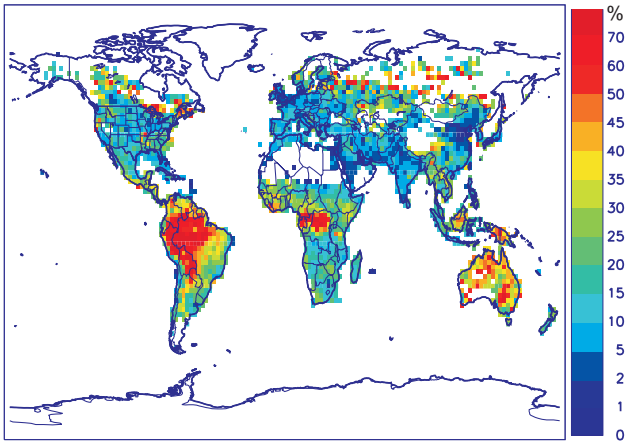

Figure 4. Percentage ratio of annual NOx net loss due to organic nitrate formation (i.e., their combined aerosol sink and deposition sink) to the total annual NOx emission. Blank areas are those with annually-averaged NOx emissions lower than $5 \cdot 10^9$ molec. cm^{-2} s^{-1}.

tertiary nitrates are assumed to undergo aerosol hydrolysis in our study (with γ=0.1). Non-tertiary nitrates might partition to the aerosol phase and possibly undergo processes preventing their eventual release to the gas-phase, in which case the overall NOx sink calculated here is underestimated.

3.3 Model evaluation against SEAC^{4}RS campaign measurements

The regional model simulation over the U.S. is evaluated against aircraft measurements of the NASA SEAC^{4}RS (Studies of Emissions and Atmospheric Composition, Clouds and Climate Coupling by Regional Surveys) campaign in August-September 2013 (Toon et al., 2016). For the most part, the SEAC^{4}RS took place over the Southeastern U.S. in areas characterized by high emissions of isoprene and other BVOCs. The observations discussed below are those obtained on the NASA DC-8 (www-air.larc.nasa.gov/missions/merges/) between 9h and 17h local time. Biomass burning plumes, urban plumes and stratospheric air are excluded from the analysis (diagnosed with $[CH_3CN] > 225$ ppt, $[NO_2] > 4$ ppbv, and $[O_3]/[CO] > 1.25$, respectively) (Travis et al., 2016).

Figure 5 present the observed and calculated average profiles of ozone, NO_2 and VOC oxidation products. As noted above, the NOx anthropogenic emissions used in the model were strongly reduced, relative to NEI official estimations, in order to match the SEAC^{4}RS observations for NO_2 (also NO) and improve the agreement for ozone, consistent with the results of Travis et al. (2016). The model is in excellent agreement with the HCHO profile measured by the Compact Atmospheric Multispecies Spectrometer (CAMS) (Richter et al., 2015), with only about 4% average overestimation below 4 km altitude, whereas a model underestimation of 8% is found relative to HCHO measurements by laser-induced-fluorescence (NASA GSFC ISAF instrument, Cazorla et al. (2015), not shown on Fig. 5). The model performance is also fairly good for the major products of isoprene + OH, with moderate overestimations of 21%, 8% and 30% for MVK+MACR, ISOPN (the family of primary hydroxynitrates from isoprene) and ISOPOOH, respectively. Note that the modelled MVKMAC accounts for the presumed interference of ISOPOOH in the measurement, as described in Müller et al. (2018). This correction increases MVKMAC by ∼10% on average for this campaign. The good consistency between the model results for the major high-NOx and low-NOx isoprene oxidation products lends confidence in the major steps of the mechanism. The underestimation for IEPOX (-18% below 4 km) is moderate in view of the highly uncertain aerosol sink (∼30% of the total IEPOX sink in the model simulation), without which the model would largely

Geosci. Model Dev. Discuss., https://doi.org/10.5194/gmd-2018-316
Manuscript under review for journal Geosci. Model Dev.
Discussion started: 19 December 2018

overestimate IEPOX observations. Not shown on Fig. 5, the model-calculated HPALD concentrations (peaking at about 20 pptv at ∼0.5 km) are about a factor of 5 lower than the Caltech CIMS (Chemical Ionisation Mass Spectrometry) measurement at the molecular weight of 116 which was previously thought to consist only (or mainly) of the HPALDs (Crounse et al., 2011; Travis et al., 2016). However, this CIMS signal includes very probably a large contribution of non-HPALD compounds presumed to be longer-lived than the HPALDs (Paul Wennberg, pers. comm., 2017).

The slightly too low ISOPN/MVKMAC ratio in the model (0.0364 vs. 0.0408) could indicate an overestimation of ISOPN aerosol sink, although the measurement uncertainties (∼30% for ISOPN, Fisher et al. (2016)) preclude a firm assessment. Aerosol hydrolysis represents ∼75% of the total sink of the tertiary hydroxynitrate ISOPBNO3 in the model (average over the model domain) or about 40% of the total ISOPN sink. On the other hand, the model overestimation of the secondary isoprene nitrates (MVKNO3+MACRNO3) shown on Fig. 5 suggests either a too high production or an underestimated sink. The main precursor of MACRNO3 being ISOPBNO3 which undergoes rapid aerosol hydrolysis, its production rate is much lower than that of MVKNO3, formed mainly from the OH-reaction of the secondary nitrate ISOPDNO3 ($CH_2{=}C(CH_3)CH(ONO_2)CH_2OH$). MACRNO3 being also much shorter-lived than MVKNO3 due to its faster photolysis (Müller et al., 2014) and its fast assumed aerosol hydrolysis sink, its abundance is very low, contributing for less than 1% of the sum MVKNO3+MACRNO3. The model overestimation could therefore be due to unaccounted aerosol reactions of either MVKNO3 or of its precursor, ISOPDNO3. The model overestimation for nitroxyacetone (NOA) reaches almost a factor of 3, in contrast with the GEOS-Chem underestimation found by Fisher et al.. This compound is mainly produced from multiple reaction sequences in the NO_3-initiated oxidation mechanism of isoprene. Although isoprene oxidation by NO_3 is primarily a nighttime process, NOA is formed after several oxidation steps favored by daylight. Our isoprene + NO_3 mechanism is more detailed and in line with the recent mechanistic conclusions from laboratory studies (Wennberg et al., 2018), but it still bears large uncertainties due to its high complexity. In addition, reactions of either NOA or of its precursors (NISOPOOHD, NISOPOOHB, ISOPCNO3, NC4CHO) on aerosols could explain part of the overestimation. Finally, the model might overestimate nitrate radical concentrations and therefore also the importance of NO_3 as oxidant of isoprene. Although the reactions of NO_3 with all major peroxy radicals are taken into account in the model, many potentially significant reactions with unsaturated oxidation products of isoprene (e.g. MVK, ISOPOOH, NISOPOOHB and NISOPOOHD, MCO3H, MPAN, etc.) are neglected in this mechanism (as in the MCM and other mechanisms). A careful assessment of the role of these reactions might be in order.

Despite the model overestimation for both NOA and MVKNO3+MACRNO3, the model underestimates the SEAC^{4}RS measurement for $RONO_2$ (the sum of all organic nitrates) by almost a factor of two. A similar model underestimation was found by Fisher et al. (2016). Part of the discrepancy might be due to a misrepresentation of alkyl and hydroxyalkyl nitrates from other precursors than isoprene. Nitrates from ethane, propane, ethene and propene oxidation are included in MAGRITTE, but their concentrations are largely underestimated with respect to SEAC^{4}RS observations (not shown on Fig. 5), in part due to underestimations of precursors emissions, in particular for ethane, propane and propene. However, these nitrates account for only a small part of the $RONO_2$ bias (∼16 pptv altogether out of 120 pptv below 4 km) based on SEAC^{4}RS observations and model results. Nitrates from monoterpenes and higher alkanes are crudely included in the model, and their contribution (11 and 19 pptv during SEAC^{4}RS) could be underestimated. Methylnitrate is well reproduced by the model (Fig. 5), but it makes only a very small contribution (∼5 ppt). The good agreement validates the low nitrate yield used in the mechanism ($2{\cdot}10^{-4}$ at room conditions, see Note N63) for the CH_3O_2 + NO reaction, well below the experimental determination (1% ± 0.7% in tropospheric conditions) of Butkovskaya et al. (2012). Although a higher yield ($\sim 3{\cdot}10^{-4}$) would still remain compatible with the SEAC^{4}RS measurement (by assuming lower oceanic emissions), much higher values as reported by Butkovskaya et al. would lead to huge overestimations of CH_3ONO_2 mixing ratios in the troposphere.

Geosci. Model Dev. Discuss., https://doi.org/10.5194/gmd-2018-316
Manuscript under review for journal Geosci. Model Dev.
Discussion started: 19 December 2018

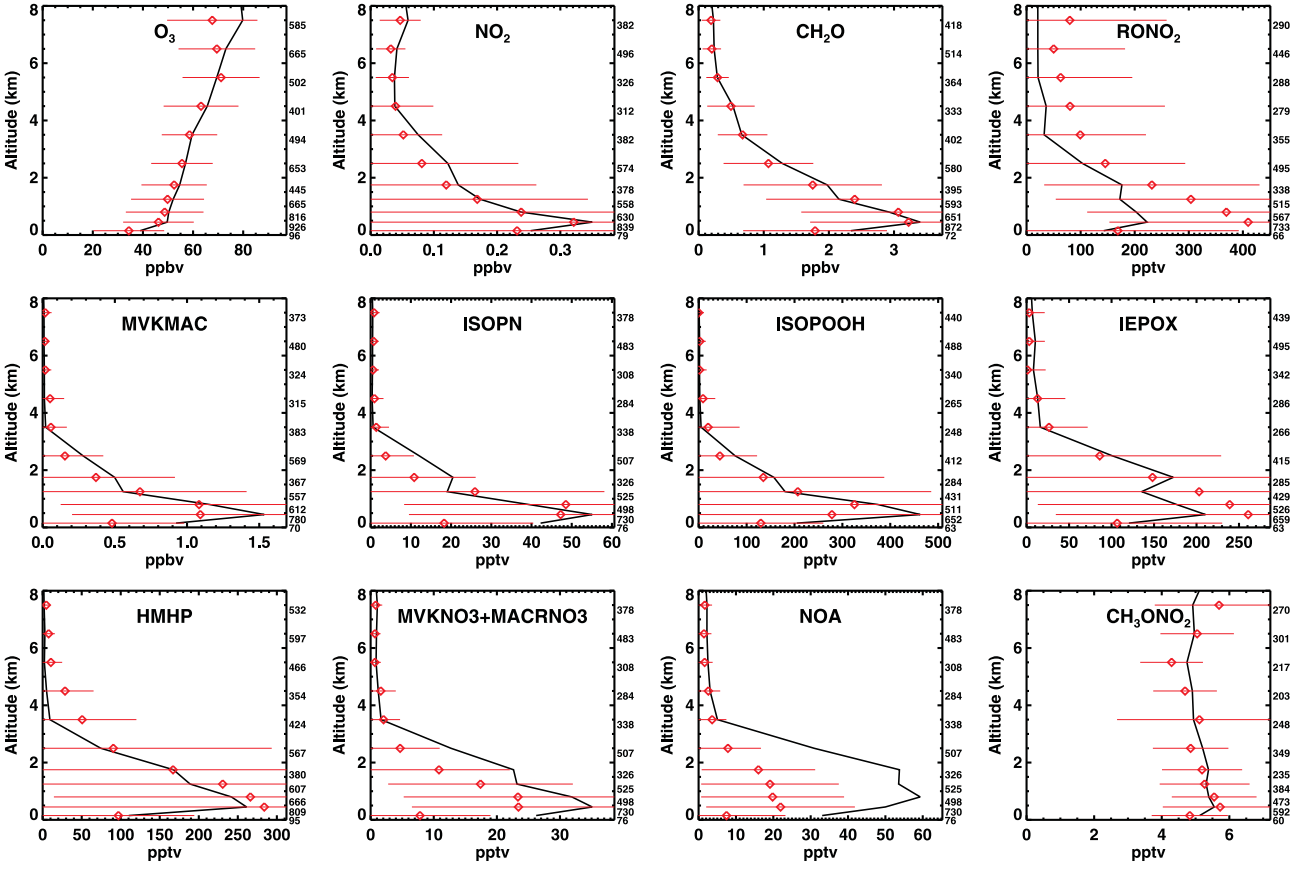

Figure 5. Observed (red symbols) and modelled (black lines) mean profiles of ozone, NO_2, and major VOC oxidation products over North America during the SEAC^{4}RS campaign. The number of measurements per altitude bin is indicated on the right for each plot. The vertical bin interfaces are 0, 0.3, 0.6, 1, 1.5 km, and from 2 to 8 km by 1 km. The horizontal lines indicate the standard deviation of the measurements within each vertical bin. MVKMAC stands for the sum MVK+MACR+0.44 ISOPOOH.

3.4 Global budget of formic and acetic acid

The calculated global photochemical source of formic acid amounts to 5.5 TgC or 21 Tg(HCOOH) per year (Table 5). Although the model simulation incorporates newly proposed formation mechanisms, as detailed below, this total is lower than several previous model estimations (Paulot et al., 2011; Stavrakou et al., 2012; Millet et al., 2015), for several reasons. Firstly, the global isoprene source in our simulation (366 TgC/yr) is near the low end of the range of previous estimates (Arneth et al., 2011; Sindelarova et al., 2014). Furthermore, the formation of HCOOH in the oxidation of glycolaldehyde and hydroxyacetone implemented in several studies is omitted here, since the original experimental findings by Butkovskaya et al. (2006a, b) could not be confirmed (Orlando et al., 2012) and might not be effective in atmospheric conditions. HCOOH production from isoprene ozonolysis (1 TgC/yr) is lower than previous estimates (e.g. 1.8 and 2.3 TgC/yr in Paulot et al. (2011) and Stavrakou et al. (2012), respectively) despite our high assumed yield (0.58) of stabilized Criegee (CH_2OO). This is due to the combination of (1) low direct formation yield of HCOOH in the CH_2OO reaction with the water dimer (Sheps et al., 2017),

Geosci. Model Dev. Discuss., https://doi.org/10.5194/gmd-2018-316
Manuscript under review for journal Geosci. Model Dev.
Discussion started: 19 December 2018

Geoscientific Model Development Discussions
Open Access
EGU

Table 5. Global sources of HCOOH in the model simulation.

	Tg(C)/yr	Tg(HCOOH)/yr
Direct emissions		
Biomass burning	0.78	3.0
Biogenic	1.46	5.6
Anthropogenic	0.58	2.2
Photochemical production		
$ISOP + O_3$	0.99	3.8
Other Alkenes ozonolysis	0.52	2.0
$C_2H_2 + OH$	0.69	2.6
$APIN + OH$	0.42	1.6
$VA + OH$	1.87	7.2
from $CH_3CHO + h\nu$	*0.76*	*2.9*
from $OCHCH_2OOH + h\nu$	*1.11*	*4.3*
$ISOP + OH$ (various pathways)	1.13	4.3
$HMAC/HMVK + OH$	*0.58*	*2.2*
$ISOPOOH + OH$	*0.45*	*1.7*
$HMML + OH$	*0.12*	*0.5*
Total source		
Global	8.4	32

(2) high deposition sink of HMHP (over ∼50% of its global production) resulting from its high solubility and high deposition velocities over forests (Nguyen et al., 2015b; Müller et al., 2018), and (3) the HCOOH yield of only 0.45 in the reaction of HMHP with OH recently estimated from experiment (Allen et al., 2018). The very good model agreement against the SEAC^{4}RS measurements of HMHP over the Southeastern U.S. suggests an essentially correct model representation of its production and sink rate, and therefore of the contribution of alkene ozonolysis to the budget of formic acid.

Vinyl alcohol (VA), originally proposed as possible source of formic acid by Archibald et al. (2007), received full attention when acetaldehyde phototautomerization to VA was shown in the laboratory to be efficient (Andrews et al., 2012) and represent a sizable source of formic acid of the order of 3 TgC/yr (Cady-Perreira et al., 2014; Millet et al., 2015). However, a recent, more detailed experimental evaluation of the phototautomerization yield led to a downward revision of the global source to about 0.8 TgC/yr (Shaw et al., 2018), in good agreement with our model calculations (Table 5). This source could be even lower if VA tautomerizes back to acetaldehyde (da Silva et al., 2010), but acid-catalyzed VA tautomerization was shown to be negligible, and aerosol-mediated tautomerization remains speculative (Peeters et al., 2015).

Another source of VA and of other enols has been identified: the photolysis of hydroperoxycarbonyls (Liu et al., 2018). Our results (Table 5) indicate that the photolysis of hydroperoxyacetaldehyde (HPAC) is a larger source of VA (and therefore of HCOOH) than CH_3CHO tautomerization. The sources of HPAC (5.6 Tg/yr globally) include the oxidation of acetaldehyde by OH (30% of total), the photolysis of MVKOOH (31%) and several other pathways in isoprene oxidation, in particular through the isoprene hydroxyperoxy radical 1,6 H-shift

Geosci. Model Dev. Discuss., https://doi.org/10.5194/gmd-2018-316
Manuscript under review for journal Geosci. Model Dev.
Discussion started: 19 December 2018

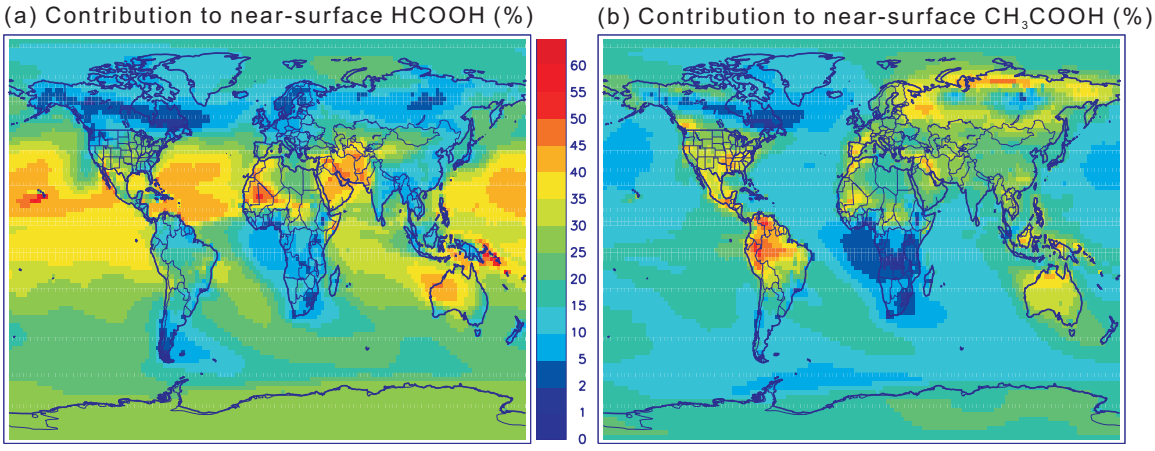

Figure 6. Calculated percentage contribution of hydroperoxycarbonyl photolysis to near-surface concentrations of (a) formic and (b) acetic acid for the month of July.

pathway as confirmed experimentally (Crounse et al., 2011; Teng et al., 2017). In addition, the photolysis of the HPALDs, of C_4 hydroperoxydicarbonyls (HPDIAL and HPKETAL) also generated from the isomerisation pathway, and of nitroxyenals (NC4CHO) formed from isoprene + NO_3 all lead partly to keto-enols (HMAC and HMVK) which are oxidized for a large part into HCOOH following their reaction with OH, following a mechanism similar as for VA (So et al., 2014). The photolysis and deposition of HMVK and HMAC are found to be minor sinks (∼5% and 10% of their global sink, respectively). Finally, hydroperoxycarbonyls formed from minor pathways in the ISOPOOH degradation mechanism are photolyzed in part into other enol compounds, which are partly oxidized to HCOOH (along with MVK or MACR). The estimated combined HCOOH source due to hydroperoxycarbonyl photolysis amounts to 2.1 TgC/yr, exceeding in magnitude the source due to alkene ozonolysis (1.5 TgC/yr). As seen on Fig. 6(a), the contribution of this source to nea-surface HCOOH concentrations is highest over remote oceanic areas (up to 50%) and is comparatively much lower over biomass burning and biogenic emission areas. This is partly due to HPAC formation due to oceanic acetaldehyde emissions, and to the significant share of direct biogenic and pyrogenic emissions to the global HCOOH budget (Table 5). Nevertheless, hydroperoxycarbonyl photolysis enhances HCOOH levels by ∼15% (up to 120 pptv) near the surface over vegetated areas such as Amazonia (Fig. 6(a)), and by $>$ 30% at higher tropospheric levels (not shown).

The largest known photochemical source of CH_3COOH is the reaction of acetylperoxy radical CH_3CO_3 with peroxy radicals (HO_2 and RO_2), amounting to ∼16 TgC/yr globally (Table 6). This is very consistent with a previous model estimate (18 TgC/yr) by Paulot et al. (2011) but significantly lower than the estimate of Khan et al. (2018) (close to 30 TgC/yr). Our calculated contribution of $CH_3CO_3 + RO_2$ reactions (∼2.3 TgC/yr) is smaller than in Paulot et al. (2011) (∼5.6 TgC/yr). It could be underestimated if the CH_3COOH-forming channel ratio for the reactions of CH_3CO_3 with major non-tertiary peroxy radicals would be significantly higher than the value assumed here for most reactions (0.1), which is based on the case of $CH_3CO_3 + CH_3O_2$ (Atkinson et al., 2006). The high reported CH_3COOH yield (0.5) (Atkinson et al., 2006) in the case of $CH_3CO_3 + CH_3C(O)CH_2O_2$ is implemented in our mechanism but assumed to be atypical.

The additional source of acetic acid due to the photolysis of hydroperoxyacetone (HPACET) and involving the oxidation of methylvinyl alcohol (MVA) by OH enhances the estimated global photochemical production of CH_3COOH by 7 TgC/yr or 43% (Table 6). The global source of HPACET (32 TgC/yr) are dominated by the acetonyl peroxy radical reaction with HO_2 (15 TgC/yr) and by the reactions of the dihydroperoxyaldehyde (DIHPCHO) formed in the isoprene peroxy isomerisation pathway, following the assumption of fast 1,4 H-shift

Geosci. Model Dev. Discuss., https://doi.org/10.5194/gmd-2018-316
Manuscript under review for journal Geosci. Model Dev.
Discussion started: 19 December 2018

Geoscientific Model Development Discussions

Table 6. Global sources of CH_3COOH in the model simulation.

	Tg(C)/yr	Tg(CH_3COOH)/yr
Direct emissions		
Biomass burning	5.7	14.3
Anthropogenic	2.6	6.6
Photochemical production		
$CH_3CO_3 + HO_2$	13.8	34.5
$CH_3CO_3 + RO_2$	2.3	5.7
$C_3H_6 + O_3$	0.1	0.2
HPACET + hν (+OH)	6.9	17.2
from isoprene oxidation	*4.4*	*11.0*
from acetone oxidation	*1.7*	*4.1*
other	*0.8*	*2.1*
Total source		
Global	31.4	78.5

of DIHPCARP2 (14 TgC/yr from DIHPCHO photolysis, 2 TgC/yr from DIHPCHO + OH). In absence of 1,4 H-shift, HPACET would be produced anyway, directly from the reactions of DIHPCARP2 with NO or HO_2 (see Table 2). The precise mechanisms for the formation of HPACET (also HPAC) in the isomerisation pathway are uncertain, but experimental evidence shows clearly that these compounds are formed. Photolysis accounts for 77% of the global HPACET sink, whereas reaction with OH and deposition account for 19 and 4%, respectively. The only significant sink of MVA, the main product of HPACET photolysis, is reaction with OH, assumed to form CH_3COOH (along with OH and HCHO) with a 50% yield, following a mechanism similar as for VA+OH (So et al., 2014). The calculated contribution of HPACET photolysis to the CH_3COOH concentration (Fig. 6(b)) is highest over forests (except in areas impacted by biomass burning), up to 40% (200 pptv) over Southeastern U.S., and 50% (up to 300 pptv) over Amazonia.

3.5 Global budget of glyoxal

The global sources of glyoxal as calculated by the model are summarized in Table 7. Contrary to previous model evaluations (Fu et al., 2008; Stavrakou et al., 2009b; Li et al., 2016; Chan Miller et al., 2017; Silva et al., 2018), isoprene oxidation is not found to be a very large source of glyoxal, except for the significant contribution of glycolaldehyde oxidation by OH which amounts to ∼4.7 TgC/yr of glyoxal. This has several causes. The oxidation of isoprene by NO_3 is now an almost negligible glyoxal source in our mechanism (as in the Caltech mechanism), whereas an overall yield of 35% glyoxal was inferred from the MCMv3.2 mechanism (Stavrakou et al., 2009b). Direct glyoxal formation from ISOP + OH with a yield of ∼2% at high-NOx through the δ-ISOPO2 + NO pathway (Galloway et al., 2011) becomes negligible under ambient atmospheric conditions due to the fast unimolecular reactions (O_2-elimination and 1,6 H-shift) of δ-ISOPO2 radicals resulting in very small δ-ISOPO2 fractions in the atmosphere (Peeters and Nguyen, 2012; Peeters et al., 2014).

Furthermore, the oxidation of isoprene hydroxyepoxides (IEPOX), which was believed to be a potentially significant glyoxal source (Bates et al., 2014; Li et al., 2016), is found to produce very little glyoxal in atmospheric conditions due to the proposed fast 1,4 H-shift in the peroxy radicals IEPOXBO2 ($HOCH_2CH(OH)C(CH_3)(O2)CHO$) formed from IEPOX + OH (Wennberg et al., 2018), outcompeting

Geosci. Model Dev. Discuss., https://doi.org/10.5194/gmd-2018-316
Manuscript under review for journal Geosci. Model Dev.
Discussion started: 19 December 2018

Geoscientific Model Development Discussions

Table 7. Global sources of glyoxal in the model simulation.

	Tg(C)/yr	Tg(GLY)/yr
Direct emissions		
Biomass burning	1.58	3.8
Photochemical production		
$C_2H_2 + OH$	2.39	5.8
Aromatics + OH	3.78	9.1
Monoterpenes oxidation	3.67	8.9
GLYALD + OH	4.69	11.3
IEPOX + OH	0.06	0.1
$OCHCH_2OOH + OH$	0.39	0.9
HPALDs	0.35	0.8
ISOPOOH + OH	0.89	2.2
ISOP + NO_3	0.12	0.3
Other pathways in isoprene oxidation	0.89	2.2
Total source		
Global	18.8	45

its reactions with NO and HO_2 (see Note N17). The 1,4 H-shift rate is very uncertain and could be overestimated, but even a factor of 10 reduction of the rate would imply a fairly small glyoxal production due to IEPOX + OH (0.6 TgC/year).

Chan Miller et al. (2017) suggested that the DIHPCARPs from the 1,6 H-shift of δ-ISOPO2 partly undergoes a 1,5 H-shift to a dihydroperoxy dicarbonyl (DHDC, e.g. $OCHCH(OOH)C(CH_3)(OOH)CHO$) which would quickly photolyze to OH + an oxy radical decomposing to glyoxal and other products. However, even under the assumption that the 1,5 H-shift would be competitive, and although DHDC photolysis should indeed be very rapid, OH elimination should be negligible (Liu et al., 2018), whereas the expected preferred dissociation pathway involves formation of a formyl radical + OH + hydroperoxy dicarbonyls which might form glyoxal upon further photolysis, but at much lower yields than in the mechanism of Chan Miller et al..

Finally, due to the fast photolysis of hydroperoxyacetaldehyde (HPAC), the fraction of the formed HPAC reacting with OH is small (23%), and only a fraction of it gives glyoxal (along with OH).

There are still large uncertainties in the mechanism, however, and direct experimental constraints on the glyoxal yields in real atmospheric conditions are lacking. Further work is needed to refine the above estimates and identify additional sources, since model evaluations against spaceborne and in situ glyoxal measurements suggest a large photochemical source (Stavrakou et al., 2009b; Li et al., 2016; Silva et al., 2018).

4 Conclusions

We have presented a new BVOC oxidation mechanism for use in large-scale tropospheric chemistry-transport models. Its main focus is on isoprene, owing to its high chemical complexity and very large share of global BVOC emissions: of the 99 organic chemical species

Geosci. Model Dev. Discuss., https://doi.org/10.5194/gmd-2018-316
Manuscript under review for journal Geosci. Model Dev.
Discussion started: 19 December 2018

included in the mechanism, 91 compounds (71 stable compounds and 20 radicals) are involved in the chemical degradation of isoprene alone. This mechanism incorporates all major mechanistic advances from recent studies, in particular those affecting the budget of HO_x and NO_x radicals. Mainly thanks to HO_x formation in isomerisation reactions of isoprene-derived peroxy radicals, and further OH recycling through secondary reactions, the mechanism goes a long way in explaining the large underestimations of modelled OH concentrations in isoprene-rich, NO_x-poor areas which prompted the community to search for OH-recycling mechanisms about a decade ago (Lelieveld et al., 2008; Hofzumahaus et al., 2009). The representation of monoterpene chemistry is much cruder, due to the still very poor understanding of its formidably complex mechanism. The simple monoterpene mechanism included here is only meant to provide an approximate reproduction of the yield of key OVOCs produced in their oxidation, based on box model simulations with the Master Chemical Mechanism (MCM).

Although smaller than e.g. the Caltech mechanism or the MCMv3.3.1, this isoprene mechanism is larger than most mechanisms implemented in large-scale models, and probably more detailed than strictly needed for many modelling purposes, such as the prediction of isoprene impacts on HOx, NOx, and ozone. Reduction techniques could be implemented to lighten the mechanism while retaining its most essential predictions, but since its current size and degree of detail can be handled by MAGRITTE, we find it useful to keep it as is in order to facilitate further analysis of model results and future mechanism updates. As pointed out by Wennberg et al. (2018), the distinction between isoprene peroxys resulting from OH addition to C1 and C4 is essential in view of the order-of-magnitude difference in bulk isomerisation rates (Fig. 2) and in the difference in the nature of the resulting products. For example, the distinction impacts also the fate of the first-generation hydroxynitrates, given the efficient hydrolysis of the tertiary nitrate formed following C1-addition. Note that the hydrolysis rates remain very uncertain. Due to our assumption of very fast tertiary nitrate hydrolysis ($\gamma = 0.1$), about 75% of the global sink of the 1,2-isoprene hydroxynitrate is due to this process. The rate might be possibly too high, but it accounts for the fast overall hydroxynitrate loss observed in campaign measurements. This aspect of the mechanism will be revised when quantitative experimental determinations of heterogeneous processes and rates will become available.

Although many parts of our isoprene mechanism rely on the Caltech mechanism, there are notable differences. For example, whereas the DIHPCARPs formed from the 1,6 H-shift of the Z-δ-hydroxyperoxy radicals are bypassed in the reduced Caltech mechanism and replaced by simple products, they are assumed here to undergo fast 1,4 H-shift to form CO, OH and C_4 dihydroperoxycarbonyl compounds. The further chemistry of the latter compounds leads in part to the same simple products implemented in the Caltech mechanism, although at different (and variable) yields. Other pathways might be possible, however (Novelli et al., 2018b); more work will be needed to reliably assess this important chemistry (60–75% of the 1,6-isomerisation pathway, or $\sim$35 Tg(C) yr^{-1}). In that context, rationalizing the laboratory constraint on the HPAC and HPACET yields is clearly desirable.

A major difference between the present and previous isoprene mechanisms lies in the very fast photolysis of α-hydroperoxycarbonyls (Liu et al., 2018), leading in several important cases to the formation of an enol which is for a large part oxidized by OH into formic or acetic acid. Also new to this mechanism, HCOOH is formed from the OH-oxidation of keto-enols (HMVK and HMAC) produced from the photolysis of several multifunctional carbonyls. This pathway of HMVK/HMAC is all the more relevant as their photolysis is likely much slower than previously thought. More generally, the oxidation of enols formed from the oxidation of isoprene, acetaldehyde and acetone by OH is a potentially large, previously unsuspected source of carboxylic acids here estimated at 8 Tg(HCOOH) yr^{-1} (slightly larger than the contribution of alkene ozonolysis) and 17 Tg(CH_3COOH) yr^{-1}. In both cases, this source amounts to >20% of the total identified global source, which remains however largely insufficient to account for the atmospheric observations (e.g., Paulot et al. (2011)). Further experimental and theoretical studies of multifunctional carbonyl photolysis and enol oxidation are required to confirm and refine those estimates. The source could be larger due to the neglected contribution of hydroperoxycarbonyls formed from higher anthropogenic NMVOCs (e.g.

higher ketones and their precursors) and possibly monoterpenes. Moreover, the contribution of acetaldehyde photooxidation could be much higher than estimated here, considering the large underestimation of its calculated concentrations at remote locations (Read et al., 2012).

Evaluation of MAGRITTE and of its new chemical mechanism against the SEAC^{4}RS campaign measurements indicates a good overall model performance for the main isoprene oxidation products. Heterogeneous reactions of IEPOX and organic nitrates on aerosols are a large area of uncertainty, with suggestions of heterogeneous sink overestimation for tertiary organic nitrates and sink underestimations for other isoprene nitrates. The total $\mathrm{RONO_2}$ concentrations are underestimated by almost 50%, possibly due to misrepresentations of nitrates due to e.g. monoterpenes and anthropogenic precursors. The low observed $\mathrm{CH_3ONO_2}$ levels are well reproduced by the model, providing a strong indication for a very low nitrate yield ($< 3 \cdot 10^{-4}$) in the $\mathrm{CH_3O_2}$+NO reaction.

Code and data availability. The chemical mechanism is available at http://tropo.aeronomie.be/index.php/models/magritte in KPP (Kinetic Pre-Processor) format (doi:10.18758/71021042, last access: 15 December 2018). Other relevant subroutines of the MAGRITTE model can be made available upon request (email: jfm@aeronomie.be). The SEAC^{4}RS airborne trace gas measurements are available from the NASA LaRC Airborne Science Data for Atmospheric Composition (https://www-air.larc.nasa.gov/missions/merges/, last access: 15 December 2018).

Author contributions. JFM and JP elaborated the mechanism and drafted the manuscript, JFM and TS conducted the model calculations, all authors analyzed the model results.

Competing interests. The authors declare that they have no conflict of interest.

Acknowledgements. This research was supported by the Belgian Science Policy Office through the projects TROVA (2016–2018) within the ESA/PRODEX programme, OCTAVE (2017–2021) within the BRAIN-be research programme, and BIOSOA within the SSD program (2006-2010). We gratefully acknowledge the PIs and data managers of the NASA SEAC^{4}RS campaign for the measurements used in this work.

Geosci. Model Dev. Discuss., https://doi.org/10.5194/gmd-2018-316
Manuscript under review for journal Geosci. Model Dev.
Discussion started: 19 December 2018

Geoscientific Model Development Discussions
Open Access
EGU

References

Allen, H. M., Crounse, J. D., Bates, K. H., Teng, A. P., Krawiec-Thayer, M. P., Rivera-Rios, J. C., Keutsch, F. N., St. Clair, J. M., Hanisco, T. F., Moller, K. H., Kjaergaard, H. G., and Wennberg, P. O.: Kinetics and product yields of the OH initiated oxidation of hydroxymethyl hydroperoxide, J. Phys. Chem. A, 122, 6292–6302, 2018.

Anderson, D. C., Loughner, C. P., Diskin, G., Weinheimer, A., Canty, T. P., Salawitch, R. J., Worden, H. M., Fried, A., Mikoviny, T., Wisthaler, A., and Dickerson, R. R.: Measured and modeled CO and NOy in DISCOVER-AQ: An evaluation of emissions and chemistry over the eastern US, Atmos. Environ., 96, 78–87, 2014.

Andrews, D., Heazlewood, B. R., Maccarone, A. T., Conroy, T., Payne, R. J., Jordan, M. J. T., and Kable, S. H.: Photo-tautomerization of acetaldehyde to vinyl alcohol: A potential route to tropospheric acids, Science, 337, 1203–1208, 2012.

Archibald, A., R., M. M., Taatjes, C. A., Percival, C. J., and Shallcross, D. E.: Atmospheric transformation of enols: A potential secondary source of carboxylic acids in the urban troposphere, Geophys. Res. Lett., 34, L21801, 2007.

Arey, J., Aschmann, , S. M., Kwok, E. S. C., and Atkinson, R.: Alkyl nitrate, hydroxyalkyl nitrate, and hydroxycarbonyl formation from the NOx-air photooxidations of C_5-C_8 n-alkanes, J. Phys. Chem. A, 105, 1020–1027, 2001.

Arneth, A., Schurgers, G., Lathière, J., Duhl, T., Beerling, D. J., Hewitt, C. N., Martin, M., and Guenther, A.: Global terrestrial isoprene emission models: sensitivity to variability in climate and vegetation, Atmos. Chem. Phys., 11, 8037–8052, 2011.

Asatryan, R., da Silva, G., and Bozzelli, J.W.: Quantum chemical study of the acrolein (CH_2CHCHO) + OH + O_2 reactions, J. Phys. Chem. A, 114, 8302–8311, 2010.

Assaf, E., Song, B., Tomas, A., Schoemaecker, C. and Fittschen, C.: The rate constant of the reaction between CH_3O_2 radicals and OH radicals revisited, J. Phys. Chem. A, 120, 8923–8932, 2016.

Assaf, E., Sheps, L., Whalley, L., Heard, D., Tomas, A., Schoemacker, C. and Fittschen, C.: The reaction between CH_3O_2 and OH radicals: Product yields and atmospheric implications, Environ. Sci Technol., 51, 2170–2177, 2017.

Assaf, E., Schoemacker, C., Vereecken, L., and Fittschen, C.: Experimental and theoretical investigation of the reaction of RO_2 radicals with OH radicals: Dependence of the HO_2 yield on the size of the alkyl group, Int. J. Chem. Kinet., 1–11, 2018.

Atkinson, R., Baulch, D. L., Cox, R. A., Crowley, J. N., Hampson, R. F., Hynes, R. G., Jenkin, M. E., Rossi, M. J., and Troe, J.: Evaluated kinetic and photochemical data for atmospheric chemistry: Volume II - gas phase reactions of organic species, Atmos. Chem. Phys., 6, 3625–4055, 2006.

Baeza-Romero, M. T., Glowacki, D. R., Blitz, M. A., Heard, D. E., Pilling, M. J., Rickard, A. R., and Seakins, P. W.: A combined experimental and theoretical study of the reaction between methylglyoxal and OH/OD radical: OH regeneration, Phys. Chem. Chem. Phys., 9, 4114–4128, 2007.

Barnes, I., Becker, K. H., Zhu, T.: Near UV absorption spectra and photolysis products of difunctional organic nitrates: Possible importance as NOx reservoirs, J. Atmos. Chem., 17, 353–373, 1993.

Baulch, D. L., Bowman, C. T., Cobos, C. J., Cox, R. A., Just, T., Kerr, J. A., Pilling, M. J., Stocker, D., Troe, J., Tsang, W., Welker, R. W., and Warnatz, J.: Evaluated kinetic data for combustion modeling: Supplement II, J. Phys. Chem. Ref. Data, 34, 2005.

Bates, K. H., Crounse, J. D., St Clair, J. M., Bennet, N. B., Nguyen, T. B., Seinfeld, J. H., Stoltz, B. M., and Wennberg, P. O.: Gas phase production and loss of isoprene epoxydiols, J. Phys. Chem. A, 118, 1237–1246, 2014.

Bates, K. H., Nguyen, T. B., Teng, A. P., Crounse, J. D., Kjaergaard, H. G., Stoltz, B. M., Seinfeld, J. H., and Wennberg, P. O.: Production and fate of C_4 dihydroxycarbonyl compounds from isoprene oxidation, J. Phys. Chem. A, 120, 106–117, 2016.

Bauwens, M., Stavrakou, T., Müller, J.-F., De Smedt, I., Van Roozendael, M., van der A, R. J., Wiedinmyer, C., Kaiser, J. W., Sindelarova, K., and Guenther, A. Nine years of global hydrocarbon emissions based on source inversion of OMI formaldehyde observations, Atmos. Chem. Phys., 16, 10133–10158, 2016.

Bauwens, M., Stavrakou, T., Müller, J.-F., Van Schaeybroeck, B., De Cruz, L., De Troch, R., Giot, O., Hamdi, R., Termonia, P., Laffineur, Q., Amelynck, C., Schoon, N., Heinesch, B., Holst, T., Arneth, A., Ceulemans, R., Sanchez-Lorenzo, A., and Guenther, A.: Recent past (1979–2014) and future (2070–2099) isoprene fluxes over Europe simulated with the MEGAN-MOHYCAN model, Biogeosciences, 15, 3673-3690, https://doi.org/10.5194/bg-15-3673-2018, 2018.

Berndt, T., Jokinen, T., Sipilä, M., Mauldin III, R. L., Herrmann, H., Stratmann, F., Junninen, H. and Kulmala, M.: H_2SO_4 formation from the gas-phase reaction of stabilized Criegee Intermediate with SO_2: Influence of water vapour content and temperature, Atmos. Environ., 89, 603–612, 2014.

Bossolasco, A., Farago, E. P., Schoemaker, C., and Fittschen, C.: Rate constant of the reaction between CH_3O_2 and OH radicals, Chem. Phys. Lett., 593, 7–13, 2014.

Bottorff, B., Lew, M. Rickly, P. and Stevens, P. S.: HOx radical chemistry in a forested environment during PROPHET-AMOS 2016: Model comparisons and radical budget, AGU (American Geophysical Union) Fall Meeting, Washington D. C., december 2018.

Browne, E. C., Min, K.-E., Wooldridge, P. J., Apel, E., Blake, D. R., Brune, W. H., Cantrell, C. A., Cubison, M. J., Diskin, G. S., Jimenez, J. L., Weinheimer, A. J., Wennberg, P. O., Wisthaler, A., and Cohen, R. C.: Observations of total $RONO_2$ over the boreal forest: NOx sinks and HNO_3 sources, Atmos. Chem. Phys., 13, 4543–4562, 2013.

Browne, E. C., Wooldridge, P. J., Min, K.-E., Cohen, R. C.: On the role of monoterpene chemistry in the remote continental boundary layer, Atmos. Chem. Phys., 14, 1225–1238, 2014.

Burkholder, J. B., Sander, S. P., Abbatt, J. P. D., Barker, J. R., Huie, R. E., Kolb, C. E., Kurylo, M. J., Orkin, V. L., Wilmouth, D. M., and Wine, P. H.: Chemical Kinetics and Photochemical Data for Use in Atmospheric Studies, Evaluation number 18. JPL Publication 15–10, Jet Propulsion Laboratory, Pasadena, 2015.

Butkovskaya, N. I., Pouvesle, N., Kukui, A., Mu, Y., and Le Bras, G.: Mechanism of the OH-initiated oxidation of hydroxyacetone over the temperature range 236-298 K, J.. Phys Chem. A, 110, 6833–6843, 2006a.

Butkovskaya, N. I., Pouvesle, N., Kukui, A., and Bras, G. L.: Mechanism of the OH-initiated oxidation of glycolaldehyde over the temperature Range 233-296 K, J. Phys. Chem., 110, 13492–13499, 2006b.

Butkovskaya, N. I., Kukui, A., and Le Bras, G.: Pressure and temperature dependence of methyl nitrate formation in the CH_3O_2 + NO Reaction, J. Phys. Chem. A, 116, 5972–5980, 2012.

Cady-Pereira, K. E., Chaliyakunnel, S., Shephard, M. W., Millet, D. B., Luo, M., and Wells, K. C.: HCOOH measurements from space: TES retrieval algorithm and observed global distribution, Atmos. Meas. Tech., 7, 2297–2311, 2014.

Calvert, J. G., Mellouki, A., Orlando, J., Pilling, M., and Wallington, T.: The mechanisms of atmospheric oxidation of the oxygenates, Oxford University Press, New York, 1619 pp., 2011.

Capouet, M., Peeters J., Nozière B. and Müller, J.-F.: Alpha-pinene oxidation by OH: simulations of laboratory experiments, Atmos. Chem. Phys., 4, 2285–2311, 2004.

Caravan, R. L., Khan, M. A. H., Z'ador, J., Sheps, L., Antonov, I. O., Rotavera, B., Ramasesha K. Au, K., Chen, M.-W., Rösch, D., Osborn, D. L., Fittschen, C., Schoemaecker, C., Duncianu, M., Frira, A., Dusanter, S., Tomas, A., Percival, C. J., Shallcross, D. E., and Taatjes, C. A.: The reaction of hydroxyl and methylperoxy radicals is not a major source of atmospheric methanol, Nat. Commun., 9, 4343, 2018.

Carter, W. P. L., and Atkinson, R.: Alkyl nitrate formation from the atmospheric photooxidation of alkanes; a revised estimation method, J. Atmos. Chem., 8, 165–173, 1989.

Cazorla, M., Wolfe, G. M., Bailey, S. A., Swanson, A. K., Arkinson, H. L., and Hanisco, T. F.: A new airborne laser-induced fluorescence instrument for in situ detection of formaldehyde thrthrough the troposphere and lower stratosphere, Atmos. Meas. Tech., 8, 541–552, 2015.

Chan, A. W. H., Galloway, M. M., Kwan, A. J., Chhabra, P. S., Keutsch, F. N., Wennberg, P. O., Flagan, R. C., and Seinfeld, J. H.: Photooxidation of 2-methyl-3-buten-2-ol (MBO) as a potential source of Secondary Organic Aerosol; Environ. Sci. Technol., 43, 4647–4652, 2009.

Chan Miller, C., Jacob, D. J., Marais, E. A., Yu, K., Travis, K. R., Kim, P. S., Fisher, J. A., Zhu, L., Wolfe, G. M., Keutsch, F. N., Kaiser, J., Min, K. E., Brown, S. S., Washenfelder, R., Gonzalez Abad, G., and Chance, K.: Glyoxal yield from isoprene oxidation and relation to formaldehyde: chemical mechanism, constraints from SENEX aircraft observations, and interpretation of OMI satellite data, Atmos. Chem. Phys., 17, 8725–8738, 2017.

Chao, W., Hsieh, J.-T., Chang, C.-H., Lin, J. J.-M.: Direct kinetic measurement of the reaction of the simplest Criegee intermediate with water vapor; Science, 347, 751–754, 2015.

Claeys, M., Graham, B., Vas, G., Wang, W., Vermeylen, R., Pashynska, V., Cafmeyer, J., Guyon, P., Andreae, M. O., Artaxo, P., and Maenhaut, W.: Formation of secondary organic aerosols through photooxidation of isoprene, Science 303, 1173–1176, 2004.

Crounse, J. D., Paulot, F., Kjaergaard, H. G., and Wennberg, P. O.: Peroxy radical isomerization in the oxidation of isoprene, Phys. Chem. Chem. Phys., 13, 13607–13613, 2011. Amendment: http://www.rsc.org/suppdata/cp/c1/c1cp21330j/addition.htm.

Crounse, J. D., Knap, H. C., Ørnsø, K. B., Jørgensen, S., Paulot, F., Kjaergaard, H. G., and Wennberg, P. O.: Atmospheric fate of methacrolein. 1. Peroxy radical isomerization following addition of OH and O_2, J. Phys. Chem. A, 116, 5756–5762, 2012.

Crounse, J. D., Nielsen, L. B., Jørgensen, S., Kjaergaard, H. K., and Wennberg, P. O.: Autoxidation of organic compounds in the atmosphere, J. Phys. Chem. Lett., 4, 3513–3520, 2013.

da Silva, G.: Carboxylic acid catalyzed keto-enol tautomerizations in the gas phase, Angewandte Chemie, 122, 7685–7687, 2010.

D'Ambro, E. L., Moller, K. H., Lopez-Hilfiker, F. D., Schobesberger, S., Liu, J., Shilling, J. E., Kjaergaard, H. G., and Thornton, J. A.: Isomerization of second-generation isoprene peroxy radicals: Epoxide formation and implications for Secondary Organic Aerosol yields, Environ. Sci. Technol., 51, 4978–7987, 2017.

Dee, D. P., Uppala, Simmons, A. J., Berrisford, P., Poli, P., Kobayashi, S., Andae, U., Balmaseda, M. A., Balsamo, G., Bauer, P., Bechtold, P., Beljaars, A. C. M., van de Berg, L., Bidlot, J., Bormann, N., Delsol, C., Dragani, R., Fuentes, M., Geer, A. J., Haimberger, L., Healy, S. B., Hersbach, H., Hólm, E. V., Isaksen, L., K P., Köhler, M., Matricardi, M., McNally, A. P., Monge-Sanz, B. M., Morcrette, J.-J., Park, B.-K., Peubey, C., de Rosnay, P., Tavolato, C., Thépaut, J.-N., and Vitart, F.: The ERA-Interim reanalysis: configuration and performance of the data assimilation system, Q. J. R. Meteorol. Soc, 137, 553–597, doi:10.1002/qj.828, 2011.

Fischer, E. V., Jacob, D. J., Millet, D. B., Yantosca, R. M., and Mao, J.: The role of the ocean in the global atmospheric budget of acetone, Geophys. Res. Lett., 39, L01807, 2012.

Fisher, J. A., Jacob, D. J., Travis, K., Kim, P. S., Marais, E. A., Chan Miller, C., Yu, K., Zhu, L., Yantosca, R. M., Sulprizio, M. P., Mao, J., Wennberg, P. O., Crounse, J. D., Teng, A. P., Nguyen, T. B., St. Clair, J. M., Cohen, R. C., Romer, P., Nault, B. A., Wooldridge, P. J., Jimenez, J. L., Campuzano-Jost, P., Day, D. A., Hu, W., Shepson, P. B., Xiong, F., Blake, D. R., Goldstein, A. H., Misztal, P. K., Hanisco, T. F., Wolfe, G. M., Ryerson, T. B., Wisthaler, A., and Mikoviny, T.: Organic nitrate chemistry and its implications for nitrogen budgets

in an isoprene- and monoterpene-rich atmosphere: constraints from aircraft (SEAC^{4}RS) and ground-based (SOAS) observations in the Southeast US, Atmos. Chem. Phys., 16, 5969–5991, 2016.

Flocke, F., Atlas, E., Madronich, S., Schauffler, S. M., Aikin, K., Margitan, J. J., and Bui, T. P.: Observations of methyl nitrate in the lower stratosphere during STRAT: Implications for its gas phase production mechanisms, Geophys. Res. Lett., 25, 1891–1894, 1998.

Fu, T.-M., Jacob, D. J., Wittrock, F., Burrows, J. P., Vrekoussis, M., and Henze, D. K.: Global budgets of atmospheric glyoxal and methylglyoxal, and implications for formation of secondary organic aerosols, J. Geophys. Res., 113, D15303 , 2008.

Fuchs, H., Hofzumahaus, A., Rohrer, F., Brauers, T., Dorn, H.-P., Häseler, R., Holland, F., Kaminski, M., Li, X., Lu, K., Nehr, S., Tillmann, R., Wegener, R., and Wahner, A.: Experimental evidence for efficient hydroxyl radical regeneration in isoprene oxidation, Nat. Geosci., 6, 1023–1026, 2013.

Galloway, M. M., Huisman, A. J., Yee, L. D., Chan, A. W. H., Loza, C. L., Seinfeld, J. H., and Keutsch, F. N.: Yields of oxidized volatile organic compounds during the OH radical initiated oxidation of isoprene, methyl vinyl ketone, and methacrolein under high-NOx conditions, Atmos. Chem. Phys., 11, 10779–10790, 2011.

Gross, C. B. M., Dillon, T. J., Schuster, G., Lelieveld, J., and Crowley, J. N.: Direct kinetic study of OH and O_3 formation in the reaction of $CH_3C(O)O_2$ with HO_2, J. Phys. Chem. A, 118, 974–985, 2014.

Guenther, A. B., Jiang, X., Heald, C. L., Sakulyanontvittaya, T., Duhl, T., Emmons, L. K., and Wang, X.: The Model of Emissions of Gases and Aerosols from Nature version 2.1 (MEGAN2.1): an extended and updated framework for modeling biogenic emissions, Geosci. Model Dev., 5, 1471–1492, doi:10.5194/gmd-5-1471-2012, 2012.

Hallquist, M., C.Wenger, J., Baltensperger, U., Rudich, Y., Simpson, D., Claeys, M., Dommen, J., Donahue, N. M., George, C., Goldstein, A. H., Hamilton, J. F., Herrmann, H., Hoffmann, T., Iinuma, Y., Jang, M., Jenkin, M. E., Jimenez, J. L., Kiendler-Scharr, A., Maenhaut, W., McFiggans, G., Mentel, T. F., Monod, A., Prévôt, A. S. H., Seinfeld, J. H., Surratt, J. D., Szmigielski, R., and Wildt, J.: The formation, properties and impact of secondary organic aerosol: current and emerging issues, Atmos. Chem. Phys., 9, 5155–5236, 2009.

Hofzumahaus, A., Rohrer, F., Lu, K., Bohn, B., Brauers, T., Chang, C.-C., Fuchs, H., Holland, F., Kita, K., Kondo, Y., Li, X., Lou, S., Shao, M., Zeng, L., Wahner, A., and Zhang, Y.: Amplified trace gas removal in the troposphere, Science, 324, 1702–1704, 2009.

Huang, G., Brook, R., Crippa, M., Janssens-Maenhout, G., Schieberle, C., Dore, C., Guizzardi, D., Muntean, M., Schaaf, E., and Friedrich, R.: Speciation of anthropogenic emissions of non-methane volatile organic compounds: a global gridded data set for 1970-2012, Atmos. Chem. Phys., 17, 7683–7701, 2017.

Jacobs, M. I., Burke, W. J. and Elrod, M. J.: Kinetics of the reactions of isoprene-derived hydroxynitrates: gas phase epoxide formation and solution phase hydrolysis, Atmos. Chem. Phys., 14, 8933–8946, 2014.

Jara-Toro, R. A., Hernandez, F. J., Taccone, R. A., Lane, S. I., and Pino, G. A.: Water catalysis of the reaction between methanol and OH at 294 K and the atmospheric implications, Angew. Chem. Int. Ed., 56, 2166–2170, 2017.

Janssens-Maenhout, G., Crippa, M., Guizzardi, D., Dentener, F., Muntean, M., Pouliot, G., Keating, T., Zhang, Q., Kurokawa, J., Wankmüller, R., Denier van der Gon, H., Kuenen, J. J. P., Klimont, Z., Frost, G., Darras, S., Koffi, B., and Li, M.: HTAP_v2.2: a mosaic of regional and global emission grid maps for 2008 and 2010 to study hemispheric transport of air pollution, Atmos. Chem. Phys., 15, 11411–11432, 2015.

Jenkin, M. E., Young, J. C. and Rickard, A. R.: The MCM v3.3.1 degradation scheme for isoprene, Atmos. Chem. Phys., 15, 11433–11459, 2015.

Jokinen, T., Sipilä, M., Richters, S., Kerminen, V.-M., Paasonen, P., Stratmann, F., Worsnop, D., Kulmala, M., Ehn, M., Herrmann, H., and Berndt, T.: Rapid autoxidation forms highly oxidized RO_2 radicals in the atmosphere, Angew. Chem. Int. Ed., 53, 1–6, 2014.

Jokinen, T., Berndt, T., Makkonen, R., Kerminen, V.-M., Junninen, H., Paasonen, P., Stratmann, F., Herrmann, H., Guenther, A. B., Worsnop, D. R., Kulmala, M., Ehn, M., and Sipilä, M.: Production of extremely low volatile organic compounds from biogenic emissions: Measured yields and atmospheric implications, Proc. Nat. Acad. Sci., 112, 7123–7128, 2015.

Jorand, F., L. Kerhoas, A. Heiss, J. Einhorn, and K. Sahetchian: Determination of the ultraviolet absorption cross section of hexyl-ketohydroperoxides in solution in acetonitrile, J. Photochem. Photobiol. A, 134, 119–125, 2000.

Jørgensen, S., Knap, H. C., Otkjaer, R. V., Jensen, A. M., Kjeldsen, M. L. H., Wennberg, P. O., and Kjaergaard, H. G.,: Rapid hydrogen shift scrambling in hydroperoxy-substituted organic peroxy radicals, J. Phys. Chem A, 120, 266–275, 2016.

Khan, M. A. H., Lyons, K., Chhantyal-Pun, R., McGillen, M. R., Caravan, R. L., Taatjes, C. A., Orr-Ewing, A. J., Percival, C. J., and Shallcross, D. E. :Investigating the tropospheric chemistry of acetic acid using the global 3-D chemistry transport model, STOCHEM-CRI, J. Geophys., 123, 6267–6281, 2018.

Kjaergaard, H. G., Knap, H. C., Ørnsø, K. B., Jørgensen, S., Crounse, J. D., Paulot, F., and Wennberg, P. O.: Atmospheric fate of methacrolein. 2. Formation of lactone and implications for organic aerosol production, J. Phys. Chem. A, 116, 5763–5768, 2012.

Knap, H. C., Schmidt, J. A., and Jorgensen, S.: Hydrogen shift reactions in four methyl-buten-ol (MBO) peroxy radicals and their impact on the atmosphere, Atmos. Environ., 147, 79–87, 2016.

Kwan, A. J., Chan, A. W. H., Ng, N. L., Kjaergaard, H. G., Seinfeld, J. H., and Wennberg, P. O.: Peroxy radical chemistry and OH radical production during the NO_3-initiated oxidation of isoprene, Atmos. Chem. Phys., 12, 7499–7515, 2012.

Lee, L., Teng, A. P., Wennberg, P. O., Crounse, J. D., and Cohen, R. C.: On rates and mechanisms of OH and O_3 reactions with isoprene-derived hydroxy nitrates, J. Phys. Chem. A, 118, 1622–1637, 2014.

Lei, X., Chen, D., Wang, W., Liu, F., and Wang, W.: Quantum chemical studies of the OH-initiated oxidation reactions of propenols in the presence of O_2, Mol. Phys., doi: 10.1080/00268976.2018.1537527, 2018.

Lelieveld, J., Butler, T. M., Crowley, J. N., Dillon, T. J., Fischer, H., Ganzeveld, L., Harder, H., Lawrence, M. G., Martinez, M., Taraborrelli, D., and Williams, J.: Atmospheric oxidation capacity sustained by a tropical forest, Nature, 452, 737–740 , 2008.

Lelieveld, J., Gromov, S., Pozzer, A., and Taraborrelli, D.: Global tropospheric hydroxyl distribution, budget and reactivity, Atmos. Chem. Phys., 16, 12477-12496, 2016.

Lewis, T. R., Blitz, M. A., Heard, D. E., and Seakins, P. W.: Direct evidence for a substantive reaction between the Criegee intermediate, CH_2OO, and the water vapour dimer, Phys. Chem. Chem. Phys., 17, 4859–4863, 2015.

Li, J., Mao, J., Min, K.-E., Washenfelder, R., Brown, S. S., Kaiser, J., Keutsch, F. N., Volkamer, R., Wolfe, G. M., Hanisco, T. F., Pollack, I. B., Ryerson, T. B., Graus, M., Gilman, J. B., Lerner, B. M., Warneke, C., de Gouw, J. A., Middlebrook, A. M., Liao, J., Welti, A., Henderson, B. H., McNeill, V. F., Hall, S. R., Ullmann, K., Donner, L. J., Paulot, F., and Horowitz, L. W. Observational constraints on glyoxal production from isoprene oxidation and its contribution to organic aerosol over the Southeast United States, J. Geophys. Res., 121, doi:10.1002/2016JD025331, 2016.

Liggio, J., Li, S.-M., and McLaren, R.: Reactive uptake of glyoxal by particulate matter, J. Geophys. Res., 110, D10304, 2005.

Lin, Y.-H., Zhang, Z., Docherty, K. S., Zhang, H., Budisulistiorini, S. H., Rubitschun, C. L., Shaw, S. L., Knipping, E. M., Edgerton, E. S., Kleindienst, T. E., Gold, A., and Surratt, J. D.: Isoprene epoxydiols as precursors to secondary organic aerosol formation: acid-catalyzed reactive uptake studies with authentic compounds, Environ. Sci., 46, 250-258, 2012.

Lin, Y.-H., Zhang, H., Pye, H. O. T., Zhang, Z., Marth, W. J., Park, S., Arashiro, M., Cui, T., Budisulistiorini, S. H., Sexton, K. G., Vizuete, W., Xie, Y., Luecken, D. J., Piletic, I. R., Edney, E. O., Bartolotti, L. J., Glod, A., and Surratt, J. D.: Epoxide as a precursor to secondary organic aerosol formation from isoprene photooxidation in the presence of nitrogen oxides, Proc. Nat. Acad. Sci., 110, 6718-6723, 2013.

Liu, Y. J., Herdlinger-Blatt, I., McKinney, K. A., and Martin, S. T.: Production of methyl vinyl ketone and methacrolein via the hydroperoxyl pathway of isoprene oxidation, Atmos. Chem. Phys., 13, 5715–5730, 2013.

Liu, J. M., D'Ambro, E., Lee, B. H., Lopez-Hilfiker, F. D., Zaveri, R. A., Rivera-Rios, J. C., Keutsch, F. N., Iyer, S., Kurten, T., Zhang, Z. F., Gold, A., Surratt, J. D., Shilling, J. E., and Thornton, J. A.: Efficient isoprene secondary organic aerosol formation from a non-IEPOX pathway, Environ. Sci Technol., 50, 9872–9880, 2016.

Liu, Z., Nguyen, V. S., Harvey, J., Müller, J.-F. and Peeters, J.: Theoretically derived mechanisms of HPALD photolysis in isoprene oxidation, Phys. Chem. Chem. Phys., 19, 9096–9106, 2017.

Liu, Z., Nguyen, V. S., Harvey, J., Müller, J.-F. and Peeters, J.: The photolysis of α-hydroperoxycarbonyls, Phys. Chem. Chem. Phys., 20, 6970–6979, 2018.

Magneron, I., Mellouki, A., and Le Bras, G.: Photolysis and OH-initiated oxidation of glycolaldehyde under atmospheric conditions, J. Phys. Chem. A, 109, 4552–4561, 2005.

Marais, E. A., Jacob, D. J., Jimenez, J. L., Campuzano-Jost, P., Day, D. A., Hu, W., Krechmer, J., Zhu, L., Kim, P. S., Miller, C. C., Fisher, J. A., Travis, K., Yu, K., Hanisco, T. F., Wolfe, G. M., Atkinson, H. L., Pye, H. O. T., Froyd, K. D., Liao, J., and NcNeill, V. F.: Aqueous-phase mechanism for secondary organic aerosol formation from isoprene: application to the southeast United States and co-benefit of SO_2 emission controls, Atmos. Chem. Phys., 16, 1603–1618 , 2016.

Matsunaga, A., Ziemann, P. J.: Yields of β-hydroxynitrates, dihydroxynitrates, and trihydroxynitrates formed from OH radical-initiated reactions of 2-methyl-1-alkenes, Proc. Natl. Acad. Sci., 107, 6664–6669, 2010.

Mebel, A. M., and Kislov, V. V.: The $C_2H_3 + O_2$ reaction revisited: Is multireference treatment of the wave function really critical?, J. Phys. Chem. A, 109, 6993–6997, 2005.

Millet, D. B., Guenther, A., Siegel, D. A., Nelson, N. B., Singh, H. B., de Gouw, J. A., Warneke, C., Williams, J., Eerdekens, G., Sinha, V., Karl, T., Flocke, F., Apel, E. C., Riemer, D. D., Palmer, P. I., and Barkley, M.: Global atmospheric budget of acetaldehyde: 3-D model analysis and constraints from in-situ and satellite observations, Atmos. Chem. Phys., 10, 3405–3425, 2010.

Millet, D. B., Baasandorj, M., Farmer, D. K., Thornton, J. A., Baumann, K., Brophy, P., Chaliyakunnel, S., de Gouw, J. A., Graus, M., Hu, L., Koss, A., Lee, B. H., Lopez-Hilfiker, F. D., Neuman, J. A., Paulot, F., Peischl, J., Pollack, I. B., Ryerson, T. B., Warnecke, C., Williams, B. J., and Xu, J.: A large and ubiquitous source of atmospheric formic acid, Atmos. Chem. Phys., 15, 6283–6304, 2015.

Müller, J.-F., and Brasseur, G.: IMAGES: A three-dimensional chemical transport model of the global troposphere, J. Geophys. Res., 100, 16,445–16,490, 1995.

Müller, J.-F., Stavrakou, T., Wallens, S., De Smedt, I., Van Roozendael, M., Potosnak, M. J., Rinne, J., Munger, B., Goldstein, A., and Guenther, A. B.: Global isoprene emissions estimated using MEGAN, ECMWF analyses and a detailed canopy environment model, Atmos. Chem. Phys., 8, 1329–1341, 2008.

Müller, J.-F., Peeters, J. and Stavrakou, T.: Fast photolysis of carbonyl nitrates from isoprene, Atmos. Chem. Phys., 14, 2497–2508, 2014.

Müller, J.-F., Liu, Z., Nguyen, V. S., Stavrakou, T., Harvey, J. N. and Peeters, J : The reaction of methyl peroxy and hydroxyl radicals as a major source of atmospheric methanol, Nat. Commmun., 7, 13213, 2016.

Müller, J.-F., Stavrakou, T., Bauwens, M., Compernolle, S., and Peeters, J.: Chemistry and deposition in the Model of Atmospheric composition at Global and Regional scales using Inversion Techniques for Trace gas Emissions (MAGRITTE). Part B. Dry deposition, submitted to Geophys. Model Dev. Discuss., 2018.

Nakanishi, H., Morita, H., and Nagakura, S.: Electronic structures and spectra of the keto and enol forms of acetylene, Bull. Chem. Soc. Jpn., 50, 2255–2261, 1977.

Neeb, P.: Structure-reactivity based estimation of the rate constants for hydroxyl radical reactions with hydrocarbons, J. Atmos. Chem., 35, 295–315, 2000.

Neu, J. L., Lawler, M. J., Prather, M. J., and Saltzmann, E. S.: Oceanic alkyl nitrates as a natural source of tropospheric ozone, Geophys. Res. Lett., 35, L13814, 2008.

Nguyen, T. B., Bates, K. H., Crounse, J., Schwantes, R. H., Zhang, X., Kjaergaard, H. G., D., S. J., Lin, P., Laskin, A., H., S. J., and Wennberg, P. O.: Mechanism of the hydroxyl radical oxidation of methacryloyl peroxynitrate (MPAN) and its pathway toward secondary organic aerosol formation in the atmosphere, Phys. Chem. Chem. Phys., 17, 17914–17926, 2015a.

Nguyen, T. B., Crounse, J. D., Teng, A. P., St Clair, J. M., Paulot, F., Wolfe, G. M., and Wennberg, P. O.: Rapid deposition of oxidized biogenic compounds to a temperate forest, Proc. Nat. Acad. Sci., 112, E392-E401, 2015.

Nguyen, T. B., Tyndall, G. S., Crounse, J. D., Teng, A. P., Bates, K. H., Schwantes, R. H., Coggon, M. M., Zhang, L., Feiner, P., Miller, D. O., Skog, K. M., Rivera-Rios, J. C., Dorris, M., Olson, K. F., Koss, A., Wild, R. J., Brown, S. B., Goldstein, A., de Gouw, J. A., Brune, B. H., Keutsch, F. N., Seinfeld, J. H., and Wennberg, P. O.: Atmospheric fates of Criegee intermediates in the ozonolysis of isoprene, Phys. Chem. Chem. Phys., 18, 10241–10254, 2016.

Novelli, A., Kaminski, M., Rolletter, M., Acir, I.-H., Bohn, B., Dorn, H. P., Li, X., Lutz, A., Nehr, S., Rohrer, F., Tillmann, R., Wegener, R., Holland, F., Hofzumahaus, A., Kiendler-Scharr, A., Wahner, A., and Fuchs, H.: Evaluation of OH and HO_2 concentrations and their budgets during photooxidation of 2-methyl-3-butene-2-ol (MBO) in the atmospheric simulation chamber SAPHIR, Atmos. Chem. Phys., 18, 11409–11422, 2018a.

Novelli, A., Bohn, B., Dorn, H. P., Hofzumahaus, A., Holland, F., Li, X., Kaminski, M., Yu, Z., Rosanka, S., Reimer, D., Gkatzelis, G. I., Taraborrelli, D., Vereecken, L., Rohrer, F., Tillmann, R., Wegener, R., Kiendler-Scharr A., Wahner, A., and Fuchs, H.: The atmosphere of a tropical forest simulated in a chamber: experiments, theory and global significance of OH regeneration in isoprene oxidation, iCACGP-IGAC 2018 Conference, Takamatsu, Japan, 2018b.

Orlando, J., Tyndall, G., and Taraborrelli, D.: Atmospheric oxidation mechanism for glycolaldehyde (and hydroxyacetone), Abstract A33L-0315, AGU (American Geophysical Union) Fall Meeting, San Francisco, Calif., December 2012.

Paulot, F., Crounse, J. D., Kjaergaard, H. G., Kürten, A., St. Clair, J. M., Seinfeld, J. H., and Wennberg, P. O.: Unexpected epoxide formation in the gas-phase photooxidation of isoprene, Science, 325, 730–733, 2009a.

Paulot, F., Crounse, J. D., Kjaergaard, H. G., Kroll, J. H., Seinfeld, J. H., and Wennberg, P. O.: Isoprene photooxidation: new insights into the production of acids and organic nitrates, Atmos. Chem. Phys., 9, 1479–1501, 2009b.

Paulot, F., Wunch, D., Crounse, J. D., Toon, G. C., Millet, D. B., DeCarlo, P. F., Vigouroux, C., Deutscher, N. M., González Abad, G., Notholt, J., Warneke, T., Hannigan, J. W., Warneke, C., de Gouw, J. A., Dunlea, E. J., De Mazière, M., Griffith, D. W. T., Bernath, P., Jimenez, J. L., and Wennberg, P. O.: Importance of secondary sources in the atmospheric budgets of formic and acetic acids, Atmos. Chem. Phys., 11, 1989–2013, 2011.

Paulot, F., Henze, D. K., and Wennberg, P. O.: Impact of the isoprene photochemical cascade on tropical ozone, Atmos. Chem. Phys., 12, 1307–1325, 2012

Peeters, J., Nguyen, T. L. and Vereecken, L.: HOx radical regeneration in the oxidation of isoprene, Phys. Chem. Chem. Phys., 11, 5935–5939, 2009.

Peeters, J., and Müller, J.-F.: HOx radical regeneration in isoprene oxidation via peroxy radical isomerisations, II: Experimental evidence and global impact, Phys. Chem. Chem. Phys., 12, 14227–14235, 2010.

Peeters, J., and Nguyen, T. L.: Unusually fast 1,6-H shifts of enolic hydrogens in peroxy radicals: formation of the first-generation C_2 and C_3 carbonyls in the oxidation of isoprene, J. Phys. Chem. A, 116, 6134–6141, 2012.

Peeters, J., Müller, J.-F., Stavrakou, T., and Nguyen, S. V.: Hydroxyl radical recycling in isoprene oxidation driven by hydrogen bonding and hydrogen tunneling: the upgraded LIM1 mechanism, J. Phys. Chem. A, 118, 8625–8643, 2014.

Peeters, J., Nguyen, V. S., and Müller, J.-F.: Tautomerization of vinyl alcohol to acetaldehyde in the atmosphere revisited, J. Phys. Chem. Lett., 6, 4005-4011, 2015.

Pinho, P., Pio, C., and Jenkin, M.: Evaluation of isoprene degradation in the detailed tropospheric chemical mechanism, MCM v3, using environmental chamber data, Atmos. Environ., 39, 1303–1322, 2005.

Praske, E., Crounse, J. D., Bates, K. H., Kurten, T., Kjaergaard, H. G., and Wennberg, P. O.: Atmospheric fate of methyl vinyl ketone: peroxy radical reactions with NO and HO_2, J. Phys. Chem. A, 119, 4562–4572, 2015.

Praske, E., Otkjaer, R. V., Crounse, J. D., Hethcox, J. C., Stoltz, B. M., Kjaergaard, H. G., and Wennberg, P. O.: Atmospheric autoxidation is increasingly important in urban and suburban North America, Proc. Nat. Acad. Sci., 115, 64–69, 2018

Pugh, T. A. M., MacKenzie, A. R., Langford, B., Nemitz, E., Misztal, P. K., and Hewitt, C. N.: The influence of small-scale variations in isoprene concentrations on atmospheric chemistry over a tropical rainforest, Atmos. Chem. Phys., 11, 4121–4134, 2011.

Read, K. A., Carpenter, L. J., Arnold, S. R., Beale, R., Nightingale, P. D., Hopkins, J. R., Lewis, A. C., Lee, J. D., Mendes, L., and Pickering, S. J.: Multiannual observations of acetone, methanol, and acetaldehyde in remote Tropical Atlantic air: Implications for atmospheric OVOC budgets and oxidative capacity, Envrion. Sci. Technol., 46, 11028–11039, 2012.

Richter, D., Weibring, P., Walega, J. G., Fried, A., Spuler, S. M., and Taubman, M. S.: Compact highly sensitive multi-species airborne mid-IR spectrometer, Appl. Phys. B, 119, 119–131, 2015.

Rindelaub, J. D., McAvey, K. M. and Shepson, P. B.: The photochemical production of organic nitrates from α-pinene and loss via acid-dependent particle phase hydrolysis, Atmos. Environ., 100, 193–201, 2015.

Roberts, J. M., and Fajer, R. W.: UV absorption cross sections of organic nitrates of potential atmospheric importance and estimation of atmospheric lifetimes, Environ. Sci. Technol., 23, 945–951, 1989.

Romer, P. S., Duffey, K. C., Wooldridge, P. J., Allen, H. M., Ayres, B. R., Brown, S. S., Brune, W. H., Crounse, J. D., de Gouw, J., Draper, D. C., Feiner, P. A., Fry, J. L., Goldstein, A. H., Koss, A., Misztal, P., Nguyen, T. B., Olson, K., Teng, A. P., Wennberg, P. O., Wild, R. J., Zhang, L., and Cohen, R. C.: The lifetime of nitrogen oxides in an isoprene-dominated forest, Atmos. Chem. Phys., 16, 7623–7637, 2016.

Röth, E.-P. and Ehhalt, D. H.: A simple formulation of the CH_2O photolysis quantum yield, Atmos. Chem. Phys., 15, 2015, 7239–7266, 2015.

Salter, R. J., Blitz, M. A., Heard, D. E., Kovács, T., Pilling, M. J., Rickard, A. R., and Seakins, P. W.: Quantum yields for the photolysis of glyoxal below 350 nm and parameterisations for its photolysis rate in the troposphere, Phys. Chem. Chem. Phys., 15, 4984–4994, 2013.

Saunders, S. M., M. E. Jenkin, R. G. Derwent, and M. J. Pilling: Protocol for the development of the Master Chemical Mechanism, MCM v3 (Part A): tropospheric degradation of non-aromatic volatile organic compounds, Atmos. Chem. Phys., 3, 161–180, 2003.

Schwantes, R. H., Teng, A. P., Nguyen, T. B., Coggon, M. M., Crounse, J. D., St. Clair, J., Zhang, X., Schilling, K. A., Seinfeld, J. H., and Wennberg, P. O.: Isoprene NO_3 oxidation products from the RO_2+HO_2 pathway, J. Phys. Chem. A, 119, 10158–10171, 2015.

Scribano, Y., Goldman, N., Saykally, R. J., and Leforestier, C.: Water dimers in the atmosphere III: Equilibrium constant from a flexible potential, J. Phys. Chem. A., 110, 5411–5419, 2006.

Seinfeld, J. H., and Pandis, S. N.: Atmospheric Chemistry and Physics: From Air Pollution to Climate Change, 2nd ed., John Wiley, Hoboken, N. J., 2006.

Shaw, M. F., Sztáray, B., Whalley, L. K., Heard, D. E., Millet, D. B., Jordan, M. J. T., Osborn, D. L., and Kable, S. H.: Photo-tautomerization of acetaldehyde as a photochemical source of formic acid in the troposphere, Nat. Commun., 9, 2584, 2018.

Sheps, L., Rotavera, B., Eskola, A. J., Osborn, D. L., Taatjes, C. A., Au, K., Shallcross, D. E., Khan, M. A. H., and Percival, C. J.: The reaction of Criegee intermediate CH_2OO with water dimer: primary products and atmospheric impact, Phys. Chem. Chem. Phys., 19, 21970–21979, 2017.

Silva, S. J., Heald, C. L., and Li, M.: Space-based constraints on terrestrial glyoxal production, J. Geophys. Res., doi: 10.1029/2018JD029311, 2018.

Simpson, I. J., Akagi, S. K., Barletta, N. J., Choi, Y., Diskin, G. S., Fried, A., Fuelberg, H. E., Meinardi, S., Rowland, F. S., Vay, S. A., Weinheimer, A. J., Wennberg, P. O., Wiebring, P., Wisthaler, A., Yang, M., Yokelson, R. J., and Blake, D. R.: Boreal forest fire emissions in fresh Canadian smoke plume: C_1-C_10 volatile organic compounds (VOCs), CO_2, CO, NO_2, NO, HCN and CH_3CN, Atmos. Chem. Phys., 11, 6445–6463, 2011.

Sindelarova, K., Granier, C., Bouarar, I., Guenther, A., Tilmes, S., Stavrakou, T., Müller, J.-F., Kuhn, U., Stefani, P., and Knorr, W.: Global dataset of biogenic VOC emissions calculated by the MEGAN model over the last 30 years, Atmos. Chem. Phys., 14, 9317–9341, 2014.

Smith, M. C., Chang, C.-H., Chao, W., Lin, L.-C., Takahashi, K., Boering, K. A., and Lin, J. J.: Strong negative temperature dependence of the simplest Criegee Intermediate CH_2OO reaction with water dimer, J. Phys. Chem. Lett., 6, 2708–2713, 2015.

So, S., Wille, U., and da Silva, G.: Atmospheric chemistry of enols: A theoretical study of the vinyl alcohol + OH + O_2 reaction mechanism, Environ. Sci. Technol., 48, 6694–6701, 2014.

Sofiev, M., Vankevich, R., Ermakova, T., and Hakkarainen, J.: Global mapping of maximum emission heights and resulting vertical profiles of wildfire emissions, Atmos. Chem. Phys., 13, 7039–7052, 2013.

Squire, O. J., Archibald, A. T., Griffiths, P. T., Jenkin, M. E., Smith, D., and Pyle, J. A.: Influence of isoprene chemical mechanism on modelled changes in tropospheric ozone due to climate and land use over the 21st century, Atmos. Chem. Phys., 15, 5123–5143, 2015.

Stadtler, S., Kühn, T., Schrüder, S., Taraborrelli, D., Schultz, M. G., and Kokkola, H.: Isoprene-derived secondary organic aerosol in the global aerosol-chemistry-climate model ECHAM6.3.0-HAM2.3-MOZ1.0, Geosci. Model Dev., 11, 3235-3260, 2018.

St. Clair, J. M., Rivera-Rios, J., Crounse, J. D., Knap, H. C., Bates, K. H., Teng, A. P., Jorgensen, S., Kjaergaard, H. G., Keutsch, F. N., and Wennberg, P. O.: Kinetics and products of the reaction of the first-generation isoprene hydroxy hydroperoxide (ISOPOOH) with OH, J. Phys. Chem. A, 120, 1441–1451, 2016.

Stavrakou, T., Müller, J.-F., Smedt, I. D., Roozendael, M. V., van der Werf, G. R., Giglio, L., and Guenther, A.: Evaluating the performance of pyrogenic and biogenic emission inventories against one decade of space-based formaldehyde columns, Atmos. Chem. Phys., 9, 1037–1060, 2009a.

Stavrakou, T., Müller, J.-F., De Smedt, I., Van Roozendael, M., Kanakidou, M., Vrekoussis, M., Wittrock, F., Richter, A., Burrows, J. P.: The continental source of glyoxal estimated by the synergistic use of spaceborne measurements and inverse modelling, Atmos. Chem. Phys., 9, 8431–8446, 2009b.

Stavrakou, T., Peeters, J., and Müller, J.-F.: Improved global modelling of HOx recycling in isoprene oxidation: evaluation against the GABRIEL and INTEX-A aircraft campaign measurements, Atmos. Chem. Phys., 10, 9863–9878, 2010.

Stavrakou, T., Guenther, A., Razavi, A., Clarisse, L., Clerbaux, C., Coheur, P.-F., Hurtmans, D., Karagulian, F., De Mazière, M., Vigouroux, C., Amelynck, C., Schoon, N., Laffineur, Q., Heinesch, B., Aubinet, M., Rinsland, C., and Müller, J.-F.: First space-based derivation of the global atmospheric methanol emission fluxes, Atmos. Chem. Phys., 11, 4873–4898, 2011.

Stavrakou, T., Müller, J.-F., Peeters, J., Razavi, A., Clarisse, L., Clerbaux, C., Coheur, P.-F., Hurtmans, D., De Mazière, M., Vigouroux, C., Deutscher, N. M., Griffith, D. W. T., Jones, N., and Paton-Walsh, C.: Satellite evidence for a large source of formic acid from boreal and tropical forests, Nat. Geosci., 5, 26–30, 2012.

Stavrakou, T., Müller, J.-F., Boersma, K. F., van der A, R. J., Kurokawa, J., Ohara, T., and Zhang, Q.: Key chemical NOx sink uncertainties and how they influence top-down emissions of nitrogen oxides, Atmos. Chem. Phys., 13, 9057–9082, 2013.

Stavrakou, T., Müller, J.-F., Bauwens, M., De Smedt, I., Van Roozendael, M., De Mazière, M., Vigouroux, C., Hendrick, F., George, M., Clerbaux, C., Coheur, P.-F., and Guenther, A. How consistent are top-down hydrocarbon emissions based on formaldehyde observations from GOME-2 and OMI?, Atmos. Chem. Phys., 15, 11861–11884, 2015.

Surratt, J. D., Chan, A. W. H., Eddingsaas, N. C., Chan, M., Loza, C. L., Kwan, A. J., Hersey, S. P., Flagan, R. C., Wennberg, P. O., and Seinfeld, J. H.: Reactive intermediates revealed in secondary organic aerosol formation from isoprene, Proc. Nat. Acad. Sci., 107, 6640–6645, 2010.

Taraborrelli, D., Lawrence, M. G., Crowley, J. N., Dillon, T. J., Gromov, S., Grosz, C. B. M., Vereecken, L., and Lelieveld, J.: Hydroxyl radical buffered by isoprene oxidation over tropical forests, Nature Geosci., 5, 190–193, 2012.

Teng, A. P., Crounse, J. D., and Wennberg, P. O.: Isoprene peroxy radical dynamics, J. Am. Chem. Soc., 139, 5367-5377, 2017.

Thuner, L. P., Rea, G., and Wenger, J. C.: Photolysis of butenedial and 4-oxopent-2-enal, in The European Photoreactor EUPHORE 4th Report 2001, ed. I. Barnes, Bergische Universitat Wuppertal, Wuppertal, Germany, pp. 41–46, 2003.

Toon, O. B., Maring, H., Dibb, J., Ferrare, R., Jacob, D. J., Jensen, E. J., J., Z., Mace, G. G., Pan, L. L., Pfister, L., Rosenlof, K. H., Redemann, J., Reid, J. S., Singh, H. B., Yokelson, R., Minnis, P., Chen, G., Jucks, K. W., and Pszenny, A.: Planning, implementation and scientific goals of the Studies of Emissions and Atmospheric Composition, Clouds and Climate Coupling by Regional SSurvey (SEAC4RS) field mission, J. Geophys. Res., 121, 4967–5009, 2016.

Trainer, M., Williams, E. J., Parrish, D. D., Buhr, M. P., Allwine, E. J., Westberg, H. H., Fehsenfeld, F. C., and Liu, S. C.: Models and observations of the impact of natural hydrocarbons on rural ozone, Nature, 329, 705–707, 1987.

Travis, K. R., Jacob, D. J., Fisher, J. A., Kim, P. S., Marais, E. A., Zhu, L., Yu, K., Miller, C. C., Yantosca, R. M., Sulprizio, M. P., Thompson, A. M., Wennberg, P. O., Crounse, J. D., St. Clair, J. M., Cohen, R. C., Laughner, J. L., Dibb, J. E., Hall, S. R., Ullmann, K., Wolfe, G. M., Pollack, I. B., Peischl, J., Neumann, J. A., and Zhou, X.: Why do models overestimate surface ozone in the Southeast United States? Atmos. Chem. Phys., 16, 13561–13577, 2016.

Tuazon, E. C., and Atkinson, R. A.: A product study of the gas-phase reaction of methyl vinyl ketone with the OH radical in the presence of NO_x, Int. J. Chem. Kinet., 21, 1141-1152, 1989.

van der Werf, G. R., Randerson, J. T., Giglio, L., van Leeuwen, T. T., Chen, Y., Rogers, B. M., Mu, M., van Marle, M. J. E., Morton, D. C., Collatz, G. J., Yokelson, R. J., and Kasibhatla, P. S.: Global fire emissions estimates during 1997–2016, Earth Syst. Sci. Data, 9, 697–720, 2017.

Vereecken, L., and Peeters, J.: Decomposition of substituted alkoxy radicals - part I: a generalized structure-activity relationship for reaction barrier heights, Phys. Chem. Chem. Phys., 11, 9062–9074, 2009.

Vu, N. D., Khamaganov, V., Nguyen, V. S., Carl, S. A. and Peeters: J. Absolute rate coefficient of the gas-phase reaction between hydroxyl radical (OH) and hydroxyacetone: Investigating the effects of temperature and pressure, J. Phys. Chem. A, 117, 12208–12215, 2013.

Wennberg, P. O., Bates, K. H., Crounse, J. D., Dodson, L. G., McVay, R., Mertens, L. A., Nguyen, T. B., Praske, E., Schwantes, R. H., Smarte, M. D., St Clair, J. M., Teng, A. P., Zhang, X., and Seinfeld, J. H.: Gas-phase reactions of isoprene and its major oxidation products, Chem. Rev., 118, 3337–3390, DOI: 10.1021/acs.chemrev.7b00439, 2018.

Wolfe, G. M., Crounse, J. D., Parrish, J. D., St Clair, J. M., Beaver, M. R., Paulot, F., Yoon, T. P., Wennberg, P. O., and Keutsch, F. N.: Photolysis, OH reactivity and ozone reactivity of a proxy for isoprene-derived hydroperoxyenals (HPALDs), Phys. Chem. Chem. Phys., 14, 7276–7286, 2012.

Wolfe, G. M., Hanisco, T. F., Arkinson, H. L., Bui, T. P., Crounse, J. D., Dean-Day, J., Goldstein, A., Guenther, A., Hall, S. R., Huey, G., Jacob, D. J., Karl, T., Kim, P. S., Liu, X., Marvin, M. R., Mikoviny, T., Misztal, P., Nguyen, T. B., Peischl, J., Pollack, I., Ryerson, T., St. Clair, J. M., Teng, A., Travis, K. R., Ullmann, K., Wennberg, P. O., and Wisthaler, A.: Quantifying sources and sinks of reactive gases in the lower atmosphere using airborne flux observations, Geophys. Res. Lett., 42, 8231–8240, 2015.

Xiong, F., Borca, C. H., Slipchenko, L. V., and Shepson, P. B.: Photochemical degradation of isoprene-derived 4,1-nitrooxy enal, Atmos. Chem. Phys., 16, 5595–5610, 2016.

Yan, C., Kocevska, S., and Krasnoperov, L. N.: Kinetics of the reaction of CH_3O_2 radicals with OH studied over the 292–526 K temperature range, J. Phys. Chem. A, 120, 6111–6121, 2016.

Yoon M.-C., Choi Y. S., and Kim, S. K.: The OH production from the transition of acetylacetone, Chem. Phys. Lett., 300, 207–212, 1999.